5.7   Beam Instrumentation *(A. Aryshev, T. Aumeyr, G. A. Blair, S. T. Boogert, G. Boorman, A. Bosco, L. Corner, A.E. Dabrowski, L. Deacon, B. Foster, A. Gillespie, E.B. Holzer, S. Jamison P. Karataev, T. Lefevre, K. Lekomtsev, M. Olvegard, S. Mallows, M. Micheler, L. Nevay, M. Sapinski, S. Smith, L. Soby, R. Walczak, C.Welsch, M. Wendt)*

5.7.1   Overview of the CLIC beam instrumentation needs

A general layout of the CLIC complex is depicted in Figure 1. The detailed description of the accelerator sub-systems is presented in paragraphs 3 and 4 for the Main and the Drive beams respectively.
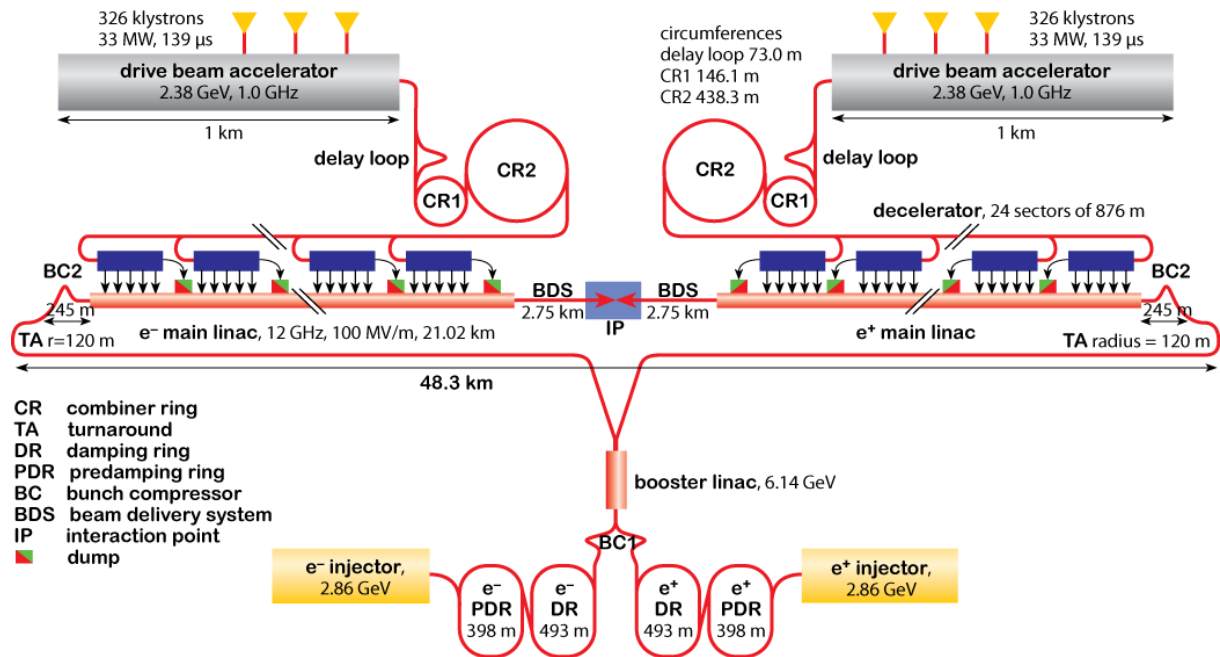
Figure 1: 3TeV CLIC Complex

Beam dynamic considerations dictate most of the requirements for Beam instrumentation and CLIC is expected to perform with extremely tight tolerances on most beam parameters. Extremely small emittance beams are generated in the damping rings and must be conserved over more than 40kms of beam lines requiring a precise control of the beam position over long distances. Before entering the main linac, the bunch length must be shortened and controlled at the femtosecond level. At the interaction point, the beam is finally focused to only a few nanometers in size. After collisions, the highly disrupted beam must be dumped in clean conditions, making sure that the 100 of megawatts of power carried by the particles are safely absorbed. Moreover, the CLIC technology relies on a two-beam acceleration scheme, where a second electron beam with a moderate energy but a high current and high bunching frequency is used to generate the radiofrequency power required to accelerate the main beam. The Drive Beam complex is nothing more than a power source, the equivalent of the 12GHz relativistic klystron distributed over a distance of 48kms, which is supposed to run with the best efficiency and reliability.

5.7.1.1   Overview of the Main Beam Requirements

The layout of the electron and positron injector complex is discussed in greater detail in paragraph 3.1. The source of polarized electrons is based on the use of a photo-injector with a DC gun. Once extracted, the electrons are directly accelerated to 200MeV in a linear accelerator using 2GHz normal conducting cavities. Contrary to the electron source, the positron source relies on a much larger accelerator complex and requires a preliminary electron injector complex of 5GeV. These electrons are then converted in a first target into high-energy photons, which then generate positron through

e$^+$/e$^-$ pair creation in a second target. The positron beam is then pre-accelerated to 200MeV. Electrons and Positrons are finally accelerated in a common 2GHz Linac up to 2.86GeV.

The transverse normalized beam emittances are then reduced from mm.rad to nm.rad in two consecutives rings, namely the Pre-Damping Ring and the Damping Ring. The main characteristics of these rings are presented in paragraph 3.2. Despite, in the injector complex, the positron beam having an emittance 100 times larger than that of the electron beam, they both finally reach similar emittance values after the PDR. At the extraction of the DR, typical values are below 500 and 5 nm.rad respectively for the horizontal and vertical emittances.

From the exit of the Damping rings, the beam enters in the 'Ring To Main Linac' (RTML, see paragraph 3.3) where the bunches are compressed in a first magnetic chicane, accelerated to an energy of 9GeV in a 'Booster Linac' and transferred to the entrance of the Main Linac through more than 20kms of beam line. After a final 1.5km long turn-around loop, bunches are compressed even further in a second magnetic chicane to a final bunch length of 44um R.M.S.

The beam is then accelerated in the Main Linac, composed of a succession of more than 70 thousands of 12 GHz accelerating structures and regrouped in working units, known as 'CLIC Modules'. This is discussed in further detail in paragraphes 3.4 and 5.6. The beam energy rises up to 1.5TeV over a total distance of 20.5kms. Along the entire linac, the beam properties (beam position, current, emittance, losses and bunch length) must be measured in a non-interceptive way to guarantee the overall performance of the machine and provide reliable information for feedback systems. In order to guarantee the design luminosity, the beam emittance growth from the Damping Ring to the Interaction Point must be kept below 20%. This of course puts very high constraints on the alignment and the stabilization of any actives devices installed on the beam line (magnet, RF cavities,..) and requires as well very precise tools to measure the beam positions and sizes.

The beam is finally transported through the Beam Delivery System (BDS) to the Interaction Point. The BDS, presented in details in paragraph 3.5, has three main functionalities. First, a beam diagnostic section characterizes the beam properties, measuring emittance, energy, and polarisation. The second part of the BDS is dedicated to the beam cleaning using a succession of collimation scheme and finally the last part provide the final optic adjustment, focussing the beam down to nanometres beam sizes at the Interaction Point.

After collisions, the beam, highly disrupted is then guided towards a huge water dump. This part of the machine, called the 'Spent Beam line' and described in further detail in paragraph 3.7 has also some crucial impact for instrumentation. The CLIC luminosity monitor is based on the detection of beamstrahlung photons generated at the IP. The 'Spent beam line' uses a combination of vertical bends to separate these high-energy photons from the charged particles themselves. An intermediate beam dumps will absorb the lowest energy particles and the oppositely charged particles coming from coherent pair creation in the IP. Each magnet comes with its own protection system composed of collimators and absorbers. The beam, with its large energy spread is then diluted using C-shape dipoles over the 30cm aperture of the vacuum window. The beam is finally stopped in a water dump. In this line, the beam diagnostic does not require high precision, but must be reliable enough to prove the beam has been dumped correctly. The instrumentation consists mainly of beam losses and intensity monitors to check the efficiency of the intermediate dump, a series of beam position monitors to steer the beam through and few beam size monitors to confirm the dilution of the particles at the entrance of the dump.

5.7.1.2 *Overview of the Drive Beam Requirements*

The unique design of the Drive Beam linac relies on the use of fully loaded accelerating structures, providing optimal conditions in terms of RF power to beam energy transfer efficiency. As a consequence, any beam intensity fluctuations from the source will be accompanied by equivalent energy fluctuations at the end of the linac. This implies a high stability over very long pulse trains of both the beam intensity of the source and the linac RF source power and phase.

The Drive Beam has also an extremely high beam charge of 590uC corresponding to a current of 4.2A over a 140.3us long pulse. This has important consequences on the technology choices for beam instrumentation. Any intercepting devices would be limited to the observation of a small fraction of the Drive Beam, most likely by reducing its pulse length or current. The average radiation level would also have an impact of the way beam diagnostics are conceived favouring radiation-hard designs and anticipating how the maintenance work of such systems could be optimized.

Another specificity of the Drive Beam scheme comes from the beam frequency multiplication technique proposed to convert a long low intensity low frequency beam into a succession of shorter high intensity high frequency beams. This is a way to distribute and provide the necessary 12 GHz RF power to the Main Beam accelerating structure. More details on the beam dynamic concepts are given in paragraph 2.7. The DB scheme uses RF deflecting cavities [i] to inject and combine bunch trains. The performance of this operation relies on longitudinal beam diagnostics capable of measuring the evolution of the bunch scaling with a good precision.

Once the Drive Beam trains have been combined, they are sent down to the CLIC tunnel and distributed to their respective decelerator sectors using Turn-Around loops. Bunches are further compressed from 2ps to 1.4ps and finally 1ps using two consecutives magnetic chicanes located respectively just before and after the turn-around. The precise tuning of the synchronization between the Drive and the Main Beam is performed in the turn-around as well. It relies on the relative phase measurement between both beams and on a fast feed-forward system, which should correct the Drive beam trajectory to keep the synchronization of the two beams better within 50femtoseconds. This scheme is presented in more details in the paragraph 4.2.

In the decelerator sector the beam energy will be gradually transformed into 12 GHz RF power over some hundreds of meters. Along the decelerator, the beam energy spread rises up linearly to finally reach a value of 90%, which makes the beam very special compared to any accelerator in the world. The beam optic must be adapted to ensure constant RF power production without consequent beam losses and it relies on the continuous monitoring of the beam properties.

5.7.1.3   Impact of the temperature tunnel evolution on the instrument's performances
With the present design of the cooling system in the CLIC main tunnel, the ambient temperature would rise by 20degrees as the beam is turned on and reached nominal parameters. For the time being, there was no analysis of all the related technical consequences. It is however anticipated that most of the devices, mechanical and electronic components, would have to be temperature controlled, most likely water-cooled. A deeper study will be launched soon in order to address this technical issue and evaluate the best solution in term of performance and cost.

5.7.1.4   Differences and Synergies between the Main and the Drive Beams
Whilst the Drive and the Main beams have very different parameters, both their charge densities can reach levels well beyond the damage threshold of any physical interceptive monitor. For this reason the choice of any instrument technologies have favored non-intercepting devices wherever possible. Nevertheless, in some case, several detector technologies must be used to cover the needs under any beam conditions. This is the true most likely for transverse and longitudinal profile measurements.

5.7.1.5   Beam instrumentation R&D for the Conceptual Design Report
For the completion of the Conceptual Design Report, the beam instrumentation requirements have been collected for the whole accelerator complex. Although this work has been initiated a long time ago and the most critical requirements have been studied for decades, the document will describe the present status of CLIC instrumentation addressing feasibility issues based on beam dynamic requirements. It is nevertheless true that several aspects of the collider, like the machine protection system and the beam commissioning strategies have been studied more recently and their impact on instrumentation has not implied any modifications at this stage.

The following paragraphs present the overview of CLIC instrumentation classified by instruments types (e.g. beam position monitor). Each paragraph starts with a summary table expressing the needs

for a given kind of measurement, both in terms of expected performance but also mentioning the number of devices to be installed along the accelerator. The tightest requirements are extracted from each table and discussed in details. The technology chosen as a baseline solution for CLIC is presented with a status of its current development. In some cases, the instruments have been already designed following the CLIC requirements, integrated in the machine layout, and some laboratory tests or even beam tests were already performed to demonstrate their performances. For some others, the design of the instruments is only discussed at the conceptual level, relying on achievements obtained in the framework of other accelerator projects, like the International Linear Collider, Free-electron Laser projects or 3rd generation synchrotron light sources. If alternative options exist, they are also discussed, highlighting what would be gained either in terms of performance or cost reduction.

5.7.1.6 *Speaking the same language!*

In the following paragraphs, most of the requirements for beam diagnostics are expressed in terms of Accuracy and Resolution. To avoid any misunderstanding, here are recalled the definitions classically adopted.

Accuracy: Value quantifying the absolute calibrated response of a measurement device within a well-defined standard frame (for example: beam position in mm relative to magnetic axis of adjacent quadrupole)

Resolution: The resolution is the smallest increment that can be induced or discerned by the measurement device within given conditions.

5.7.2 **Beam Position Monitoring Systems**

An overview of the requirements for beam position monitoring is shown in table 1. The requirements are expressed in terms of the expected position accuracy and resolution, and time resolution. The variation of the beam intensity and of the beam pipe aperture are also quoted to highlight the various situations found along the entire accelerator complex.

Machine Sub-Systems	Intensity (A)	Train duration (ns) / Bunch frequency (GHz)	Accuracy / Resolution (um)	Time Resolution (ns)	Quantity	Beam aperture (mm)
Main Beam						
e- & e+ injector Complex	0.5	156 / 1	100 / 50	10	83	40
Pre-Damping Rings	0.5	156 / 1	40 / 20	10 Turn by turn	600	20 / 9
Damping Rings	0.5	156 / 1	40 / 2	10 Turn by turn	600	20 / 9
RTML	1	156 / 2	40 / 10	10	1424	various
Main Linac	1	156 / 2	**5 / 0.05**	**10**	**4196**	8
Beam Delivery System	1	156 / 2	**5 / 0.003**	**10**	**200**	various
MDI & Post-collision Line	1	156 / 2	1000 / 100	10	12	various
Drive Beam						
Source and Linac	4	140 us / 0.5	20 / 20	10	660	40
Frequency Multiplication Complex	4→100	140us → 24 x 240ns 0.5 → 12	40 / 10	10	210	80
Transfer to Tunnel	100	24 x 240ns / 12	40 / 10	10	872	200
Turn around	100	240ns / 12	40 / 10	10	1920	40
Decelerator	100	240ns / 12	**20 / 2**	**10**	**41484**	26

Dump lines	100	240ns / 12	20 / 2	10	96	40

Table 1: Beam Position Monitors by Region and Function

The beam position monitor (BPM) system is extensive; the luminosity beams contains about 7500 BPMs while the drive beams require about 45000. There is a wide variety of different types of BPM with differing beam pipe apertures and performance requirements.

Very tight tolerances are required all along the CLIC main linac and in the Beam Delivery System. To serve these various types of BPMs, we expect to design a few types of electronics modules (BPM processors), listed in Table 7 to report beam position.

5.7.2.1   Main Beam Linac BPM

The main beam linac requires one BPM per quadrupole, a total of 4196 BPMs. Resolution requirements of 50nm (even tighter in the Beam Delivery System) as well as accuracy and stability requirements make resonant cavity position monitors an obvious choice. Single-bunch spatial resolution better than these requirements has been demonstrated in several systems [ii]. Even if this is expected to be a major problem, the required temporal resolution implies to design a BPM with a broader bandwidth than is typical for resonant BPMs. The largest present such systems consist of 36 BPMs [iii,iv], so the CLIC system is novel in scale.

Parameter	Value
Quantity	4196
Nominal current	1.2 Amp
Bunch frequency	2 GHz
Single bunch charge	3.72×10^9 e$^-$ (600 pC)
Beam duct aperture	8 mm
Position resolution	50 nm rms
Temporal resolution	10 ns
Accuracy	5 μm
Stability	100 nm

Table 2 Main Beam Linac Beam Position Monitors

Baseline Choices:

The main beam linac BPM consists of two cavities [v] as depicted in Figure 2, a position cavity measuring both X & Y, and a reference cavity measuring beam charge and phase. The position cavity supports degenerate X and Y dipole modes at 14 GHz. The signals are brought out on four dipole-mode selective couplers, two for each of the X and Y position signals. The reference cavity, with monopole mode frequency also at 14 GHz, provides the beam charge and phase signal used to normalize the position signals. The reference cavity has two monopole mode coupling ports. Redundancy of readout is required to insure that one can identify spurious measurements, which might otherwise risk machine damage from mis-steering by orbit feedback.

Monopole mode in dipole cavity

As the BPM position cavity output waveguides are designed to couple only to cavity dipole modes, the monopole mode of the dipole cavity has essentially no external damping. We have studied the effect of this undamped monopole mode on longitudinal beam dynamics. We require that the energy variation due to the BPM longitudinal mode along the bunch train is small ($< 10^{-4}$) when summed over

all BPMs. We find this condition is met if the monopole mode frequency of the dipole cavity is sufficiently far from a harmonic of the 2 GHz bunch spacing. For example, if the monopole mode frequency is at least 200 MHz away from N*2GHz, we find that the monopole mode, summed over the main beam bunch train, leads to an energy variation along the train of ~1kV per cavity, or ~2MeV if summed coherently over the 2000 cavities in one linac. This amounts to less than 10^{-5} of total energy at 250 GeV operation or ~10^{-6} at 1.5 TeV, compared to the requirement of <10^{-4}. The energy difference is reduced even more by detuning of cavity monopole mode.
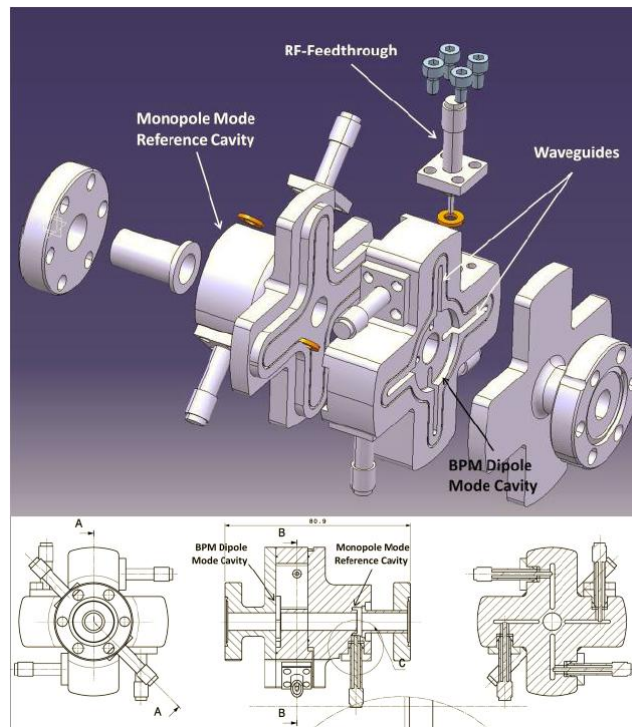
Figure 2: Main Beam Linac Cavity BPM

Future Activities and Options

Three MB BPMs will be fabricated and tested, both on the bench in 2011 and in CTF3 in 2012. Bench tests will include verification of design including manufacturability, mode frequencies and couplings, and accuracy of mode centers. Beam tests will include verification of coupling, resolution, accuracy, and stability. We will proceed with design and prototyping of cavity BPM processing electronics. We will investigate an alternate design for the pickup based on a choke-mode cavity.

5.7.2.2   *Beam Delivery System BPMs*

The Beam delivery system requires BPM resolution as good as or better than the main beam linac with the added complication of widely-varying beam pipe apertures as shown in Figure 3. The larger aperture BPMs must operate at a lower frequency than that chosen for the main beam BPMs, as low as 3 GHz. The required performance can be achieved by scaling the demonstrated performance of existing BPMs. Fortunately the BPMs requiring 3 nm resolution have small pipe diameter and can be handled with essentially the same pickup and electronics as envisioned for the main beam linac BPM. The signal-to-noise in these BPMs is adequate to meet the resolution requirements. Though this resolution has not yet been observed in a particle beam, recent results approach the requirement [**Error! Bookmark not defined.**]
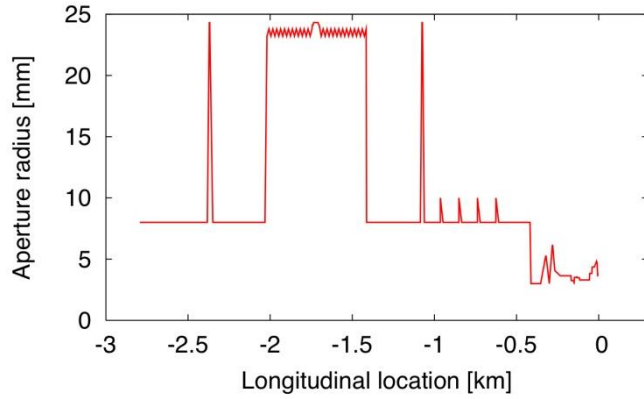
Figure 3: Beam pipe diameter evolution along the BDS

5.7.2.3 Damping Ring BPMs

The CLIC damping ring complex, including pre-damping rings, requires BPMs capable of turn-by-turn resolution. Given the short length of the bunch train (152 ns) compared to the revolution time of the ring (1.6 µs), RF transient loading is an important issue. Therefore a few BPMs must provide temporal resolution within the 156 ns bunch train. We expect it will be convenient to provide 10 ns temporal resolution for all of DR and PDR BPMs.

Parameter	Value	Comments
Quantity	1200	e$^+$ & e$^-$ PDR's & DR's
Nominal current	600 mA	During train passage
Revolution frequency	608 kHz	
Bunch frequency	1 GHz	
Single bunch charge	600 pC	
Beam duct aperture	20 / 9 mm	
Position resolution	10 µm	
Temporal resolution	100 ns	
Accuracy	20 microns	Center wrt external fiducials

Table 3: Main Beam Linac Beam Position Monitors

Baseline Choices

A conventional high-current ring BPM system is appropriate. Small button pickups will be used to maintain low beam impedance. Low coupling to the beam is adequate given the large beam current here. In general, the requirements are similar compared to those of many light sources.

5.7.2.4 Drive Beam Decelerator BPM

The BPMs for the drive beam decelerator represent a unique combination of issues:

- Quantity: these account for 75% of all CLIC BPMs

- Bunch structure; the function of the DB decelerator is to produce > 100 MW RF power at 12 GHz, some small fraction of which can propagate to the BPM, making the bunch frequency a poor choice for processing BPM signals.

- Temporal resolution of 10 ns requires developing an adequate position signal throughout the bunch train.

- Required resolution of 2 microns in a beam aperture of 23 mm requires amplitude measurement at high resolution, about one part in 6000 in amplitude and requiring accurate calibration.

- Survival: the system must survive any beam trajectory within the beam pipe at any fill pattern up to 240 ns pulse length up to 8.3 nC/bunch.

Parameter	Value	Comments
Quantity	41580	Total for all decelerators
Nominal current	100 Amps	
Bunch frequency	12 GHz	
Single bunch charge	8.3 nC	
Beam duct aperture	23 mm	
Position resolution	2 microns rms	Full charge, single bunch to 240 ns train
Temporal resolution	10 ns	
Accuracy	20 microns	Center wrt external fiducials
Wake fields	TBD	

Table 4: Drive Beam Decelerator Beam Position Monitors

Baseline Choices:

The initial plan is to use short stripline BPMs, only 25mm long, with position signals processed at baseband in a bandwidth of 4 – 20 MHz. The striplines are built into the quadrupole vacuum chamber as shown in Figure 4.
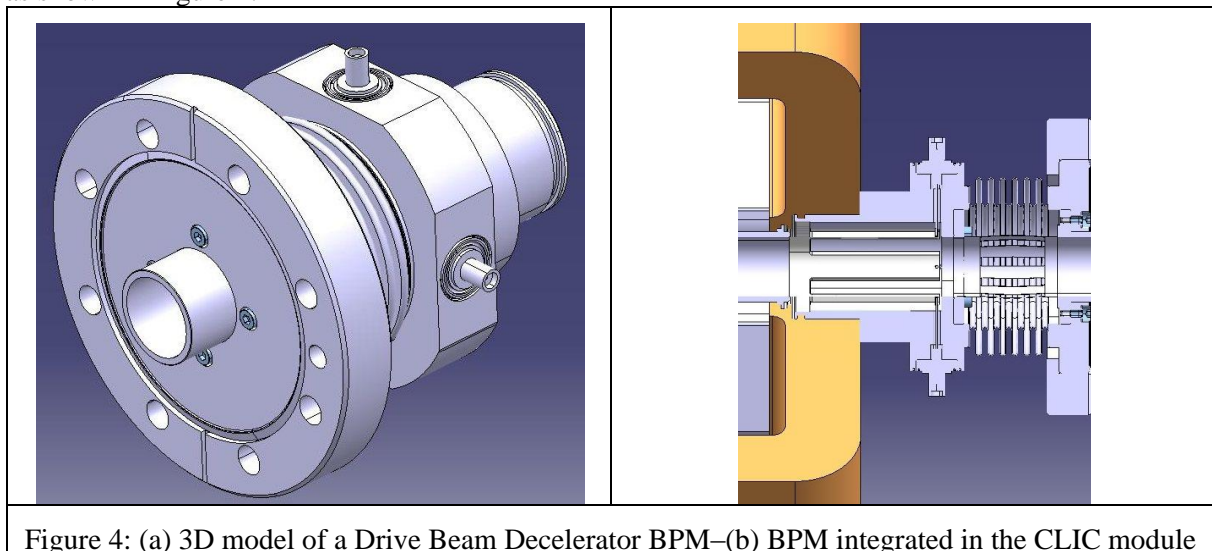
Figure 4: (a) 3D model of a Drive Beam Decelerator BPM–(b) BPM integrated in the CLIC module

Time-Domain Analysis

The BPM is modeled in GdfidL (see Figure 5) for beam response and wakes (see Figure 6). Initial analysis indicated trapped modes; in particular we find a resonant mode close to the 12 GHz bunch spacing apparent in the transverse wake. Addition of a ring of SiC rf damping material at the base of the striplines damps this resonance without significantly affecting the beam position signal as depicted in Figures 7 and 8.
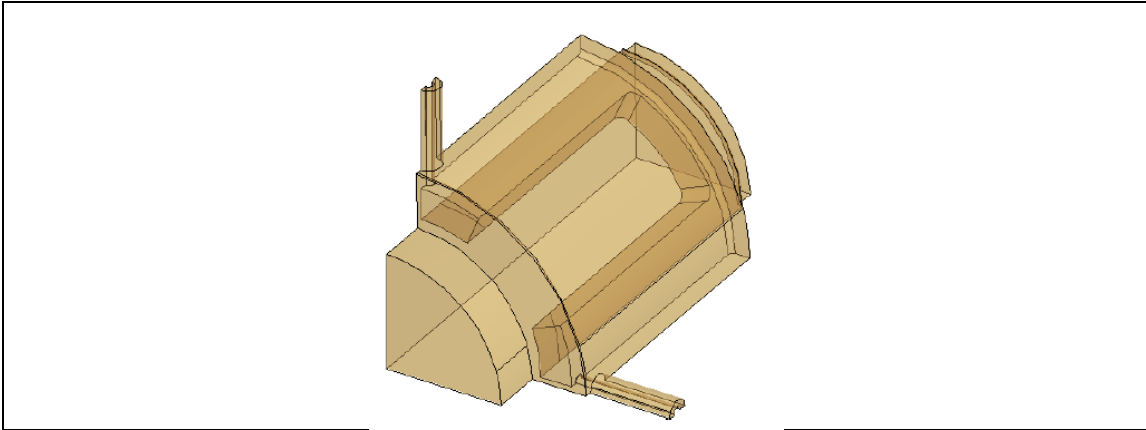
Figure 5: GdfidL model of Drive Beam BPM.
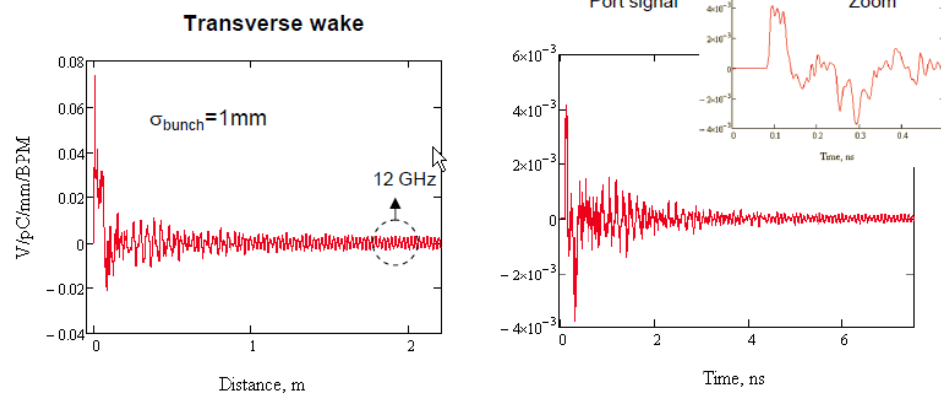
Figure 6: Undamped stripline BPM transverse wake and port signal.
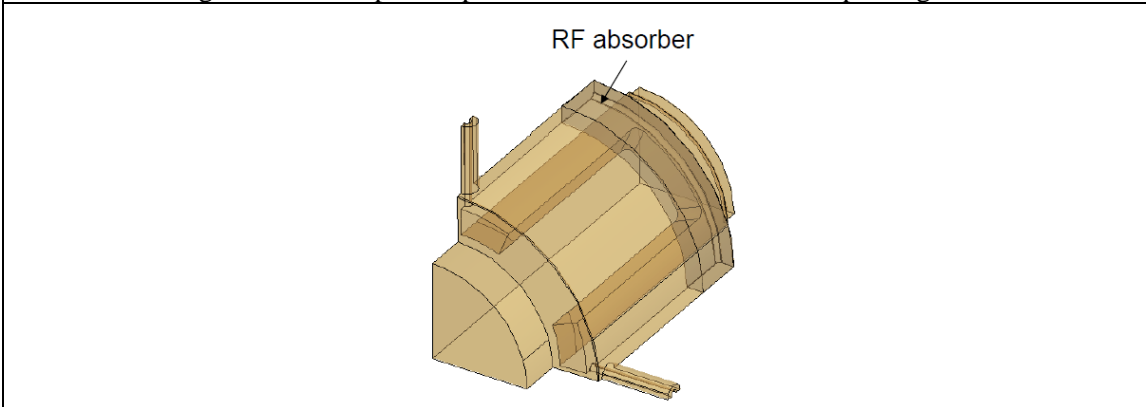
Figure 7: Drive Beam BPM with RF absorber added.
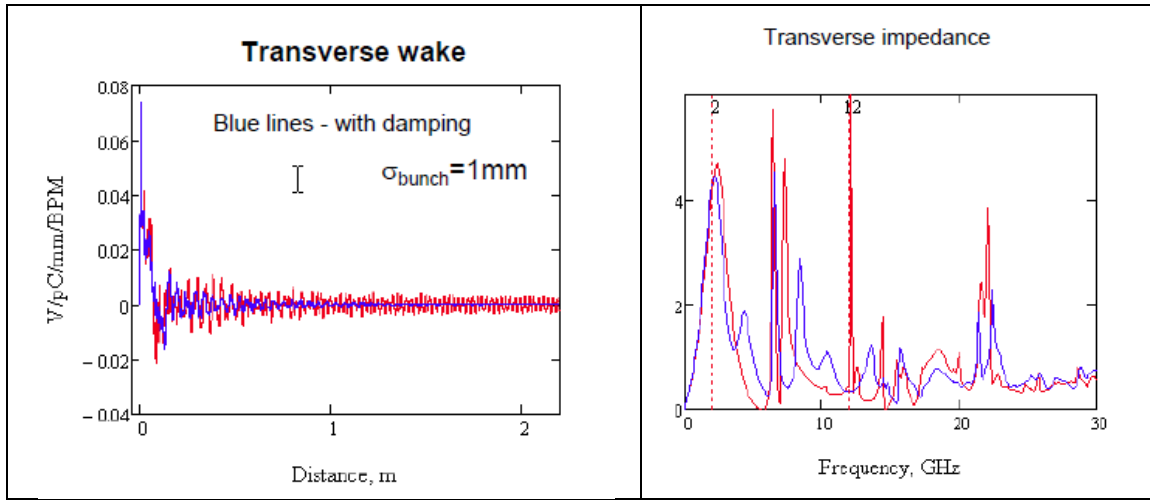
Figure 8: Transverse wake and transverse impedance of drive beam BPM. Undamped (red) and damped (blue). The damping material removes the narrow lines above the BPM processing frequency.

We then analyze the damped BPM design for beam response and wakes. We compare the time-domain analysis with an analytic model and find excellent agreement (see table 5). Transverse wakes are calculated for the analytical model from the beam voltages induced on the striplines, integrated over the number of bunches in the round-trip time of the stripline signal [vi].

Parameter	GdfidL	Analytic	Comments
Signal Amplitude	0.16 fJ	0.15 fJ	Signal energy for 1 pC single bunch, evaluated at 2 GHz in 100 MHz bandwidth
Transverse scale	0.146/mm	0.148/mm	Dipole/monopole sensitivity
Transverse wake	31 mV/pC/mm	27 mV/pC/mm	

Table 5: Comparison of GdfidL and analytic model of drive beam BPM response.

The bunch train longitudinal wake is obtained by convoluting the single bunch wake from GdfidL with the 12 GHz bunch fill pattern. The results are depicted on Figure 9. No coherent buildup of the wake over the train is observed.
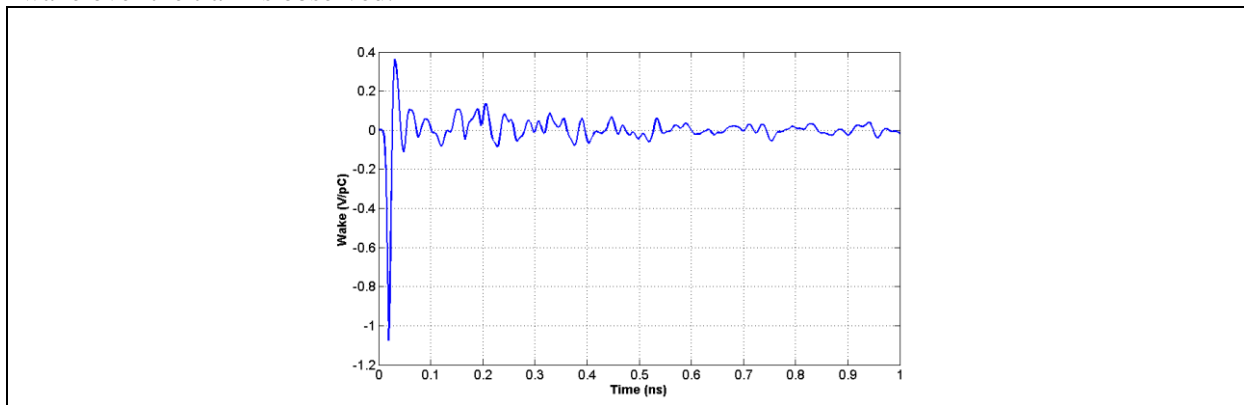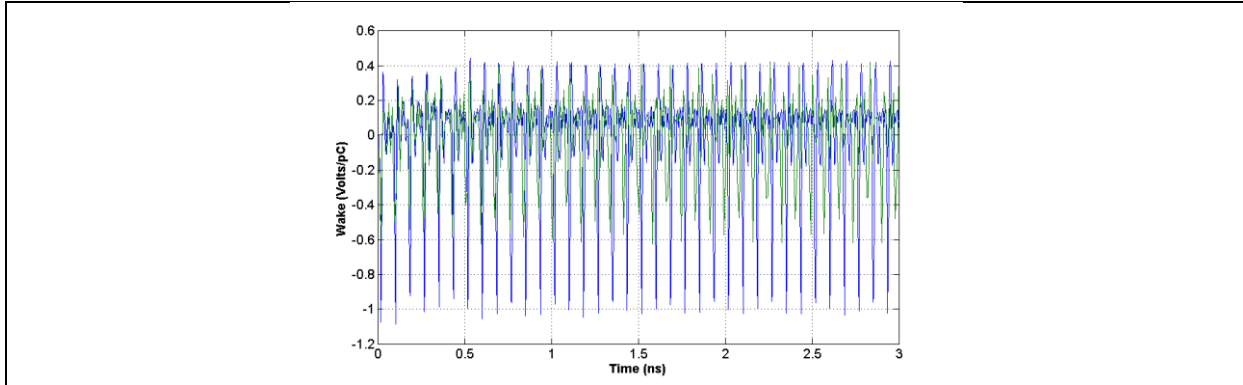
Figure 9: Single bunch and bunch train longitudinal wake calculated by GdfifL.

A prototype drive beam BPM will be tested in the lab in 2011, followed by beam tests of four units in CTF3.

5.7.2.5 Other BPMs: Drive Beam Transfer Line Example

The drive beam linac, its transfer lines and turnarounds and other beam systems require another 5000 BPMs with requirements less demanding than those of the main beam linac or drive beam decelerator. We plan to instrument these areas with slightly modified versions of the previous BPM systems. As an example we look at the one of the more challenging of these systems, the drive beam long transfer line BPMs, made challenging by the large beam duct diameter. Here we chose for the baseline design a button BPM with 6mm diameter buttons. Note that the presence of high frequencies in the beam bunch spectrum lead us to avoid large buttons due to the existence of narrow-band beam impedances at the TE11 mode resonance around the button edge at $F=c/\pi d$ for button diameter d. Choosing to process the signal in a 20 MHz bandwidth around a center frequency of 200 MHz, we find that we can meet the 10 micron resolution requirement for as few as a single bunch at nominal bunch charge.

Parameter	Value	Comments
Quantity	872	e^+ & e^- long transfer lines
Nominal current	100 Amp	
Bunch frequency	12 GHz	
Single bunch charge	8.3 nC	
Beam duct aperture	200 mm	
Position resolution	10 microns	
Temporal resolution	10 ns	
Accuracy	40 microns	Center wrt external fiducials

Table 6: Long Transfer lines BPM requirements

5.7.2.6 BPM Electronics

We plan to design three types of BPM processor to serve the various types of BPM. These have much in common; they are all based on maximizing the processing done digitally to take advantage of modern, high resolution, fast sampling ADCs. We minimize the amount of critical analog components, especially ones requiring critical matching. Online calibration is an important aspect of these designs.

At this point we base the designs on 16-bit, 160 Msample/sec ADCs, but the designs scale easily to faster sampling devices. The higher the sampling rate, the easier it is to meet requirements for analog

components, especially the large and potentially expensive analog filters in the signal paths. Digital filters are intrinsically matched; analog filters are difficult to match.

Processor Type	Freq	BW	Ultimate	Temp	Pickup	Qty
Cavity BPM	14 GHz	40 MHz	50 nm	10 ns	cavity	4800
Damping Ring	2 GHz	40 MHz	1µm	10 ns	button	1200
Direct sampling	2–500 MHz	40 MHz	1 µm	10 ns	Button/strip	48000

Table 7: Beam Position Monitor Processor Types

Cavity BPM Processor

A cavity BPM processor acquires 6 signals at 14 GHz, two each for X, Y and Reference channels. In principle we only need one each X, Y, & Ref channel for full reconstruction of the bunch train in X, Y and Z, but with two pickups processed per signal, we achieve redundancy. For convenience, and further redundancy, the six signals are spread across two mezzanine acquisition boards, either of which is able to provide full measurement capabilities to the required accuracy and resolution. The processing scheme (see Figure 10) consists of bandpass filters, programmable attenuation, downconversion, lowpass filtering, low-noise amplification, anti-alias filtering and the standard high-resolution ADC per channel. Further processing is performed digitally, including down-conversion from IF, digital filtering, normalizing to amplitude and phase of the Reference channel, phase rotation, real projection, scaling and offset compensation. A digital filter with bandwidth less than the analog bandwidth of the system is chosen since the band-limiting digital filters are exactly matched.

Each processing channel is capable of injecting a test tone into its cavity to verify operation of its complementary processing channel. The real calibration, to establish the phase and scale of the position signal may be done with beam.
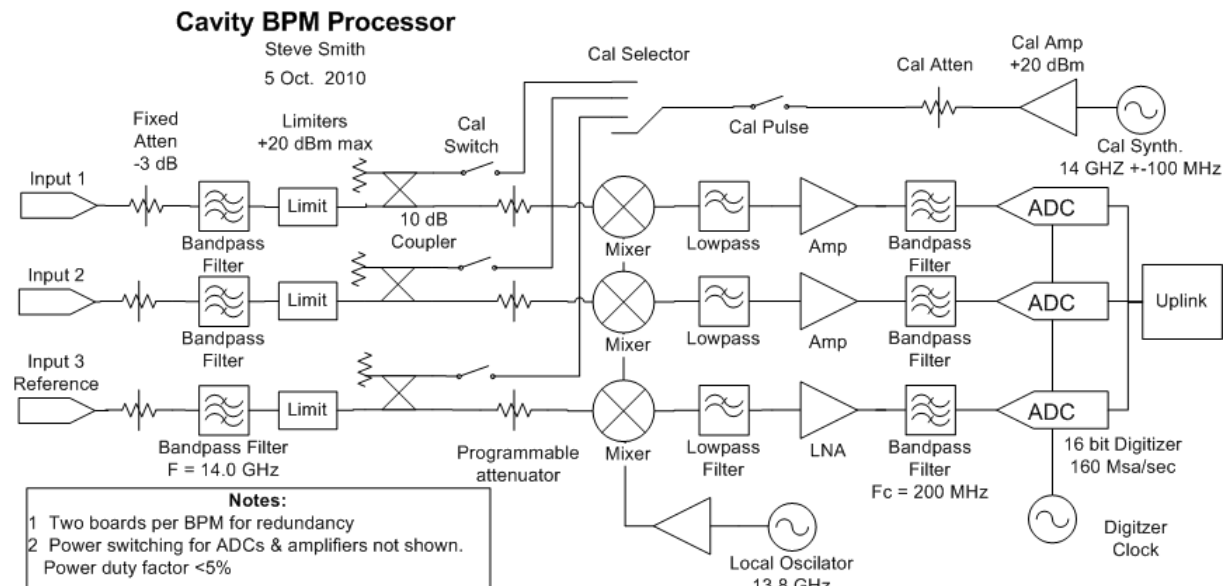
Figure 10: Cavity BPM Processor Mezzanine Card, two required per cavity BPM for redundancy.

The ADC is assumed to be at least as fast and accurate as the present Linear Technologies 16-bit, 160 Msamples/s LTC2209, with a low-power sleep mode suitable for <=5% duty factor at 50 Hz operation. At 160 Msamples/s, position can be reported in 6 ns intervals, though successive measurements at this rate are correlated due to rolloff from the processing bandwidth, probably about 20 MHz.

Button/Stripline Baseband BPM Processor

Used principally for the drive beam decelerator BPMs, this type of processor acquires 4 signals in a bandwidth of 2-200 MHz from a button or stripline BPM. The processing scheme (see Figure 11) consists of lowpass filters, programmable attenuation, low-noise amplification, anti-alias filtering and the standard high-resolution ADC per channel. Further processing is performed digitally, including digital filtering, amplitude estimation, and estimating position from $Y = R/2*\Delta/\Sigma$. Two of the input channels are capable of emitting a test tone to calibrate the gain ratio of the two adjoining channels via the inter-pickup coupling. The ADC is assumed to have the same performances as the ones chosen for the cavity BPM described previously.
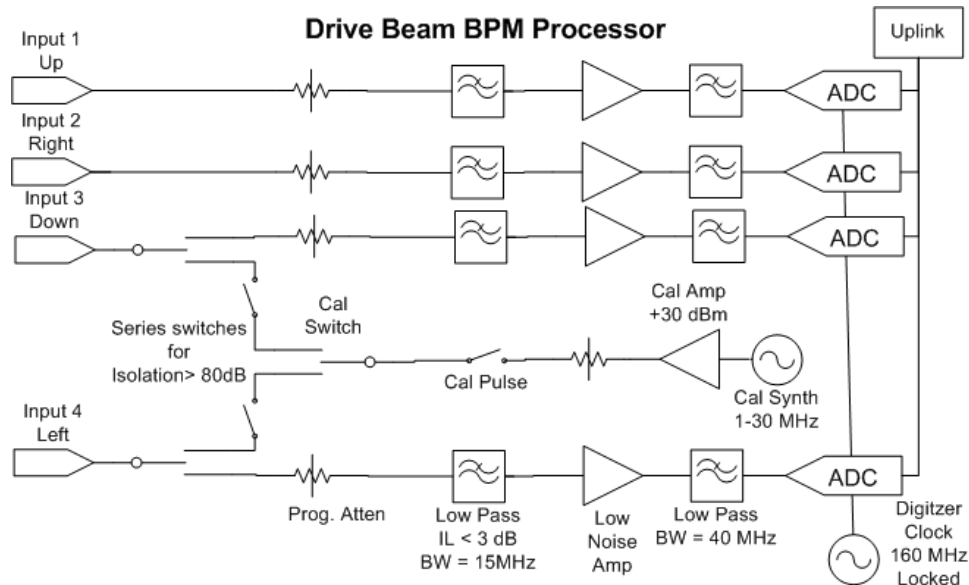
Figure 11: Baseband Button/Stripline BPM Processor mezzanine card.

Damping Ring BPM Processor

The damping ring processor looks very much like the Baseband Button/Stripline BPM processor with the addition of analog downconversion from 1 or 2 GHz to a finite IF before the digitizer. Nevertheless since it likely has many more operational modes and deeper turn memory, we expect a different implementation. There are commercially available electronics for ring BPMs that meet these needs. This will be further investigated in the technical design phase of the project.

5.7.2.7   Summary of BPM System baseline choice

A summary of the beam position monitoring systems is presented in table 8 and indicates our technology choice for the different parts of the accelerator complex. The choice for both the pick-up and the processing electronics are mentioned in the table, as well as laboratories where the devices could be tested.

Machine Sub-Systems	Quantity	Technology choice		Place to be Tested
		Pick-up	Processor	
Main Beam				
e⁻ & e⁺ injector Complex	83	Button 6mm	Baseband BPM	CERN
Pre-Damping rings	600	Button 6mm	DR type	Sync light sources
Damping rings	600	Button 6mm	DR type	ATF2
RTML	1424	Button 6mm	Baseband BPM	
Main Linac and Beam Delivery system	4796	14GHz Cavity BPM	Cavity type	ATF2

MDI & Post-collision Line	12	Button / Strip line	Baseband BPM	CERN
Drive Beam				
DB source and Linac	660	Button 6mm	Baseband BPM	CERN
Frequency multiplication complex	210	Button 6mm	Baseband BPM	CERN
Transfer to tunnel	872	Button 6mm	Baseband BPM	CERN
Turn-arounds	1920	Button 6mm	Baseband BPM	CERN
Decelerator	41484	Stripline 25mm	Baseband BPM	CERN
Dump lines	96	Stripline 25mm	Baseband BPM	CERN

Table 8: Beam Position Monitors by Region and Function

5.7.3   *Transverse Profile Measurements*

5.7.3.1   *Overview*

An overview of the requirements for transverse profile monitoring is shown in table 9. It presents the evolution of the normalized beam emittance through the CLIC complex with the corresponding expected spatial resolution and the number of devices requested. The beam energy is also indicated as it may influence the choice of detector technology. The typical charge densities are mentioned, as they will set an upper limit above which intercepting devices like screens or wire scanners would get damaged. For best thermal-resistant materials like C, Be or SIC, the limit corresponds to charge density of 10^6 nC/cm^2 [vii]. This number refers to the survival of material to single shot pulse, and does not take into account the heat dissipation effects that would need to be considered in the final design (repetition rate of the machine, cooling of the material).

In most cases, the measurement of the beam size serves directly to compute the transverse beam emittance. For ultra-relativistic beam energy, it is classically done using either the 4 profiles method [viii] or a quadrupolar scanning method [ix]. The first method relies on the use of several beam size monitors installed at different locations on the beamline and the emittance can be deduced using the nominal optic of the machine. The other method only requires one profile monitor, where the beam size is measured as a function of the strength of a focusing element. This latter method is obviously cheaper because only requires a single monitor but the beam optic needs to change accordingly, which may lead to unexpected beam losses. An alternative solution has been proposed and tested on the CTF2 [x] scanning five quadrupoles or more in such a way that the beam size stays constant at the profile monitor while the phase advance through the beam line changes.

Moreover the use of intercepting devices, like screens, degrade the beam emittance due to multiple scattering effects as the beam passes though the screen and for this reason it becomes safer to dump the beam afterwards. The best solution would then be to measure the beam emittance using 4-profiles method and non-intercepting devices, which in some cases is unfortunately not feasible.

Machine Sub-Systems	Emittance (nm.rad)	Energy (GeV)	Resolution (um)	Quantity	Charge density (nC/cm^2)
Main Beam					
e$^-$ source & pre-injector Complex	10^5	$\rightarrow$ 0.2	50	2	< 5 10^5
e$^+$ source & pre-injector Complex	93 10^5	$\rightarrow$ 0.2	50	4	< 5 10^5
Injector Linac (e$^-$/e$^+$)	1/93 10^5	$\rightarrow$ 2.86	50	2	< 5 10^5
Pre-Damping Rings (H/V)	63000/1500	2.86	50/10	4	**< 5 10^6**
Damping rings (H/V)	< 500/5	2.86	**10/1**	4	**< 5 10^8**
RTML	510/5	2.86 $\rightarrow$ 9	**10/1**	70	**< 5 10^8**
Main Linac	600/10	9	**10/1**	48	**< 5 10^8**

		→1500			
Beam Delivery System	660/20	1500	**10/1**	8	**< 5 10^8**
MDI & Post-collision Line	>660/20	< 1500	1000	6	< 5 10^3
Drive Beam					
Source and Linac	100	→ 2.37	50	10	**< 40 10^6**
Frequency Multiplication Complex	100	2.37	50	20	**< 40 10^6**
Transfer to Tunnel	100	2.37	50	2	**< 40 10^6**
Turn around	100	2.37	50	**96**	< 1.5 10^6
Decelerator	150	< 2.37	50	**576**	> 1.5 10^6
Dump lines	> 150	< 2.37	100	**96**	> 1.5 10^6

Table 9: Transverse beam size requirements

With a total number of required devices of 948, the measurements of transverse beam size is a becoming a very large system, corresponding to the 3 times the total number of such devices actually in use at CERN in the accelerator complex. Typical imaging systems used in CTF3 are presented in paragraph 5.7.3.2.

The nominal charge density available in most of the CLIC complex requires the development of non-intercepting devices, for both the Main and the Drive beams. It also implies that several detector technologies should be envisaged in order to cover the dynamic range required, starting with reduced charge during the commissioning period and increasing the charge up to the nominal beam conditions. This will be summarized in the paragraph 5.7.3.9, with the baseline technology choices.

The beam emittance is significantly reduced in the damping rings and the performances of transverse profile become extremely challenging from the damping rings till the end of the Beam delivery system, with a 1micron resolution. Several detection systems, which have already proven their capability to measure very small beam size are presented in paragraphs 5.7.3.3-4-5-6.

The special needs of the post-collision beam line and of the Drive Beam decelerators are discussed respectively in paragraphs 5.7.3.7 and 5.7.3.8.

5.7.3.2 *Bread and butter with Optical Transition radiation imaging system*

The spatial resolution of 50microns, as requested from the Main Beam source to the end of the injector linac, can be easily achieved using Optical Transition Radiation screens [xi] or Wire scanners [xii]. Moreover, the expected charge densities are still compatible with the use of standard and robust interceptive techniques. OTR screens provide images of the beam in a single shot, whereas Wire scanners only give beam profiles over several shots. However, wire scanners have the advantage of being less interceptive than screens, where the beam in normally required to be dumped afterwards. These technologies are used since 20-30 years and state of the art devices have even pushed the resolution limit down to few microns resolution [xiii,xiv].

A typical imaging system, as used on CTF3, is depicted in Figure 12. It is composed of a vacuum tank equipped with a motorized arm, capable of inserting two OTR screens with different reflectivity coefficients and a calibration target. Visible photons are emitted by the screen, reflected vertically downwards and focused onto a CCD camera using a radiation-hard lens. The light intensity is adjustable using a remotely controlled Optical density filter wheel. Lead shielding blocks are installed all around the camera to minimize radiation damage as much as possible.
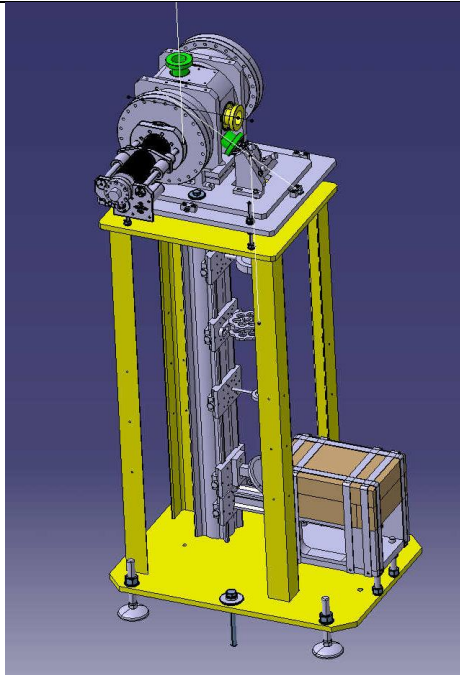
Figure 12: CTF3 OTR screen assembly

The major limitations for the use of OTR screen resides in the beam induced thermal load. As an example, the instantaneous temperature rise in thin graphite screen has been calculated as a function of beam energy and beam size for the case of the Main Beam and the Drive Beam. The results are shown on Figure 13 and clearly indicate that below 500um for the MB and 3mm for the DB screen cannot survive the full beam charge. This is a strong constraint, which can only be overcome by limiting the number of bunches or reducing the pulse train length.
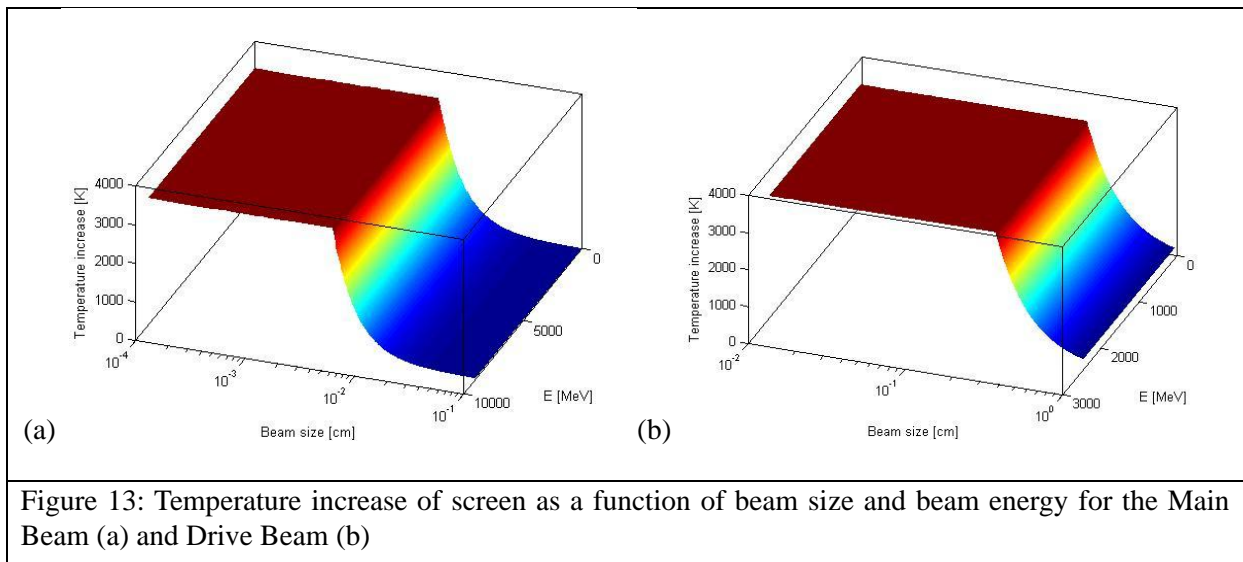
Figure 13: Temperature increase of screen as a function of beam size and beam energy for the Main Beam (a) and Drive Beam (b)

5.7.3.3 *Measuring small emittance in the PDR and DR*

CLIC would collide beams with nanometers beam size, which strongly relies on the generation of ultra-low emittance. Thus, the Main Beam emittance is reduced in two consecutives stages, in the Pre-Damping Ring and Damping Ring. Typical beam sizes shrink in consequence, putting very tight requirements on the spatial resolution of beam size monitors. Nevertheless, this problem has been studied in detail during the last 10 years either in the context of performance optimization of 3rd generation synchrotron light sources or in the framework of the ILC / CLIC studies with R&D

program performed to prove the feasibility of low emittance generation in damping rings. This work has led to the developments of several techniques, which can provide beam size measurements with resolution of the order of one micron. Two of them are based on the use of Synchrotron Radiation (SR) [xv]. For highly relativistic particles, the spatial resolution of SR imaging system is intrinsically limited by diffraction, which can be minimized by using shorter wavelength. To provide micron size resolution, imaging systems were further developed in the X-ray regime [xvi] [xvii]. Another innovative techniques has been proposed and successfully tested in PSI [xviii] based on the measurements of the Point Spread Function (PSF) on an imaging system. The beam size is not seen anymore as an image of the beam, but as a modulation of the PSF of a simple imaging system and sub-micron resolution have already been achieved. At ATF2 in KEK, very small beam profiles have been measured as well using a Laser Wire Scanner [xix]. The latter device is discussed in more details in the next paragraph.

5.7.3.4   *Micron-size resolution Transverse profile monitoring using Laser Wire Scanner*

The most critical issue for transverse profile monitoring has been identified since several years and refers to one-micron resolution beam size measurements in a linear part of the machine. In the CLIC complex, this type of device will be required from the exit of the Damping Ring to the Beam Delivery system. This covers more than 80kms of beam line and a total of more than 100 devices will be required. Contrary to the rings or turn-arounds, where synchrotron radiation could be envisaged as a natural source of light for instrumentation, there is no natural source of photons in a linear accelerator. And the use of intercepting devices must be restricted to single bunch mode to prevent any beam-induced damages as described previously in paragraph 5.7.3.2.

Basic principle of Laser wire scanner

Laser-wire systems employ a finely focused laser beam to scan across an electron beam to measure its transverse profile and thereby determine its emittance [xx]. Laser light is Compton scattered off the electron beam and either the scattered photons (or, at high electron beam energy, the scattered electrons) are detected downstream. Laser-wires are well suited for use at CLIC because they are relatively non-invasive devices that can be used continuously during machine operation and they can also be used for very high intensity beams, whereas solid wires would be destroyed. They can also be used for beam sizes approaching the wavelength of the laser-light. Typically light of wavelength 532 nm has been used to date, however shorter wavelength light has been used at SLC [xxi]. The interplay between laser-wire location and the corresponding technical requirements on the laser-wire systems, including Compton signal extraction, needs to be integrated into the beam-line design throughout the machine.

Existing Systems at Electron Machines

The state of the art at electron ring machines was achieved at the ATF [xxii] using a CW laser plus focusing cavity centered on the electron beam and at PETRA [xxiii], where a Q-switched injection-seeded laser is used. A schematic of the optical set-up is presented on Figure 14.

Both the ATF and PETRA systems measure the horizontal and vertical dimensions of the electron beam. The ATF system measured successfully electron beams of size 5.5 microns. The PETRA system measured electron beams of size of 48 microns, aiming at automation and turnkey operation; a single scan at PETRA takes less than one minute, limited by the laser repetition rate (20 Hz).
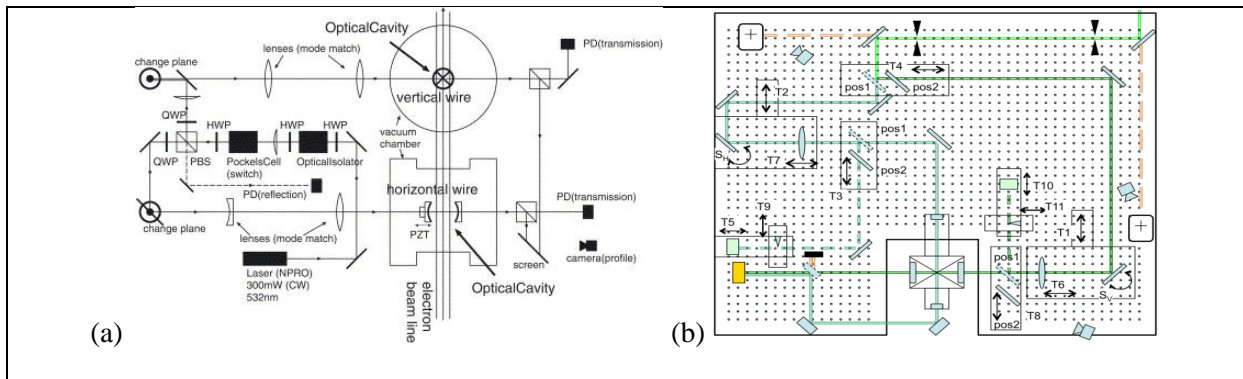
Figure 14: (a) Layout of the optical components of the ATF Damping ring laser-wire [xxii]; The symbols stand for photodiodes (PD), half-wave plate (HWP), quarter-wave plate (QWP), polarizing beam splitter (PBS), and piezo actuator (PZT). (b) Layout of the PETRA3 laser-wire system; in this system the vacuum chambers are fixed and the laser light is scanned from a vertically mounted optical table

Micron Scale Laser-wires

At the micron scales needed for some locations in CLIC (e.g. the BDS) systematic effects are very important, including uncertainties due to laser optical aberrations and the unknown horizontal size of the electron beam, which enters via a convolution with the laser intensity distribution at the focus.

Micron scale electron beams were measured at the ATF extraction line [xxiv] where beams of order 3 microns vertical size have been measured.

At the ATF2 laser wire, the laser is focused at the interaction point by a custom doublet lens of focal length 56.6 mm. The lens consists of three elements, the first two elements with curved surfaces and then a vacuum window, which is an integral part of the lens design. The first curved surface is aspheric to correct for spherical aberrations. All of the optical elements are made of fused silica to withstand both high laser power and a high radiation environment; the use of a single material has implications for the chromatic aberrations of the system, which in turn has implications for the spectral energy spread of the laser system. The lens also has a high damage threshold anti-reflective coating to prevent the formation of ghosts within the lens, which could destroy it. A full discussion is provided in [xxiv].

Ongoing R&D at ATF2 is concentrated on understanding these systematic effects and on pushing the measurement scale down to one micron or less. Other challenges include increasing the speed of scanning and the ease of turnkey operation; ongoing R&D at PETRA3 is addressing these aspects.
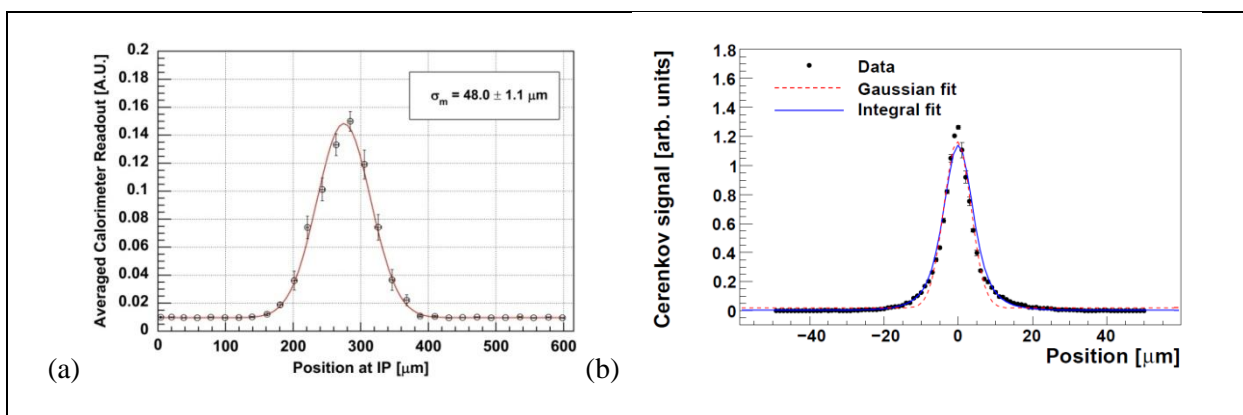
Figure 15: Vertical laser-wire scans. (a): PETRAIII [xxiii]. Right: ATF-Extraction line [xxiv] including a fit to a Gaussian and also an integral fit incorporating Rayleigh range effects. These affect the convoluted laser-wire scan shape as the Rayleigh range of the laser is comparable to the horizontal size of the electron beam and therefore the assumption that the laser size is the same across the whole

electron beam is no longer valid. However, it is difficult to disentangle this effect from aberrations of the laser or lens and requires careful modeling

Laser System

Additional challenges are presented by the laser-systems themselves; ongoing R&D [xxv] is centred on developing fibre lasers because of their many attractive properties which are important for laser-wire operation. To achieve the smallest beam size possible (limited by the optics and the laser wavelength), it is important that the spatial beam quality of the laser is as close as possible to a perfect Gaussian. This is measured by a quantity called the M^2 of the laser, where an M^2 of 1 is a perfect Gaussian and beams with poorer quality spatial output have higher M^2s. So that the focused spot of the laser is not limited by its spatial quality it is desirable to have an $M^2 < 1.1$. This can be difficult to achieve with high power solid state lasers (e.g. Nd:YAG), as thermal effects in the laser rod tend to distort the output mode. Optical fibres are waveguides, and if a single mode waveguide is used as a fibre laser the output will be very nearly perfectly Gaussian, at any level of amplification. For visible and near infrared light, a single mode fibre will be < 10 μm in diameter, which limits the amount of energy it would be possible to extract from the fibre. However, recently photonic crystal fibres have been developed [xxvi] which have a core surrounded by air holes that mean it is possible to have large diameter cores (up to 100 μm is possible) while still remaining single spatial mode, allowing the use of these fibres for high power applications.

For the laser-wire experiments at the ATF [xxiv] a pulse energy of 200 mJ and duration 400 ps (FWHM, so σ ~168 ps) was used, giving a peak power of 500 MW. However, the electron pulse duration was σ ~ 30 ps, so it would be possible to use a less energetic shorter pulse. Calculations have shown that a power of 10 MW (e.g. 50 μJ in 5 ps) should be acceptable for these experimental conditions, an energy achievable in fibre systems (although not at high repetition rates). Research is ongoing to produce energies greater than 100 mJ in the near infrared at repetition rates high enough for intra train scanning.

Pointing Stability

Fibres can also be made polarization maintaining, that is, the polarization state of the light out of the fibre is the same as that coupled in. This is important as the smallest achievable spot size depends on the laser wavelength and therefore it is preferable to work in the visible or UV regions. However, Er and Yb doped fibres lase in the near infrared (1.55 μm and 1 μm respectively) and so it is necessary to convert this output via harmonic generation to shorter wavelengths, which requires linearly polarized light.

Another advantage of fibre lasers is their efficiency. Continuous wave fibre lasers can have efficiencies (absorbed pump power to laser output) of 85%, which means that very little pump power is transferred to the fibre as heat and this, combined with the high surface area to volume ratio of fibres, means that they do not need active cooling which considerably reduces the complexity of the system and removes the need for circulating water. The pump diodes require water-cooling but as pump light can be delivered via fibre the pump diodes can be situated at a distance from the main fibre laser somewhere more accessible and easier to service.

In terms of pulse width, Yb doped fibres can support pulses down to 50fs [xxvii], which enables the use of very high peak powers for the laser-wire, which is important because the cross section for Compton scattering is small. This may also be useful as electron bunch durations become shorter.

Light Distribution

Depending on the type of laser employed for the laser-wire scanner, different approaches for light distribution to the interaction location have to be considered. Where the power of the laser exceeds 10 GW per pulse, or pulse duration falls below 100 fs, a vacuum piped transport system must be used; this is not expected to be necessary for CLIC laser-wire systems where, instead, simple pipes to

protect people from accidentally crossing the beam path should be sufficient. Laser transport can be achieved by expanding the beam to a large spot size and using mirrors to steer it from the laser room to the interaction region (final focus and scan location). Depending on the total distance and the laser power, optical components of different sizes might be used. For example, at the PETRA laser-wire, transport of the laser beam of approximately 10 MW power is achieved by expanding the laser beam to approximately 20 mm diameter by a Galilean telescope with output lens aperture of 2". Mirrors of 2" diameter are sufficiently large to accommodate the beam without diffraction effects.

The Rayleigh range for a perfect Gaussian laser mode ($M^2 = 1$) with 20 mm diameter is about 600 m. According to the propagation equation of a Gaussian beam [xxviii] within 100 m propagation the size of the laser changes by only ±1.5%. In real conditions, when $M^2 > 1$, the same collimation of the laser beam can be achieved on a reduced distance. For the case of the laser employed at PETRA, $M^2 = 2.6$ and the maximum distance with a variation of the size within 1.5% reduces to approximately 40 m. A cost estimate for such system is around 6 k€. For longer transport distances, collimated beams must be expanded to larger sizes therefore optics of 3 to 4 inches diameters must be used. The costs of optics scale almost as D^2 (being D the diameter of the optical element).

The last case to consider is that of a laser with power < 100 kW. This includes a configuration where a master mode-locked oscillator, synchronized to the accelerator, is transported to different locations to be successively amplified by a local amplifier. In this case it would be possible to transport the laser using 100s of meters of optical fibers thus making the transport line practically alignment-free. Moreover, costs are drastically reduced due to the diminished number of necessary optical elements.

Scanning Systems

The scanning system at the ATF DR employs motors to move the vacuum chamber, to which the laser final focus system is fixed. A similar moving system is employed at the ATF2, where the laser final focus lens is fixed to the vacuum vessel in order to know precisely the relative position of the laser waist with respect to the beam position. The scanning system at PETRA3 has two modes; one where the laser final focus lens systems are moved using stepper motors using a feedback readout system and the other employing a tilted mirror driven by a piezo stack; both stepping modes have intrinsic step resolution better than 1 micron. The scanning range of the stepping motor mode is 25 mm, with a 500 ms overhead for stepping the stages; combining this with the 20 Hz repetition rate of the laser and using 20 steps for a scan, with 5 shots per step = (5 × 50ms + 500ms) × 20 = 15s for a complete scan. The piezo driven mode has a scanning range of the order of 1 mm and, after moving the stages into place, can perform a scan with 20 steps and 5 shots per step in 5 × 50ms × 20 = 5s.

By employing a mode-locked laser system that is locked to the inter-bunch spacing, significantly faster scan rates could be achieved and this would be necessary in order to determine the beam size train by train in some locations in CLIC. Potential solutions involving electro-optic scanning systems have been explored [xxix]; it may be possible to test this system, which should be capable of scanning at a laser repetition frequency of 130 kHz, at PETRA3.

Electron Bunch Jitter

Transverse position jitter between bunches (and, depending on the scanning scheme, trains of bunches) will add in quadrature to the laser-wire scan and must be subtracted [xx] either from an overall average, or bunch-by-bunch using information from BPMs. Preliminary simulations [xxx] of wakefield effects in the ILC linac have indicated that wakefields do not seem to affect significantly the Gaussian nature of ILC bunches, but do affect their centroid positions early in the train. Similar studies need to be performed for CLIC.

Laser Wire Scanner at very high energy

All the LWS developments and tests are actually performed on electrons of few GeV's. Some extrapolations of the laser wire scanner properties are discussed below. The behaviour at high energy of the Compton cross-section and the corresponding characteristics of the scattered photons and

degraded electrons, are particularly important to define the best detection scheme [xix]. Figure 16 shows how the Compton scattering cross-section changes with beam energy. Above 1GeV, the cross-section starts decreasing and for 50GeV electrons it has been already reduced by a factor 2. At CLIC top energy, the initial value is dropped by one order of magnitude. Even if it is not major issue, this must be taken into account in the design of the final system, adapting the laser power accordingly to still provide a decent signal to be detected. Moreover, at very high energies, the cross-section for electron-positron pair creation is increasing and must be taken into account as well.

Figure 16: Evolution of the Compton Scattering cross-section as a function of the electron beam energy. The value is normalized to the Thomson cross-section. The calculation assumes a 266nm wavelength laser and a 90degree collision angle between the laser and the particles.
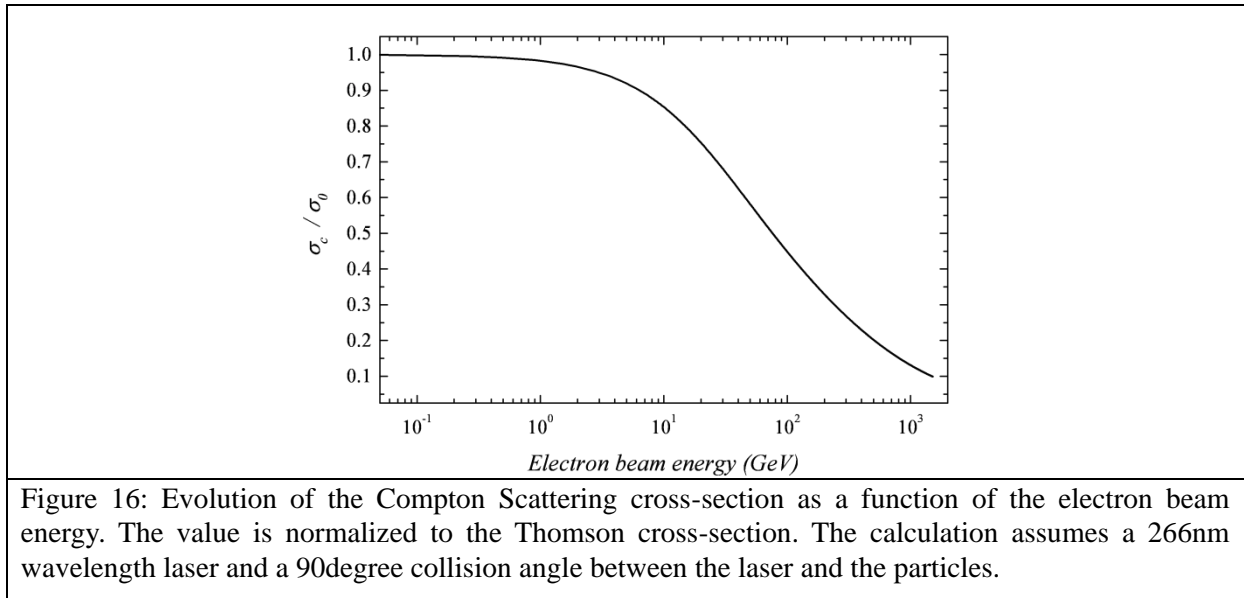
Signal Detection

The properties of the scattered photons and degraded electrons depend on the electron beam energy as depicted respectively in Figures 17 and 18.
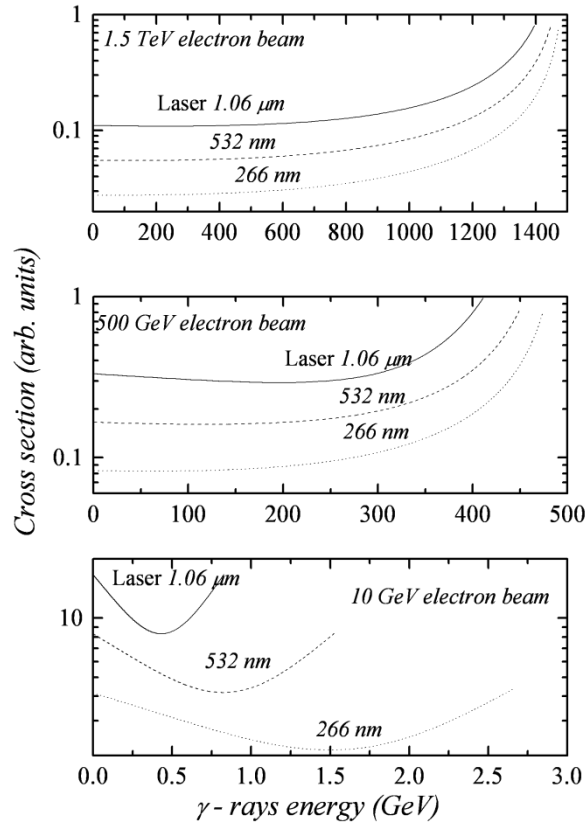
Figure 17: Energy spectrum of the scattered photons assuming 1.5TeV (a) 500GeV (b) and 10GeV (c) incident electron energy and three different laser wavelength (1060, 532 266nm)

At very high energies, the initial electron energy is mostly converted into the emission of a high-energy γ-ray and the scattered particles are left with only a small fraction of its initial energy. The scattered photon spectrum peaks on the highest energy photons. Moreover, the photon's spectrum, which remains fairly broad for electron beams of moderate energy, gets sharply peaked around the highest energy as the electron beam energy increases. In linear collider, detecting these high-energy photons is a real concern, particularly difficult because most of the photons flux is emitted in a small angle inversely proportional to the electron energy. At energies close to 1TeV, this cone angle becomes smaller than one µrad. Along a linac, their measurement becomes unpractical and would require deviating the initial electron beam in order to insert the detector. On the contrary, the measurement of the degraded electrons could be simpler. Their energy spectrum is relatively independent of the initial electron beam energy (see Figure 18) and, at very high energy the energy difference between the main beam and the scattered particle is large enough to design an efficient detection scheme.
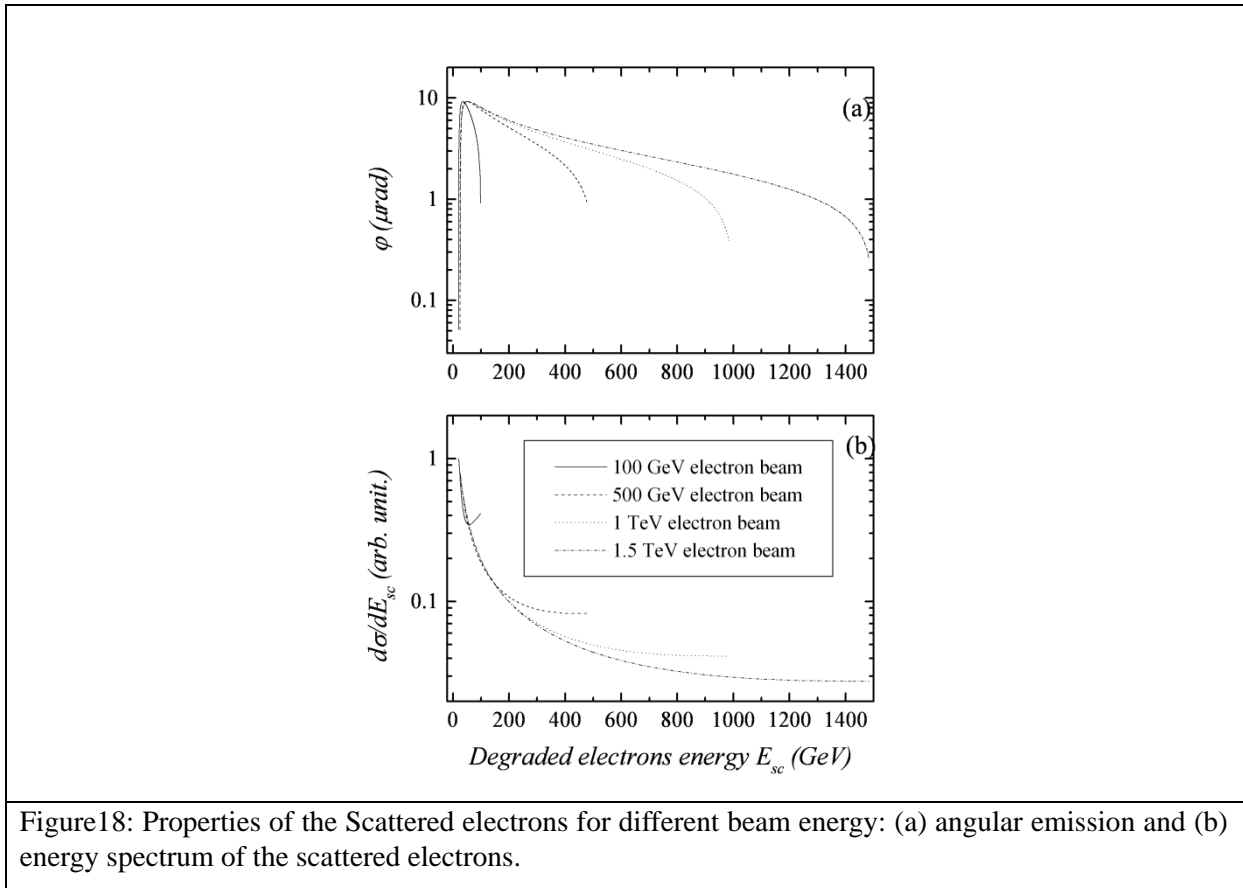
Figure18: Properties of the Scattered electrons for different beam energy: (a) angular emission and (b) energy spectrum of the scattered electrons.

For light of wavelength 532nm, the energy loss of the electron beam is insignificant (< 5%) for electron beam energies less than about 2GeV and for the CLIC drive beam (2.4GeV) the maximum energy loss is 6%. Below this approximate energy, the Compton signal must be detected via the scattered photons, and in order to do this, a magnetic field is necessary to separate them from the main electron beam. At energies above this level, the scattered electrons can be measured because they will be over-focused by downstream quadrupoles, however the energy spread of these scattered electrons is large and so they will leave the main beam at widely different locations, making efficient detection difficult. Full simulation of a laser-wire system for the ILC was performed in [xxxi] where it was shown that it would preferable to locate laser-wire after a large bend downstream of the linac in order to reduce linac-related backgrounds

At the ATF and PETRA, the scattered Compton photons are detected by a crystal calorimeter (scintillation crystals attached to a photomultiplier), respectively CsI crystals at ATF (extraction line and DR systems) and lead tungstate crystals at PETRA. A Cherenkov detector was also employed at the ATF extraction line to verify that there were no systematic differences from the crystal detectors. A system based on Cherenkov detector is useful in order to differentiate the signal from synchrotron related backgrounds; such a system can also be located in difficult to access positions in the beam-line, with the Cherenkov light directed to photomultipliers situated well away from the beam-line. Such a system is currently under test at the ATF2.

Laser Wire Scanner in the BDS

The implementation of the 4 laser wire scanners foreseen in the CLIC BDS is shown in Figure 19. They are distributed along the diagnostic section over some hundred's of meters.
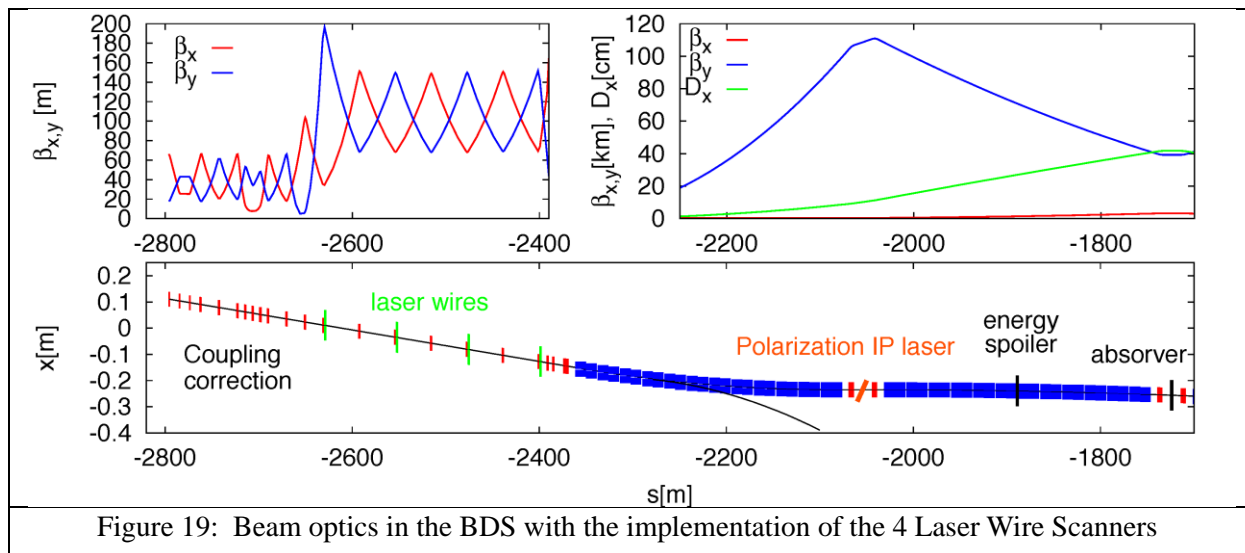
Figure 19: Beam optics in the BDS with the implementation of the 4 Laser Wire Scanners

The detection of scattered electrons (photons) is foreseen to be integrated in the first dipoles of the energy collimation area as indicated on Figure 20.
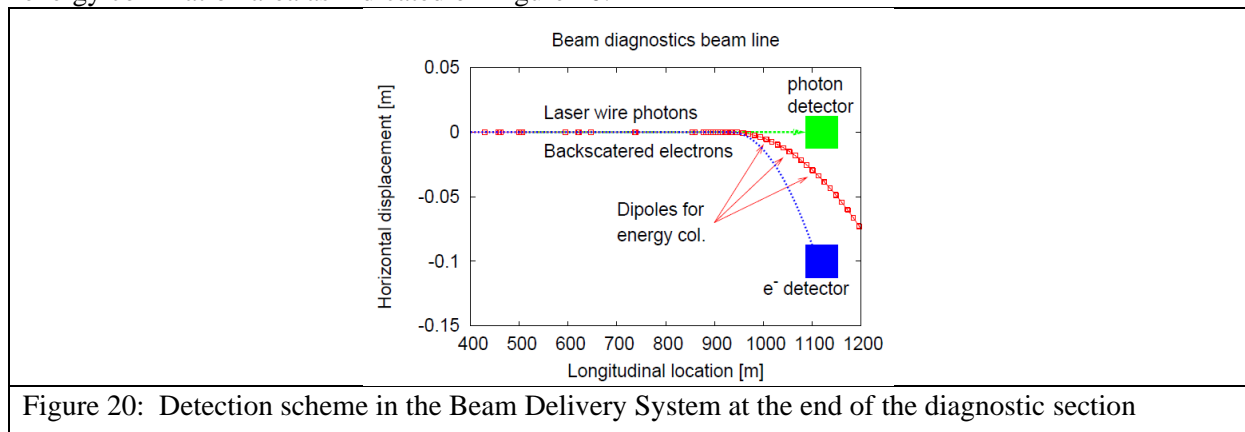
Figure 20: Detection scheme in the Beam Delivery System at the end of the diagnostic section

5.7.3.5 *High Resolution transverse profile measurement using OTR*

Spatial resolution better than one micron have been recently measured by observing the beam size contribution to the Point Spread Function (PSF) of a standard OTR imaging system [xxxii]. Originally the PSF is an image generated by a point-like source and projected by an optical system on a detector (e.g. CCD camera). The source is provided by optical transition radiation from a conductive target. The PSF must bear information about the source structure, the optical system, and the distribution of electrons (the beam size). It was predicted that the source is non-uniform, but has a minimum in the centre. The width of the PSF (as well as the sensitivity to the transverse beam size) is defined by the optical system, but the visibility is determined by the beam size. A typical vertical polarization component of OTR PSF measured at ATF2 is shown in Fig. 21(left) [xxxii]. Fig. 21(right) was measured for three different beam sizes. A clear sensitivity to a micrometer beam is observed. Nevertheless, additional investigations and systematic measurements are required to optimize the optical system and light density on a CCD and to convert the current system into a "turn-key" device.
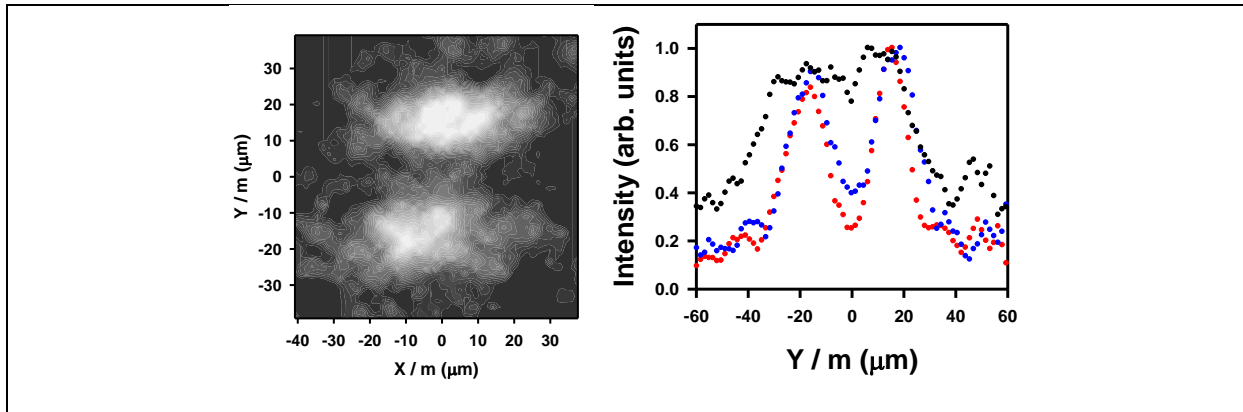
Figure 21: High-resolution beam size measurement using OTR PSF technique (m is the magnification factor and X and Y are the CCD coordinates). Left - typical OTF PSF vertical polarisation component; Right - projected OTR PSF measured for three vertical beam sizes: SAD predictions are σ = 7.2um (black), σ = 3.4um (blue), and σ = 1.7um (red).

Of course, thermal limitations linked to the use of an intercepting device remain true in this case and would most likely limit this technique to single bunch observation or low intensity beams.

5.7.3.6   *Diffraction radiation as a non-invasive beam size measurements*

Diffraction Radiation (DR) appears when a relativistic charged particle (typically an electron) moves in the vicinity of a medium (a target) with impact parameter (the shortest distance between the target and the particle trajectory) as depicted on Figure 22. The electric field of the particle interacts with the target atoms polarizing them. The polarized atoms oscillate emitting radiation known as DR with a very broad spectrum. The spatial-spectral properties of the radiation are very sensitive to a very broad range of electron beam parameters. However, the energy loss due to the process is so small that the electron parameters remain nearly the same as the initial ones. It makes it possible to develop non-invasive diagnostics tools.
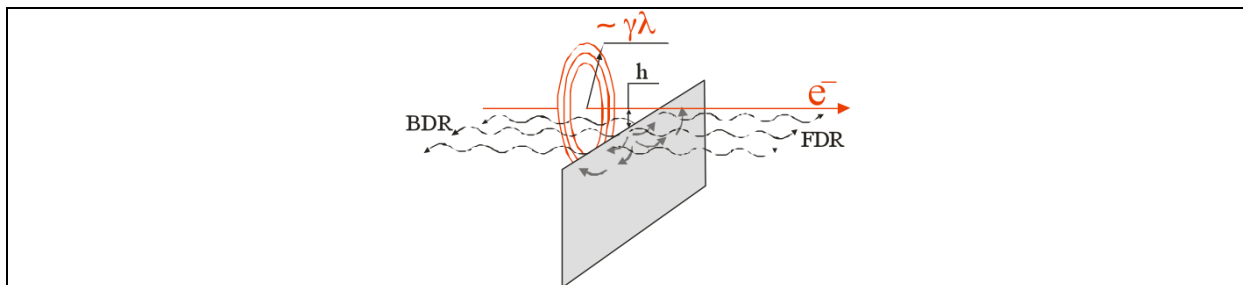
Figure 22: Principle of Diffraction Radiation Generation

DR in optical wavelength range (ODR) was applied for transverse beam parameter monitoring at ATF@KEK [xxxiii], FLASH@DESY [xxxiv] and APS@ANL [xxxv]. Since 2000 the properties of ODR from a slit target [xxxvi] were investigated as a possible tool for high-resolution non-invasive transverse beam size measurement (see Fig. 23 left). Fig. 23 right represents a typical ODR vertical polarization component measured with a CCD camera at KEK-ATF.
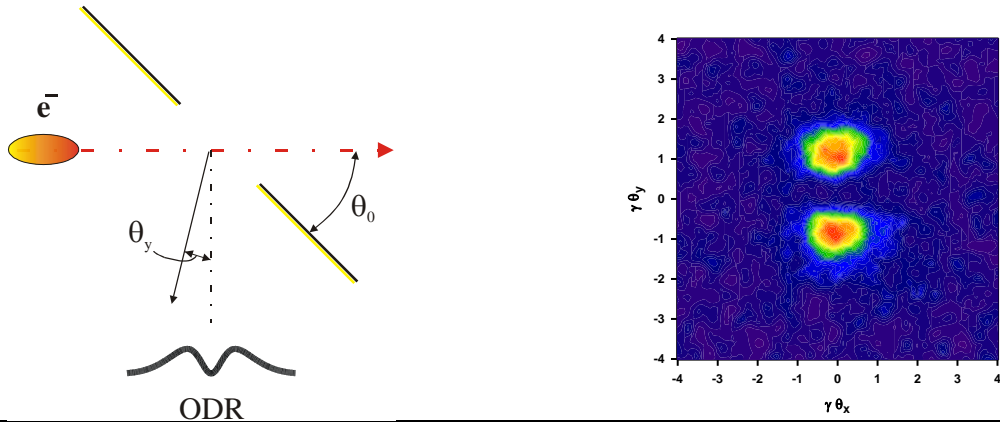
Figure 23: Scheme of ODR generation from a slit target (left), Typical ODR vertical polarization component measured with a CCD camera

The visibility of the ODR pattern was measured on ATF2, compared with the simulated data and the beam size was determined. The comparison between the wire scanner and the ODR measurement is represented in Figure 24. The achieved sensitivity to the beam size was as small as 13μm.

$$\sigma_{ODR} = \sqrt{a_0^2 + \sigma_{WS}^2}$$
$$a_0 = 12.7 \pm 1.0$$
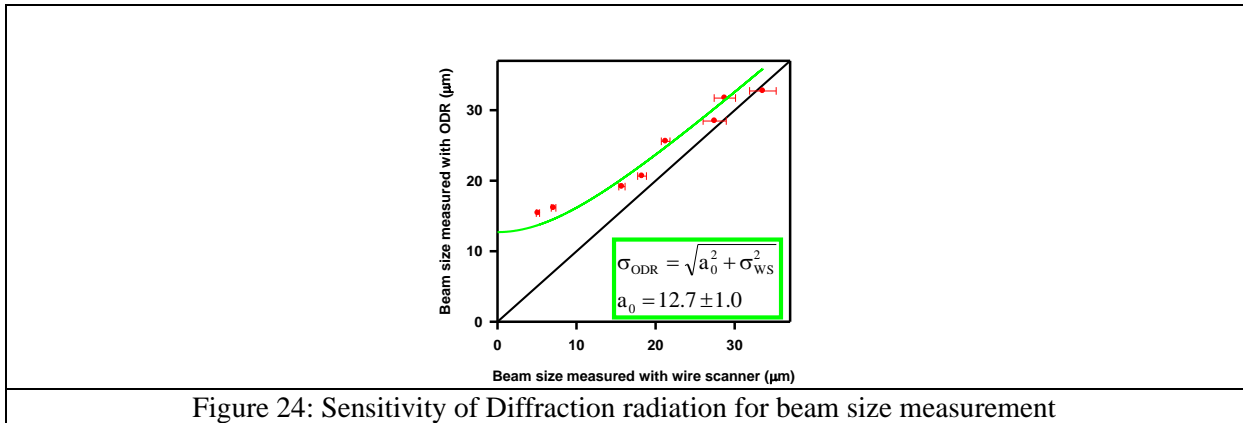
Figure 24: Sensitivity of Diffraction radiation for beam size measurement

The resolution of the current system was defined by the diffraction limit, system configuration (like the precision of the slit geometry and alignment), non-optimal measurement system, as well as by the residual contribution from synchrotron radiation (SR). To be able to achieve the resolution smaller than 10 μm, an upgrade of such a system should be followed up measuring DR in EUV or X-ray spectral-range. An experimental validation of such a scheme has been proposed during the next years on the CESR-TA ring at Cornell/USA.

5.7.3.7   *Transverse profile monitoring in the Post-collision line*

After the collisions, the beam is finally dumped. A set of beam imaging system is foreseen along the line to make sure the beam is steered and diluted correctly over the dumps. These systems do not require a high resolution since the beam in the dump line is growing in size to few millimeters at minimum.

Typical beam footprints on the entrance window of the water dump are shown in Figure 25 for non-colliding and colliding beams. The typical beam size is as big as few millimeters for non-colliding beams and increases up to several centimeters in the vertical axis for largely disrupted beams.
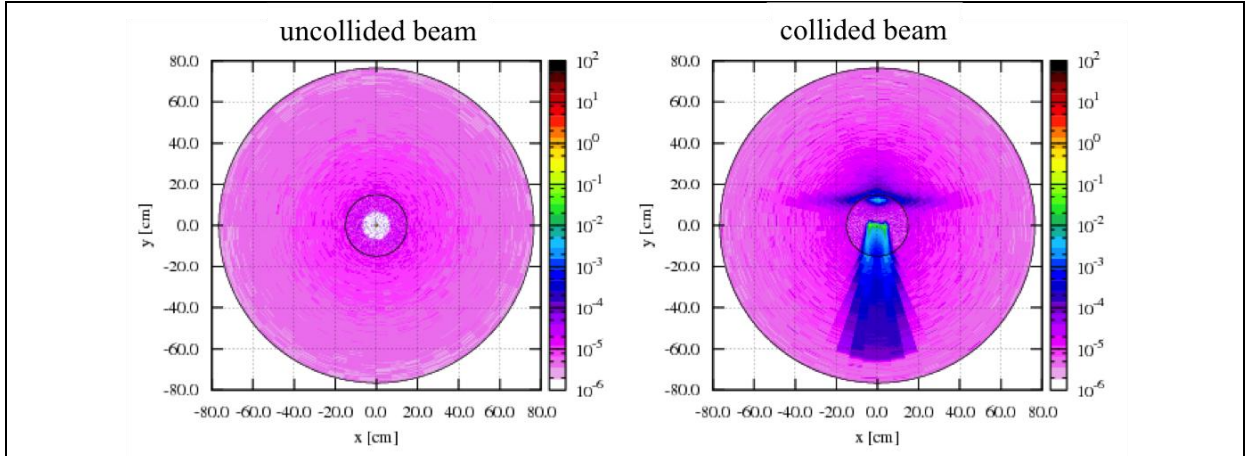
Figure 25: Beam footprint on the water-dump entrance window. 1mm thick 30cm diameter Titanium window. Non-collided beam deposits 4.3 J/cm^3 compared to only 0.13J/cm^3 once the beam is colliding (~ 6.3W). The two different vertical spots visible on the entrance window during collisions correspond to the beamstrahlung photons (up) and the disrupted beam (below).

The total diameter of the screen should be as large as 30cm. Similar screens with 60cm diameter have been already developed for the LHC beam dumping system [xxxvii] and do not represent any critical issues.

5.7.3.8   Imaging systems for the high-energy spread beam in the Drive Beam Decelerator

The beam intensity reaches up to 100A in the CLIC Drive Beam complex and especially in the decelerator. With such large intensities, the impedance of the beam line must be kept as low as possible to avoid instabilities and resonances, potentially degrading the beam quality. Thus a replacement chamber has been incorporated in the mechanical design of such OTR tank in such a way that the beam propagates in constant beam pipe when the screens are not used. Such an assembly is depicted in Figure 26 with the replacement chamber is red.
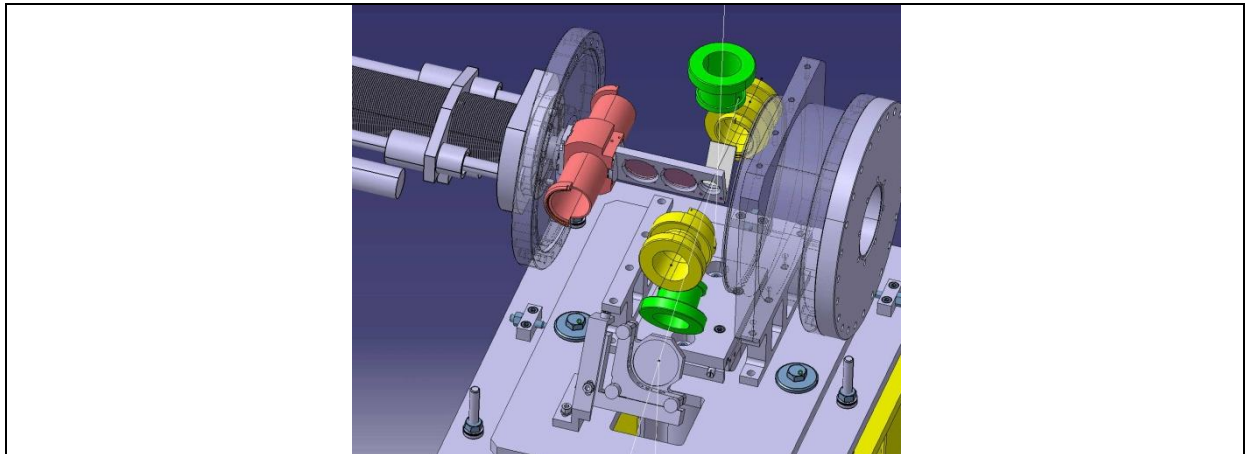
Figure 26: CTF3 OTR vacuum vessel and its replacement chamber

Optical Transition Radiators provide a very reliable source with a total number of photons per proton in the wavelength range [λ_a, λ_b] given by:

$$N_{OTR} = \frac{2\alpha R}{\pi} \left[\left(\beta + \frac{1}{\beta} \right) \cdot \ln \left(\frac{1+\beta}{1-\beta} \right) - 2 \right] \ln \left(\frac{\lambda_b}{\lambda_a} \right)$$

with α the fine structure constant, β the proton velocity, γ the relativistic factor and R the optical reflectivity of the screen.

At the end of the decelerator, the beam is characterized by a large transverse size and a very high energy spread. Following the equation mentioned just before, the OTR photon yield and the cone angle of emitted light present a not negligible dependency on the beam energy as depicted in Figure 27. In the case of the CLIC decelerator, it leads to a factor 2 difference in light intensity emitted by electrons of low and high energy. Full simulations including the efficiency of the optical system should be done to estimate the errors in imaging such beams with OTR.

Several decades of research on ceramic phosphors at CERN [xxxviii] and at other laboratories has led to the extensive use of doped alumina ceramic screens, i.e., Al_2O_3:Cr^{3+}, for accelerator beam observation. Alumina (type AF995 [xxxix]) is doped with 0.5% chrome sesquioxide and at room temperature two principal lines of luminescence at 692.9 and 694.3 nm are generated with a decay time of 3.4ms [xl]. These screens are also compatible with ultrahigh vacuum systems, they exhibit good response linearity, and their radiation resistance is high. For example, in tests made at CERN, screens have withstood integrated relativistic proton fluxes of up to 10^{20} protons/cm^2.

The energy dependence of both a carbon OTR screen and chromium-doped alumina is presented in Table 10. The number of photons generated by the Al2O3 screen is proportional to the deposited energy inside the screen. The photon yield mentioned for alumina is expressed in photon per MeV of deposited energy and does not change strongly in the typical energy range of the CLIC decelerator. Moreover, the number of photons generated by luminescence is much higher than the OTR photons. For high-energy particles, alumina has shown sensitivities starting for 10^7-10^8 protons [xli] when observed with a normal CCD camera. Even if the melting point for alumina is 2000°C, one should not use it with temperature higher than 1650°C.

Screen	OTR Carbon	Al_2O_3:Cr^{3+}
Density (g/cm^3)	1.7	3.96
Specific heat (J/gK)	0.7-2.4	1.09
Melting point (^{o}C)	3527	2000
Light directivity	0.07mrad	isotropic
Photons yield	10^{-2} (ph/p$^+$)	10^4 (ph/MeV)

Table 10: OTR and luminescent screen parameters
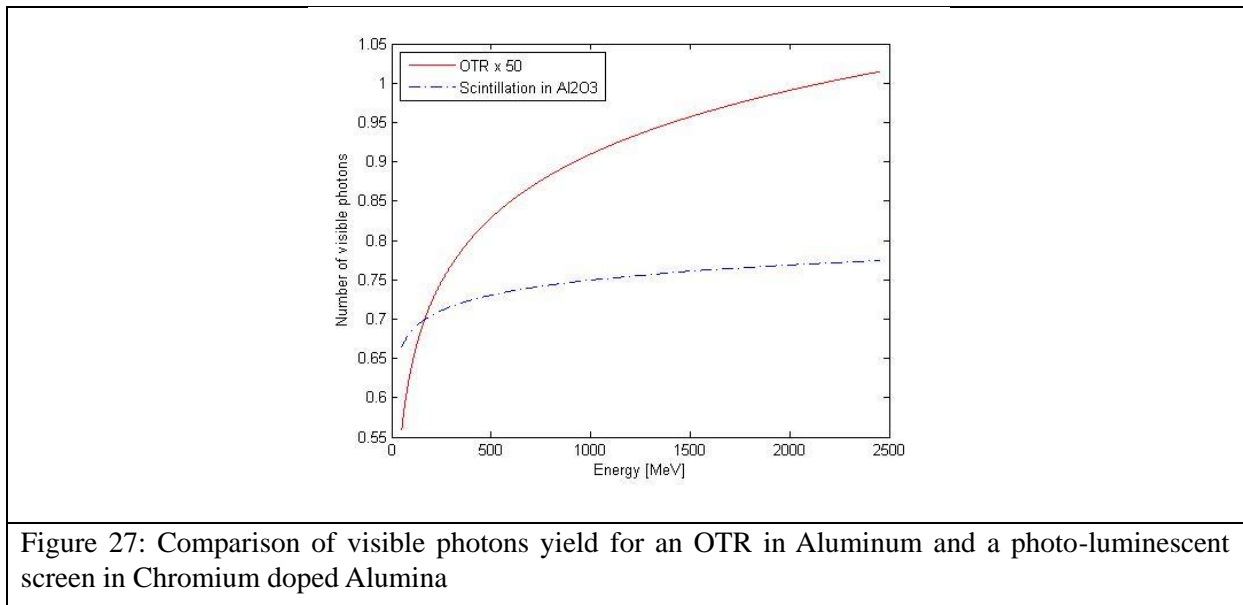
Figure 27: Comparison of visible photons yield for an OTR in Aluminum and a photo-luminescent screen in Chromium doped Alumina

5.7.3.9 *Summary of CLIC Transverse profile monitor*

A summary of the transverse profile monitoring systems is presented in Table 11 and indicates what would be the technology choice for the different part of the accelerator complex. It gives baseline

scenario, where existing developments are mature enough to fulfill the requirements. In many cases, there are two technologies mentioned, as required to cover the full dynamic range of beam intensities.

Machine Sub-Systems	Quantity	Technology choice		Place to be Tested
		Baseline	Alternatives	
Main Beam				
e⁻ & e⁺ injector Complex	10	OTR		CERN
Pre-Damping and Damping rings	8	XSR	LWS / OSR-PSF	SLS, PETRA, Soleil, Diamond,..
RTML	70	OTR	OTR/OSR PSF	ATF2
		LWS	XDR	CESR-TA
Main Linac and Beam Delivery system	56	OTR	OTR-PSF	ATF2
		LWS	XDR	CESR-TA
Post-collision Line	6	OTR	Scintillating screens	CERN
Drive Beam				
DB source and Linac	10	OTR / LWS	ODR	FEL's
Frequency multiplication complex	20	OSR/XSR	XSR	SLS, PETRA, Soleil, Diamond,..
Transfer to tunnel	2	OTR / LWS	ODR	FEL's
Turn-arounds	96	OSR	XSR	SLS, PETRA, Soleil, Diamond,..
Decelerator and Dump lines	672	OTR	Scintillating screens	CERN

Table 11: Transverse beam size monitors: Color code – Feasibility under investigation / Feasibility proven / CLIC design

   Alternative solutions are indicated as well, if they exist. They would correspond to better technologies in term of performance or cost but would need further R&D to prove their feasibility in the case of CLIC beams. For information, the places where such technologies could be tested are mentioned in the last column.

5.7.4   Longitudinal Profile Measurements

5.7.4.1   Overview

An overview of the specifications for longitudinal profile monitors is given in Table 12. It presents the evolution of the bunch length and spacing all along the CLIC complex with the expected time resolution and the number of devices requested. Similarly to transverse profile monitoring, the typical charge density is quoted in the table and highlights the preference for non-intercepting devices as soon as this value gets higher than 10^6 nC/cm^2. The time resolution mentioned in the table is specified for both bunch and train length, the latter value expressing the needs to measure the evolution of the bunch length along the pulse duration. Several diagnostic techniques can be envisaged at the moment to measure the longitudinal behavior of the beam with high resolution. Four of them are actually considered to cover the CLIC requirements as non-interceptive devices: Streak camera using optical radiation [xlii], Measurements of the frequency spectrum of Coherent radiation, power spectrum of the direct electro-magnetic field of the particles and electro-optical techniques using short laser pulses [xliii]. These techniques should then be classified depending on their expected performances either in terms of resolution but also on their capacity to fully resolved the longitudinal beam profile (^{P}) or simply provide an R.M.S bunch length (^{L}). It is generally agreed that in locations like bunch

compressors where the bunch length is modified on purpose, the tuning of the system would require the full knowledge of the longitudinal profile, which can only be measured using expensive and complex system. The evolution the bunch length in straight sections could be done only using an R.M.S value, hopefully performed using simpler and cheaper devices.

Machine Sub-Systems	Bunch length (mm)	Energy (GeV)	Resolution Bunch (ps)/Train (ns)	Quantity	Charge density (nC/cm^2)
Main Beam					
e$^-$ injector Complex	5	→ 0.2	2 / 10	3 ^{P}	< 5 10^5
e$^+$ injector Complex	11	→ 0.2	5 / 10	5 ^{P}	< 5 10^5
Injector Linac (e$^-$/e$^+$)	1 / 5	→ 2.86	0.5 /10	2 ^{P}	< 5 10^5
Pre-Damping Rings (H/V)	5	2.86	2 / 10	2 ^{P}	< 5 10^6
Damping rings (H/V)	1.5	2.86	0.5 /10	2 ^{P}	< 5 10^8
RTML - Bunch compressors 1 - Booster Linac - Transfer lines - Turn arounds - Bunch compressor 2	 **0.300** **0.300** **0.300** **0.044**	 2.86 2.86 → 9 9 9 9	 **0.1 /10** **0.1 / 10** **0.1 / 10** **0.02 / 10**	 4 ^{P} 0 4 4 ^{P}	**< 5 10^8**
Main Linac	**0.044**	9 →1500	**0.02 / 10**	**48^L**	< 5 10^8
Beam Delivery System	**0.044**	1500	**0.02 / 10**	2 ^{P}	**< 5 10^8**
Drive Beam					
Source and Linac	4 / 0.5	→ 2.37	1 / 10	8	**< 40 10^6**
Frequency Multiplication - Delay Loops - TL1 - Combiner ring 1 - TL2 - Combiner ring 2 - TL3	length (mm)/Spacing (GHz) **2 / 0.5** **2 / 1** **2 / 3** **2 / 3** **2 / 12** **2 / 12**	2.37	1 / 10	 6 2 2 2 2 2	**< 40 10^6**
Transfer to Tunnel	2 / 12	2.37	1 / 10	4	**< 40 10^6**
Turn arounds - Bunch Compressor 1 - Turn-arounds - Bunch Compressor 2	 **2 / 12** **1.4 / 12** **1 / 12**	2.37	**0.5 / 10**	 96 ^{P} 0 96 ^{P}	< 1.5 10^6
Decelerator	1 /12	< 2.37	**0.5 / 10**	48 ^{L}	> 1.5 10^6
Dump lines	1 / 12	< 2.37	**0.5 / 10**	48 ^{L}	> 1.5 10^6

Table 12: Longitudinal beam profile requirements

The bunch length is manipulated several times along the complex. The way positrons are generated induces that they would have a longer bunch length than the electron roughly by a factor 2 (see paragraph 3.1). Nevertheless on the Main Beam from the source to the end of the damping ring the bunch length is never shorter than 1ps and can be measured with a resolution better than 500ps using optical photons emitted either from SR in the rings or TR in straight sections and state of the art Streak

Cameras [xliv] and. This would also satisfy most of the requirements on the Drive Beam side. An example of a bunch length measurement using the streak camera in CTF3 is shown in Figure 28.
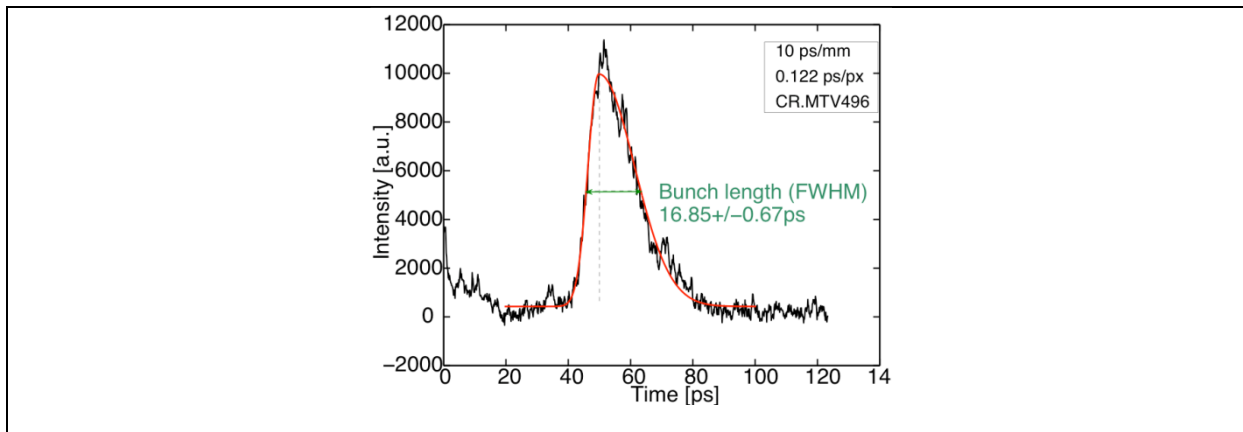
Figure 28: An example of the CTF3 single bunch spectrum measured with the streak camera using synchrotron light from the Combiner Ring
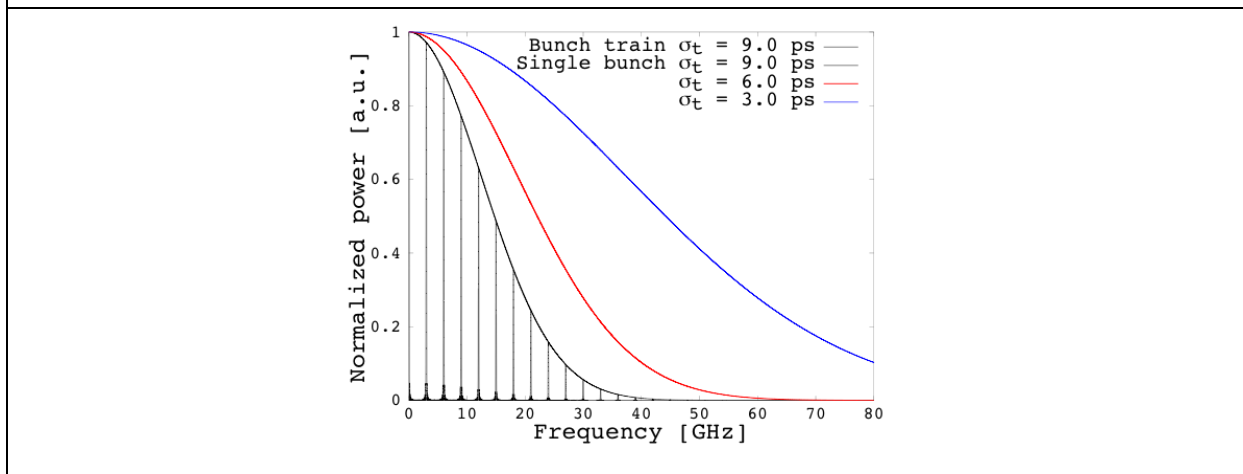
Figure 29: Power spectrum for a train of Gaussian bunches, with r.m.s. bunch length $\sigma_t = 9$ps and separated by $\tau = 333.3$ ps (black) and the single bunch envelope for $\sigma_t = 9$ps (black), $\sigma_t = 6$ps (red) and $\sigma_t = 3$ps (blue).

Although streak cameras can provide an accurate single shot measurement of a single bunch profile, they cannot measure in a single shot the evolution of the bunch length over the full pulse train length. RF devices measuring the beam power spectrum at high frequency, see Figure 29, would then cover this requirement. Such systems have been developed at CTF2 [xlv], CTF3 [xlvi, xlvii] and elsewhere, based on either diode a power measurement using diodes, or down-mixing techniques where more sensitivity is required. The choice of operational frequency, f_{op}, of the detector depends on the required bunch length dynamic range needing to be covered and should be chosen to be $f_{op}= 1/(2\pi\sigma_b)$ to obtain the highest sensitivity, where, f_{op} is in GHz, and σ_b is in femtoseconds. Although there is in principle no limit to the bunch length that these devices can measure, D-band waveguide based RF detectors are the highest frequencies currently used for this type of measurement and hence put a recommendation on the sensitivity reach to about 0.09 mm (300 fs). RF based detectors should be installed close to a streak camera for an initial calibration, and once calibrated can be used as online monitoring tool of the bunch length, if the bunch shape is known, or of the form factor, see Figures 30 and 31.
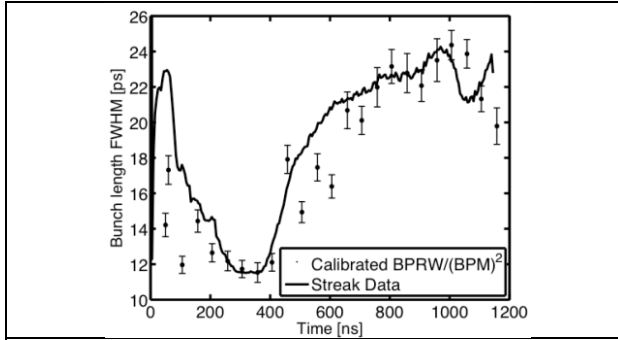
| Figure 30: Bunch Length measurement comparing a calibrated BPRW and the Streak Camera measurement in CTF3. | Figure 31: Examples of calibrated 33 and 39 GHz RF pickup signals in CTF3 compared to Streak Data. |
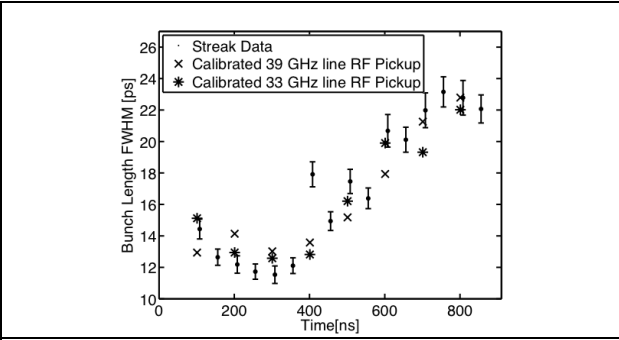
For areas of the machine where the bunch length is shorter than 0.15 mm, alternate techniques to the RF pickup should be investigated, as described in more details in the following paragraphs.

5.7.4.2 20femtosconds time resolution Longitudinal Profile monitor

Table 12 shows that for the Main Beam the most stringent requirements for bunch profile measurement occur at bunch compressor BC2 and downstream from BC2. The requirement is to measure the detailed longitudinal profile of the 44μm (150 fs) rms bunch with a resolution of 6 μm (20 fs) rms, at high charge density. A full knowledge of the bunch profile is desired rather than just a moment of the bunch distribution, and the measurement must be totally non-intercepting. The optimum solution to this problem is electro-optic measurement of the bunch Coulomb field, which can yield very reliable results at CLIC parameters of energy, charge and emittance.

Principle of Operation

Electro-optic and related techniques have proved to be extremely promising for the measurement of electron beam longitudinal profiles where the ultra-short electron bunches have structure in the range from picoseconds down to tens of femtoseconds (and indeed below). The principle of electro-optic longitudinal diagnostics (see Figure 32) is to accurately measure the temporal profile of the Coulomb field of the extreme relativistic electron beam, without intercepting the beam itself, through optical non-linearities induced in an electro-optic crystal within the electron beam line. The crystal is placed adjacent to the electron beam, but the beam does not traverse the crystal, making this a completely non-intercepting technique. The Coulomb field sweeping through the appropriately chosen crystal renders the material birefringent during the field transit; this birefringence is probed by a chirped (or sometimes ultra short) optical probe laser pulse that is passed through the crystal parallel to the electron beam axis, and in synchronism with the electron bunch.

Once the probe laser beam has interacted with the electron (or positron) bunch, the bunch is then extracted from the beamline. The resulting time-varying rotation of the polarization of the optical pulse can then be sensitively detected using all-optical techniques to yield a temporal (or longitudinal) evolution of the Coulomb field, which itself is a measure of the charge density longitudinal profile within the bunch.
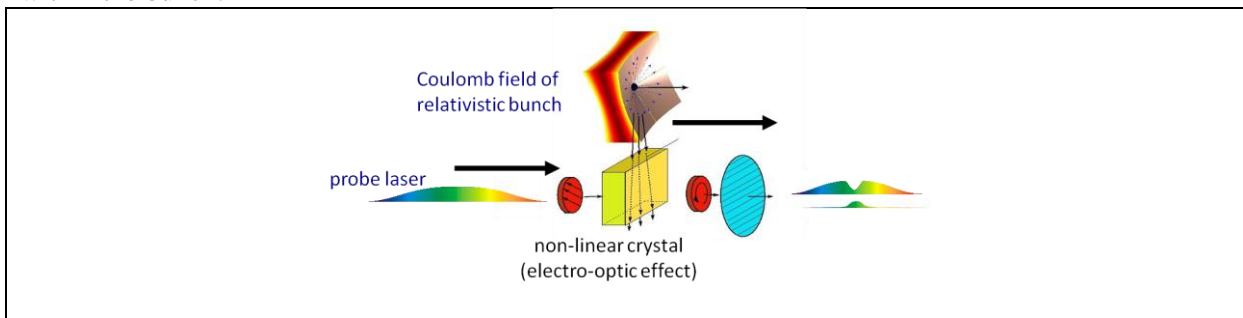
Figure 32: Principle of operation of electro-optic detection

There are a number of different ways of implementing this general principle that have been applied to single shot electron beam diagnostics, each with its own particular merits. We discuss each of the demonstrated techniques briefly, before a more detailed discussion of the preferred (baseline) choice for CLIC high resolution profile monitoring. It is useful in discussing the capabilities to separate the effects of the non-linear laser-electron beam interaction (the encoding process), and the readout of the optical information (the decoding of the temporal information).

Demonstrated time-explicit single-shot EO techniques

Three techniques of EO longitudinal diagnostics have been demonstrated in accelerator experiments, spectral decoding (SD) [xlviii], Spatial Encoding [xlix], and Temporal Decoding [l] (see Figure 33). Of these, SD and TD have been most extensively developed and demonstrated.

In all techniques, the encoding of the bunch profile is via the Coulomb field at a radially offset distance. This introduces a time resolution limit through the relativistic angular spread of the Coulomb field, which dictates the faithfulness of the Coulomb field temporal profile as a measure of the bunch charge density profile. This limit, with $\Delta t_{res} \sim 2R/c\gamma$, can be ignored for multi-GeV and TeV electron beams. Note that the same limit applies to any technique reliant on the temporal structure of Coulomb field at a radially offset position, such as in coherent diffraction radiation techniques.

Figure 33: Schematic of different EO techniques. In both Spectral Decoding and Temporal an ultrashort laser pulse is chirped before injection into the accelerator and interaction with the electron beam. In TD, the encoded information is retrieved by optical cross-correlation with a synchronized ultrashort pulse. In Spatial Encoding, an ultrashort pulse is used for the beam-interaction, with the cross-correlation integral to the geometry of the interaction region.

Spectral decoding: While SD is the simplest, and most widely implemented, technique it is fundamentally limited in its time resolution through the readout process. While the precise value of the time resolution limit will depend on the laser parameters in a given implementation, in practice the resolution will always be $\Delta t_{res} > 1ps$. We therefore do not discuss this technique further here, other than to note that with further developments by e.g. FEL facilities, this technique may become a feasible alternative for certain streak camera diagnostics.

Spatial encoding: In SE an ultrashort laser pulse with a large (~5mm) transverse beam size interacts with the Coulomb field pulse in a non-collinear geometry. This arrangement leads to a time-space mapping of the EO interaction, as different transverse parts of the probe arrive at the EO crystal with different time delays. Through imaging of the probe beam, and use of polarization optics to convert the EO interaction into an optical intensity variation, it becomes possible to read out the effect of the EO interaction as a function of time. Spatial encoding has been demonstrated at the FFTB (SLAC) [xlix], and at FLASH (DESY) [li], with observed temporal signals of ~300fs and ~100fs respectively.

In both of these implementations a contribution to the limited time resolution can be attributed to the complex fibre-optic ultrashort optical pulse transport required for their specific implementations, but which is not inherent to the technique itself. In the FLASH example, the limitations expected from the encoding process (as will be described below) were being approached. SE has a significant advantage over TD, in that the low pulse energies available from commercial ultrafast laser oscillator systems are sufficient. This follows from the fact that the decoding process is linear in laser intensity. The limitations arise from i) the encoding process, which will be broadly similar to all the other techniques, and (ii) the pulse duration of the probe pulse. In practical implementations this second constraint restricts the ultimate time resolution to an estimated $\Delta t_{res} > 50$ fs.

Temporal decoding: In TD, the ultrafast optical beam is split into two separate beams, a probe and a gate. The probe is stretched to a pulse length of ~20ps, typically by passing through a grating pair. This stretched pulse samples the bunch-induced birefringence in the electro-optic crystal, and the stretched duration sets the time window for the measurement. The decoding process is through an optical cross correlation measurement, where the gate beam serves as a short-pulse reference. The cross-correlator produces a time-space mapping in a similar way to that described for SE.

The stretched probe pulse is *focused* on to the electro-optic crystal inside the accelerator beam pipe at the measurement location – the measurement of the Coulomb field is done at a specific point, rather than an extended region as in SE. The phase retardation induced in the crystal by the bunch field is translated into an intensity modulation on the stretched pulse by passing it through an arrangement of polarisers. This encoded intensity is then cross-correlated with the short pulse in a β-Barium Borate (BBO) crystal. The non-collinear nature of the cross correlation geometry provides a mapping of time to spatial position in the BBO crystal and the CCD [lii], as shown schematically in fig 34. The use of a time-space mapping for the decoding avoids the limitation seen in SD. However, it comes at the expense of requiring significantly higher laser pulse energies for the non-linear decoding process. The probe laser typically used for TD has been a 1kHz repetition rate amplified Ti:S laser with pulse length ~30 fs, wavelength 800 nm and pulse energy >1 mJ.

Figure 34: Shortest measured electron bunch profile (at DESY FLASH).
The optimum fitted Gaussian curve sigma is 79.3 ± 7.5 fs.
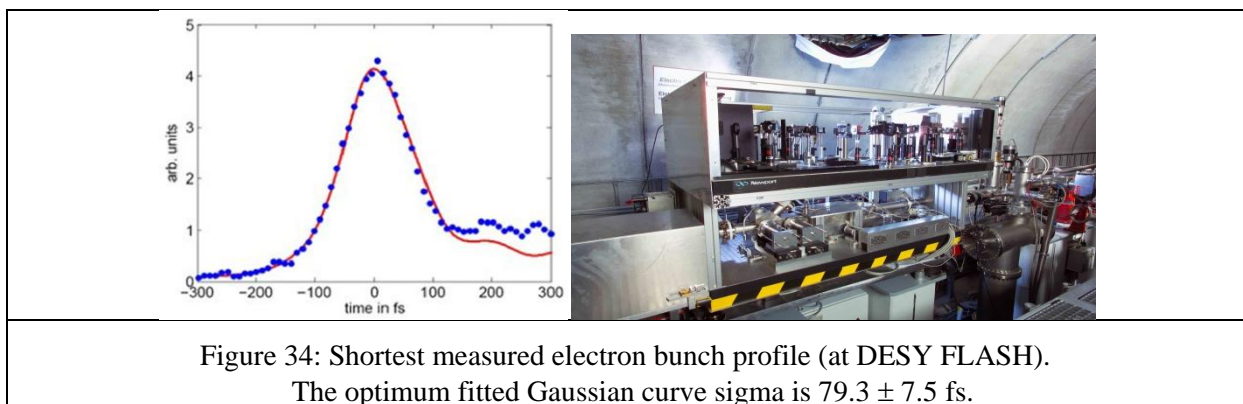
In experiments undertaken at FLASH, single-shot TD has been demonstrated with time resolution of 120fs FWHM (~60fs rms). The same campaign of measurements was also able to successfully benchmark the EO-determined profile against transverse deflecting cavity measurements. A scheme for in-situ absolute time calibration of the diagnostic, through effectively recording two snapshots of the same electron bunch with known 1-20ps time delay between snapshots, was also demonstrated. The high time resolution measurements were near the limit of the gate pulse duration, but were principally restricted by the temporal limits of the encoding process. To minimize the encoding limit, a very thin 65μm thick GaP crystal was used. To achieve the improved ~20fs time resolution for CLIC, it will be necessary to improve on both the encoding and the decoding capability.

Both SE and TD (in the form described above) may reasonably be expected to have similar time resolution capabilities. Both require a short gate pulse or probe pulse for the time-space mapping, and both have similar encoding limitations. However, the use of an optical cross-correlator, albeit with the additional requirement for high pulse energies, opens up the potential to exploit established ultrafast optical characterization processes such as Frequency Resolved Optical Gating (FROG) or its many

variants. In the following "FROG" is taken to refer to this general class of ultrafast measurement techniques, rather than a specific implementation. In a FROG measurement the temporal profile of a cross-correlation is obtained, together with the spectra (of the cross-correlation) as a function of time. This two-dimension time-frequency information can then be deconvolved to provide temporal information on a time resolution shorter than that of any individual pulse in the cross-correlation. It is this capability that is routinely applied in autocorrelation-FROG characterization of sub-10fs optical pulses, with information obtained at a resolution shorter than the optical pulse. In the context of CLIC diagnostics, it is proposed that TD, enhanced with FROG capability, will allow the optical characterization to deliver the desired 20fs resolution.

Electro-optic materials and temporal resolution

There are temporal resolution limitations that arise from the EO crystal response. These limitations are often best summarized as a detection frequency cut-off, rather than directly as a temporal resolution. For example, for a 0.2 mm thick ZnTe crystal electric field Fourier components with a frequency lower than 2.8 THz are detected with minimal distortion, while higher frequency Fourier components are detected with reduced efficiencies. For a 0.2 mm thick GaP crystal, Fourier components up to about 8 THz are detected with minimal distortion.

The EO material response curves are strongly dependent on the material, and on the material thickness. The two materials ZnTe and GaP, shown in Figure 35 are the most common used in EO diagnostics, and in electro-optic THz spectroscopy. The cutoff shown at ~5THz and 9THz, respectively, can be described as arising from a propagation phase mismatch between the probe laser and the Coulomb field propagating within the material; for thinner crystals the relative mismatch is reduced, giving rise to the higher cutoff. However, this comes advantage comes simultaneously with a reduction of signal magnitude. For even vanishingly thin crystals a cutoff in the response will remain, arising from the rapid change in refractive index of the material for frequencies approaching the optical phonon resonances. An ideal detection material would be free from such resonances and response cutoffs, and have a near uniform response from 0-20THz or higher. Alternative EO materials exist that have both large EO coefficients and a response curve that can include frequencies up to 20THz or higher (e.g. DAST, GaSe). However, the response for a fixed crystal orientation and Coulomb field - laser geometry does not span the full bandwidth; the crystal orientation can be chosen to provide a broad response centered at a given frequency. To achieve the full bandwidth required for 20fs rms resolution diagnostics, it is proposed that a detector comprising multiple crystals, of different orientation or material, is used to provide a small set (2-3) of simultaneous measurements. These measurements will then be `spliced' into a single faithful temporal profile of the beam; we note that the algorithms necessary for this splicing of explicit temporal information remain to be developed and tested. The `splicing of time-implicit spectral information from spectral upconversion measurements should be straightforward. A single laser system, and single beam-interaction assembly, is envisaged for the multiple-crystal detection, and should not add significantly to the system complexity over that of a single-crystal arrangement.
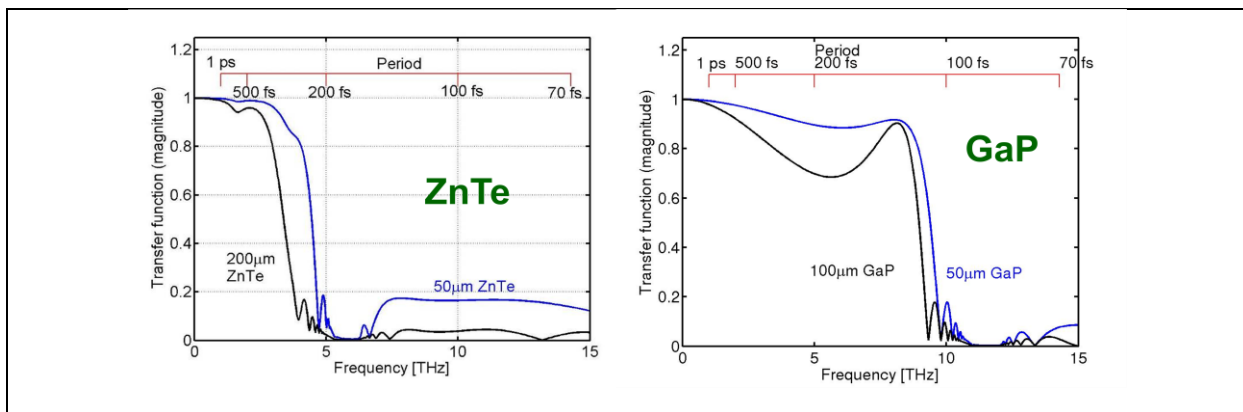
Figure 35: Normalised amplitude spectral response functions for the two commonly used EO crystals, and for different crystal thicknesses. The form of these response functions means that the temporal

response of the EO encoding cannot be treated as a simple rms-like quantity.
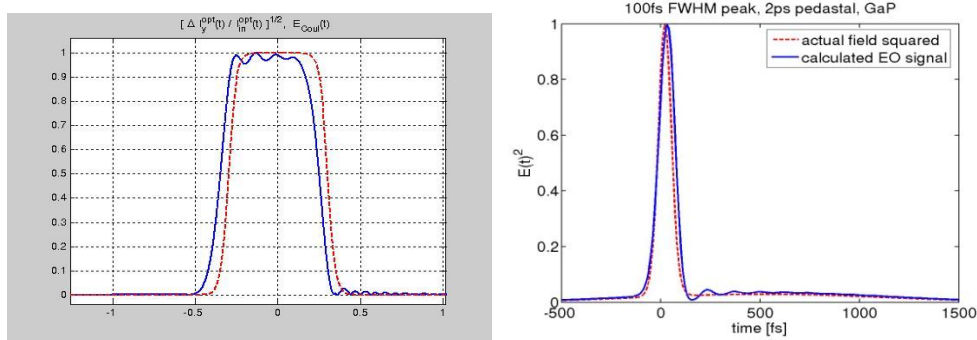
Figure 36: Example simulations of EO profiles (blue) obtained for given charge bunch profiles (red). The choice of bunch profiles demonstrates the effect expected for ultrashort time scale charge density variations

High resolution (& time implicit) Techniques – spectral upconversion

Based on a more detailed description of the EO encoding process described in [liii] which explains the encoding in terms of optical sideband generation via sum and difference frequency mixing of the optical and terahertz fields in the crystal, a new technique called Spectral Upconversion [liv] has been developed (see Figure 37). The technique directly measures the Fourier spectrum of the electron bunch, through first upconverting the far-IR-mid-IR spectrum to the optical region, followed by optical spectral imagining. The technique uses a long-pulse (>10ps pic) laser probe, for which laser transport in optical fibre becomes relatively trivial. The laser system can be significantly simpler than the ultrafast amplified systems of TD. In measuring the Fourier spectrum of the bunch, there is a loss of phase and explicit time information when compared with TD, but this comes at the gain of diagnostics system simplicity and expected reliability. When coupled to the multiple-crystal detection arrangement, the response bandwidth is sufficient to characterize bunches with 20fs resolution, and potentially even shorter.

Note that through up converting the Coulomb spectrum to the optical, region, the relative bandwidth of the spectrum is reduced by more than an order of magnitude; it becomes possible to measure the full spectrum with a single CCD detector with well-calibrated response. Single-bunch, or intratrain measurements become possible through selected timing of the probe laser pulse. In addition this method can measure non-propagating long wavelength components not accessible to radiative techniques such as CSR, CTR, CDR and Smith-Purcell.
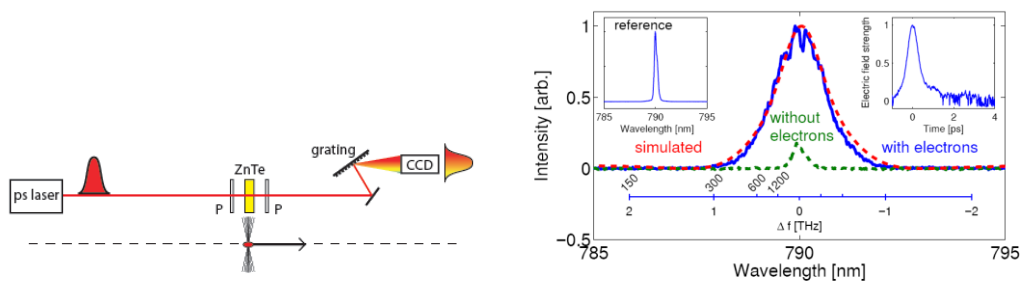
Figure 37: (Left) general concept of the Spectral Up-conversion technique. A quasi-monochromatic ~10-50ps duration pulse interacts with the electron-beam, to produce an output optical pulse that has the spectrum of the bunch coulomb field imposed on it as optical sidebands. (Right) Results from a demonstration experiment, as described in reference [liv]

Envisaged CLIC systems

Of the systems described above, temporal decoding has best demonstrated time resolution, and the potential for even higher time resolution with the FROG-TD system. TD currently requires complicated, and expensive, amplified ultrafast lasers to obtain the higher time resolution. Single-shot SD requires much simpler ultrafast laser oscillators, but suffers from an intrinsic temporal limitation that can, in certain circumstances, causes severe measurement artifacts in the measured bunch profile [xlviii] which make it unsuitable for the 20fs resolution monitors (although for low time resolution measurements it may still be a suitable approach).

Spectral upconversion offers a relatively simple method for obtaining spectral information of the bunch temporal profile, including the long-wavelength non-propagating spectral components; it is able to do this with high repetition rate laser systems, so when coupled to optical array detectors and suitably fast read-out will be able to perform single bunch measurements, or a sequence of measurements throughout a bunch train. It therefore provides an option for intratrain feedback systems.

It is proposed that for 20fs time resolution requirements, both time explicit FROG-EO systems and time-implicit spectral up-conversion system be developed for CLIC. The specific locations of time-explicit, low rep rate diagnostics and systems appropriate for feedback still remains to be identified.

Development work required for CLIC Technical Design Phase

For CLIC implementation, development will need to address operational reliability of the diagnostic, as well as the more challenging task of achieving the higher time resolution to the 20 fs rms.

The higher time resolution is to be achieved by the use of current and alternative EO materials, and the yet-to-be demonstrated multiple-crystal detectors to achieve sufficient detection bandwidth. The testing of a range of alternative materials in EO diagnostic systems will need to be undertaken; this will address issues of signal calibration and splicing of multiple-crystal data; of signal-noise and bandwidth relationships, and crystal robustness in accelerator environments; Much of the initial development can be undertaken with laser-lab experiments only, without the need for more complicated accelerator tests.

The material investigations and multiple-crystal developments will feed into both of the two approaches for the EO diagnostic systems, the time-explicit "FROG" Temporal Decoding EO system, and the time-implicit spectral up-conversion system. The amplified laser systems currently required for Temporal Decoding, and which will certainly be required for the FROG-TD systems, suffer significant problems of day-day reliability and alignment stability. Development should be aimed at first demonstrating FROG-TD, and then minimising the pulse energy requirements for FROG-TD detection. Minimising the laser pulse energy requirements will allow the complexity of the laser system to be reduced, with concurrent improvement in reliability. Optical-fibre ultrafast oscillators, which are now commercially available, have shown themselves to be reliable systems for low pulse energy ultrashort pulses. While fibre systems delivering the ultrashort pulses with the expected requirement of 10-50uJ pulse energy are not available currently, independent developments in laser technology (driven partly by accelerator applications such as FEL seeding) offer the likelihood that such system will be available in the 2-5 year time frame. The spectral up-conversion approach has a distinct advantage in simplicity, cost, and reliability of the required laser systems, albeit at the loss of explicit time profile information. Low pulse energies are suitable, as no optical-nonlinear process is required in retrieving the coulomb field spectral information. The quasi-monochromatic laser would deliver relatively long pulse durations (~10 ps), which greatly simplifies the laser transport requirements. Appropriate laser systems will need to be identified or developed; Yb fibre laser systems are a potentially low-cost and robust option, and are being developed in the context of EO diagnostics by FEL laboratories. The spectral up-conversion laser power requirements will be largely driven by signal-noise; to adequately specify the laser requirements, further testing and development of spectral up conversion is needed.

5.7.4.3 Cost-effective high-resolution bunch length monitor

Bunch length and profile can be derived from the spectral analysis of a coherent radiation generated by an electron/positron beam at a wavelength range comparable to or longer than the bunch length [lv]. The advantage of the method is that it does not have any theoretical limitation on the resolution for the bunch length measurements, i.e. for shorter bunches a shorter wavelength range has to be measured. In practice, the accuracy depends on the technology of the detection system. The technology is significantly different when comparing optical, near-infrared or far-infrared wavelength ranges. Therefore, each bunch length range must be considered separately.

The coherent radiation spectrum, $S(\omega)$, is defined by the following equation

$$S(\omega) = Se(\omega) \ [N + N \ (N-1) \ F(\omega)]$$

Here $S_e(\omega)$ is the single electron spectrum, N is the bunch population, $F(\omega)$ is the longitudinal bunch form factor and the measurement purpose.

Coherent Diffraction Radiation (CDR) generated by a charged particle passing by a conducting screen is one of the best candidates [lvi]. Recent developments in theory of the phenomenon allow us to predict the single electron spectrum with relevant accuracy [lvii].

There are two major tasks the CDR technique can fulfill. The first one is the online monitoring of the bunch length both throughout a train and shot-by-shot, when the bunch length is shorter than 500fs, where RF pickup reaches its sensitivity limit. The second task is to measure longitudinal bunch form factor and bunch profile through the analysis of CDR spectrum.

CDR vacuum system

The CDR monitor only requires a moderate space in the accelerator beam line, i.e. be compact, robust and light. A schematic drawing is demonstrated in Figure 38. It will be based on a typical accelerator vacuum chamber with a CDR generating cavity. The current design is based on accumulative experience of many groups developing CDR diagnostics. Nevertheless the cavity length, depth and angle of the incoming surface will be finalized during the TDR phase. For that purpose we shall use advanced electromagnetic simulation tools (Gdfidl and ACE3P (SLAC)) to optimize the cavity and to predict the single electron spectrum essential for determining the longitudinal bunch form factor and profile.
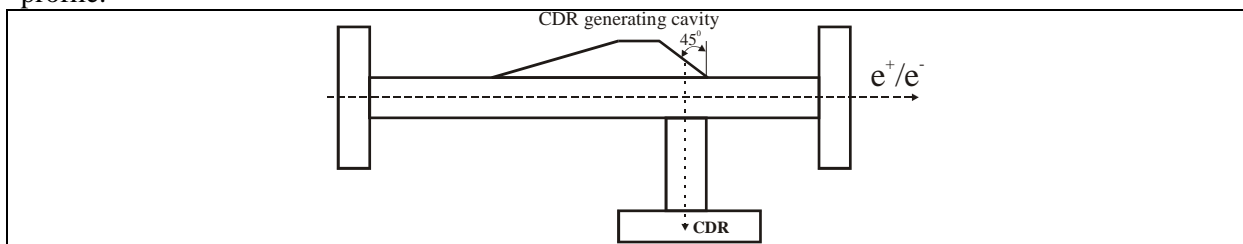
Figure 38: Schematic drawing of a CDR generator

During the TDR phase a prototype of the CDR generator will be built and tested with beam in the CTF3 facility.

Measurement system

To fulfill the challenging requirements of 10ns train resolution, an extremely fast detector should be envisaged. Schottky Barrier Diode (SBD) based detector would be an appropriate choice with a typical time response of FWHM=250ps (see, for instance, Figure 39 [lviii]). One may see that the detector has a long tail of about 2 ns, nevertheless, it still satisfies the CLIC requirements of 10ns resolution throughout the train.
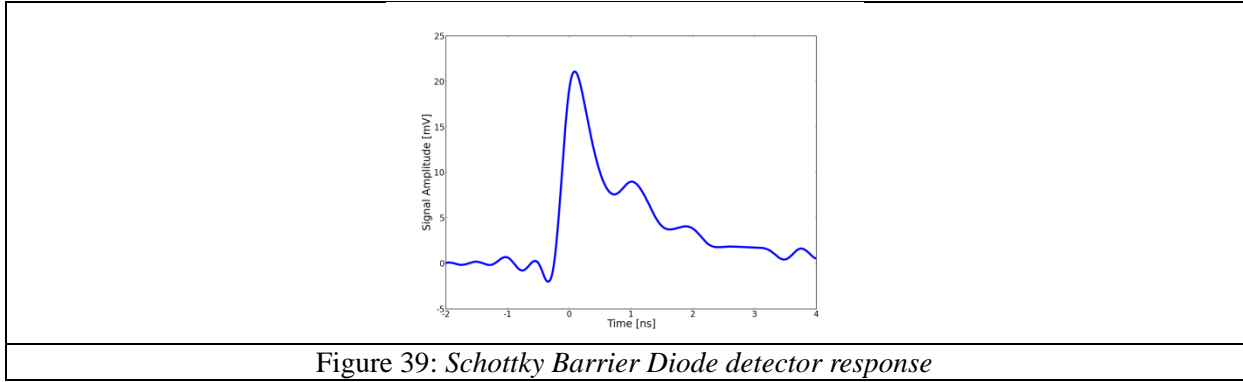
Figure 39: *Schottky Barrier Diode detector response*

Typical beam signals measured at CTF3 by a CDR target are shown in Figure 40. They are capable to follow the fast bunch length variation observed along the pulse. Higher amplitudes indicate shorter bunches.

Figure 40: CDR power signals measured with two SBD detectors: DXP-08 40 - 60 GHz (left) and DXP-12 60 - 90 GHz (right) [lix].

There are a few SBD detectors commercially available (see Table 13 and 14). They cover the optimal bunch length (σ_z) region from 9 ps to 90 fs. With a lower accuracy bunch lengths of a few femtoseconds long can be monitored.

Table 13: SBD detectors from Millitech, Inc.

Type	DXP-42	DXP-28	DXP-22	DXP-19	DXP-15	DXP-12	DXP-10	DXP-08	DXP-06	DXP-05
Band	K	Ka	Q	U	V	E	W	F	D	G
GHz	18-26	26-40	33-50	40-60	50-75	60-90	75-110	90-140	110-170	140-220
σ_z (ps)	6.1-8.8	4.0-6.1	3.2-4.8	4.0-2.7	2.1-3.2	1.8-2.7	1.4-2.1	1.1-1.8	0.9-1.4	0.7-1.1

Table 14: SBD detectors from VDI Virginia Diodes, Inc.

Type	WR4.3ZBD	WR3.4ZBD	WR2.8ZBD	WR2.2ZBD	WR1.9ZBD	WR1.5ZBD	WR1.2ZBD	WR1.0ZBD	WR0.8ZBD	WR0.65ZBD
Freq. GHz	170-260	220-330	260-400	330-500	400-600	500-750	600-900	750-1100	900-1400	1100-1700
σ_z (ps)	0.61-0.94	0.48-0.72	0.40-0.61	0.31-0.48	0.27-0.40	0.21-0.31	0.18-0.27	0.14-0.21	0.11-0.18	0.09-0.14

The CLIC bunch length monitor using coherent diffraction radiation should measure the bunch spectrum in single shot using a grating and an array of diode. The final design of detector will be finalized during the TDR phase.

5.7.4.4   *Measuring the Beam Frequency Combination on the Drive Beam Complex*

The evolution of the bunch combination frequency needs to be monitored in order to optimize the drive beam generation process. Phase errors should be measured after the delay loop and within the combiner rings in order to diagnose potential optics or ring length errors contributing to phase errors in the final 12 GHz drive beam, which should be less than a few picoseconds of phase error for optimal efficient power production. Studies have shown [lx], that a path length error in the delay loop, resulting in 15ps of bunch spacing error, can introduce a power production efficiency drop by as much as 30%.

Non-interceptive phase monitor diagnostics based on either streak cameras imaging synchrotron radiation or button pickups coupled to electronics based on either high frequency diodes or down mixing techniques, have been developed at CTF3 [lxi, lxii], and can be adapted for use in the CLIC drive beam. These techniques are complementary and are based on a single shot measurement. The streak camera provides a phase measurement within a few hundreds of picoseconds time window and a few picoseconds or sub-picoseconds of resolution. The button pickup, see Figure 41, with the corresponding electronics, see Figure 42, can monitor phase errors, along the full pulse train with nanoseconds of time resolution, determined largely by the ADC sampling choice, and a phase precision of about 5 degrees of 12 GHz (1-2 ps) in CTF3. Improved sensitivity could be obtained with more sensitive electronics components.

Concept for the button pickup ring length measurement based on down-mixing electronics – "BPRS"

Figure 41: Button Pickup "BPR" installed in the CTF3 combiner ring

The BPRS electronics has a 3 GHz local oscillator with an adjustable phase shifter control. As a consequence, the output of the down mixed signal will be maximized if the signal is in phase with the local oscillator and zero if $\pi/2$ out of phase. A perfect factor of x4 combination, without phase errors, the ring length of the combiner ring should be $(C + \lambda/N)$, where C is a constant and λ is the wavelength corresponding to the 3 GHz RF deflector in the combiner ring, see Figure 43. Hence, the periodicity of the output BPRS signal, for a well adjusted ring length should be exactly the time taken for the beam to complete 4 turns, and shown in Figure 44. This signal is hence used to adjust the ring length in a multi turn measurement and can also monitor any phase variations along the pulse train, which will be reflected in an amplitude drop in the resulting down mixed signal, for a uniform current.
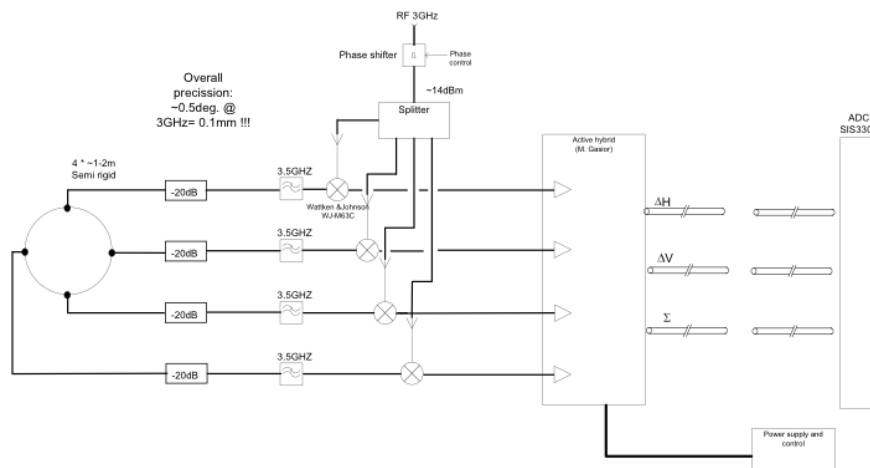
Figure 42: Button Pickup "BPR" Electronics installed in CTF3 for ring length measurements
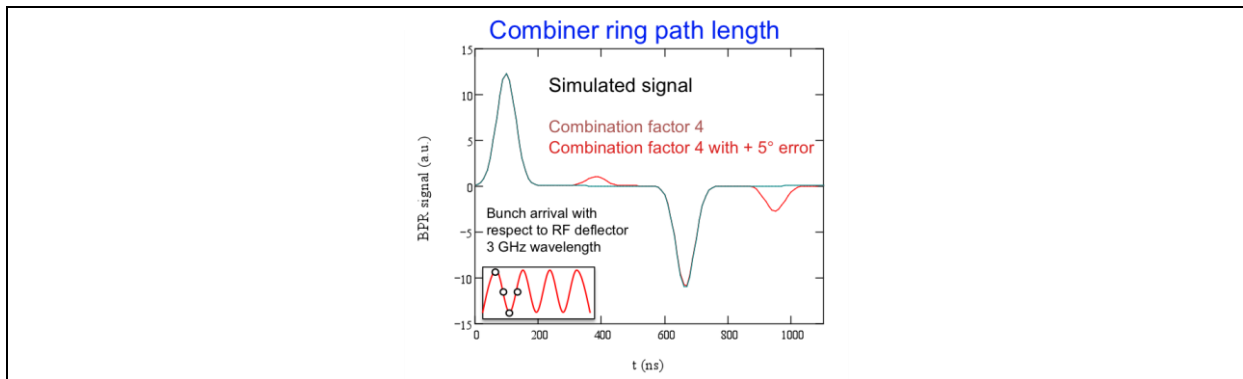
Figure 43: A schematic of the sensitivity of the BPR sum signal to phase errors during a factor of N=4 combination, with a perfect 3 GHz incoming beam
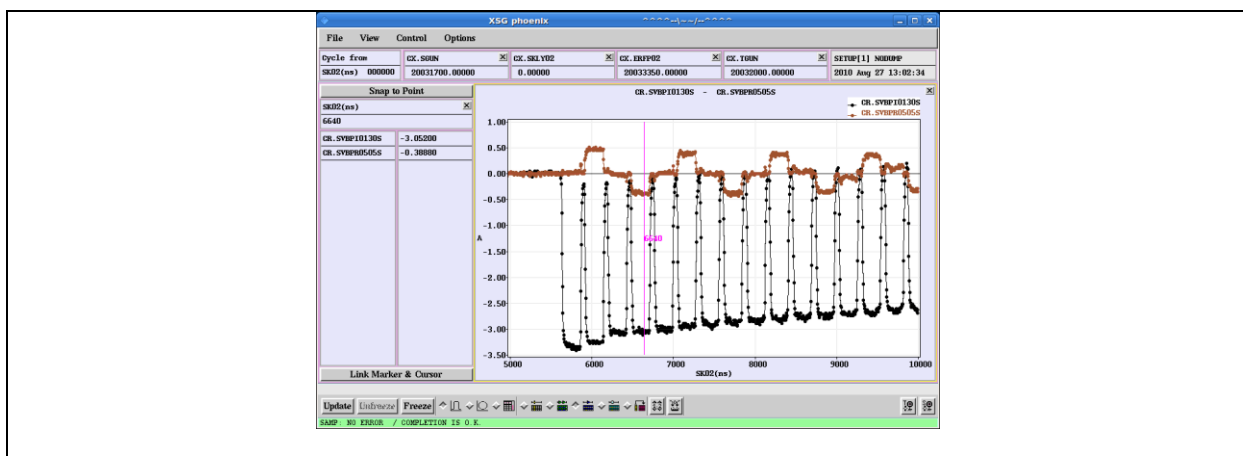
Figure 44: Measurement of the combiner ring length, tuned for a factor of X4 combination, using the BPRS signal, with the beam stored over many turns.

The concept of the BPRS measurement can be extended to monitoring path length errors in the delay loop, or in other combiner rings in CLIC, by modifying the electronics in order to be sensitive to phase errors of different frequencies of interested. For example, it is foreseen in CTF3 to modify the electronics of a button pickup after the delay loop, in order to be sensitive to residual 1.5 GHz phase errors, originating from a path length error in the delay loop. Simulations have shown [lxiii], that by using a 1.5 GHz reference local oscillator, with an adjustable phase control, and with small modifications to the down mixing components in the electronics, that such a detector can be sensitive to phase errors of the order 1-2ps.

Concept for the button pickup phase measurement based on high frequency diodes – "phase monitor"

Another method to identify errors in the combination is by measuring directly the beam power contained in various beam harmonics of interest as depicted in Figure 29. Two "phase monitor" devices have been installed in CTF3, one just after the delay loop, and the other one inside the combiner ring. The principle of these two detectors, explained in the following, can be adapted to measuring the particular beam frequency spectrum, during the various beam combinations of the CLIC drive beam generation.
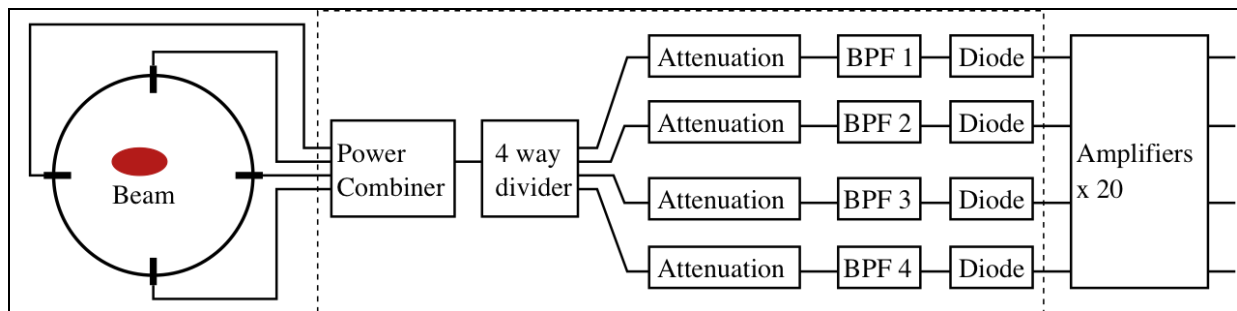
Figure 45. A schematic of the "phase monitor" electronics based on bandpass filters and diodes.

In CTF3, the beam power spectrum is collected by the 4 antennae of the BPR button pickup depicted in Figure 41. The 4 signals are combined, to be position insensitive, and re-divided into four channels where attenuation is applied where needed. The signals are then band pass filtered around a particular beam harmonic of interest, with a bandwidth of ~100MHz and measured with a diode, see Figure 45. The signals are digitized with a 12 bits ADC sampling at 96 MS/s. The phase monitor in the delay loop monitors the beam power at central frequencies of 7.5 GHz, 9.0 GHz, 10.5 GHz and 12.0 GHz to be sensitive to residual 1.5 GHz spacing errors in the combined 3 GHz beam. The one in the combiner ring monitors the frequency bands around 6.0 GHz, 9.0GHz, 12.0 GHz and 15.0 GHz where after a perfect 12.0 GHz combination, the 12.0 GHz component should increase to a maximum in the 4th turn, whilst the other signals are suppressed.
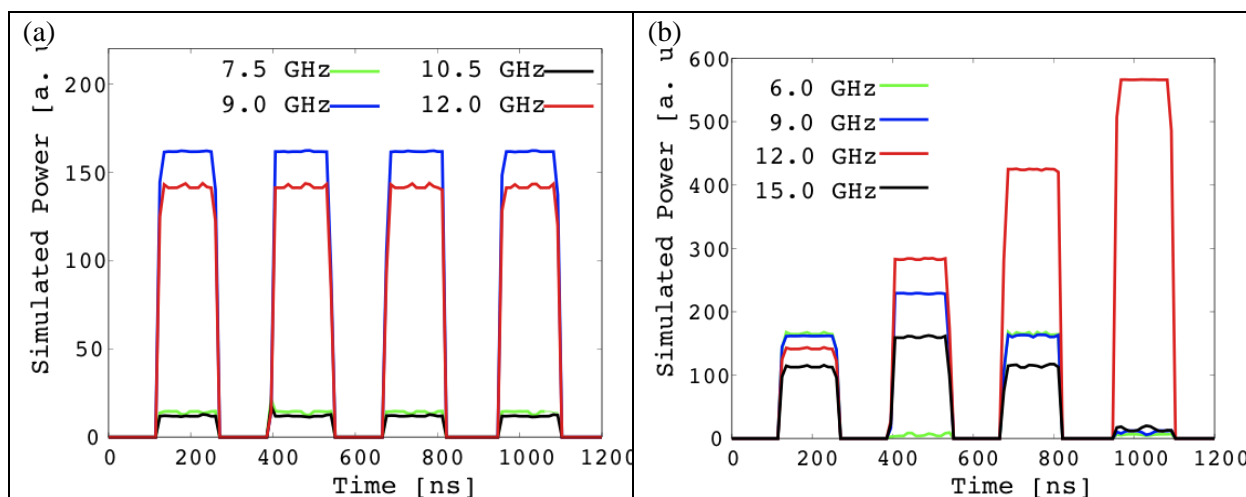
Figure 46: Simulation of the expected phase monitor signals after the delay loop (a) and in the combiner ring (b) for a perfectly combined beam with uniform bunch length along the train.

Figure 46 shows a simulation of the expected phase monitor signals measured in the CTF3 delay loop and the combiner ring for a combination without phase errors and a uniform bunch length, $\sigma_b=15ps$, along the bunch train. Deviations from the relative power measurements, in each frequency for each turn, would indicate a path length error, and hence these signals can provide tuning knobs for the operators. Relative changes to these signals can also be sensitive to bunch length variations, in particular if the bunches are $\sigma_b >10ps$ and hence measurements with the phase monitor should be normalized, on-line, to calibrated bunch length measurements using the BPRW, see Figure 30.

(a)   (b)
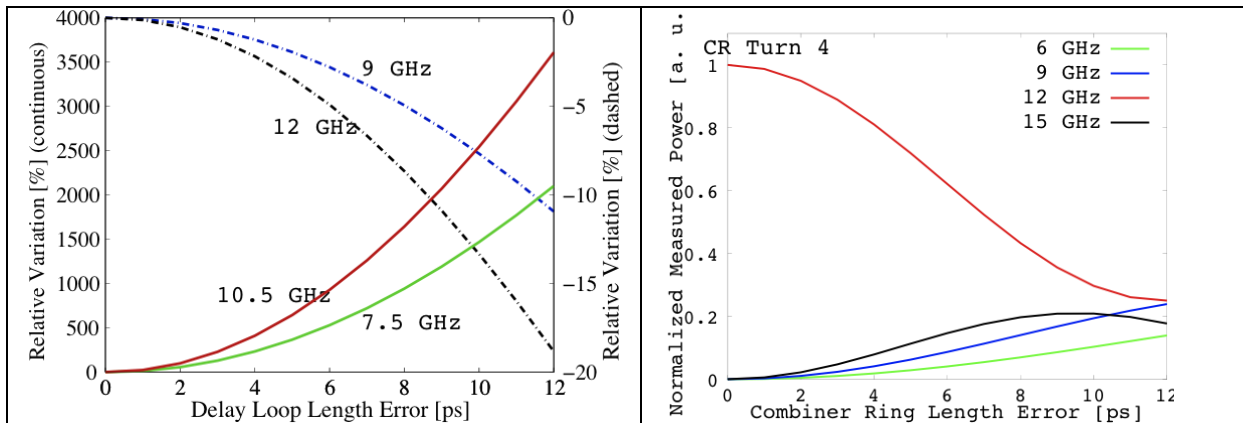
Figure 47: Sensitivity of the phase monitors to path length errors in the delay loop (a) and in the combiner 4th turn (b), for different detection frequencies.

The amplitude changes of the phase monitor signals are shown as a function of the error in the ring lengths in picoseconds in Figure 47(a) for the delay loop and Figure 47(b) for the combiner ring, during the 4th turn.

Although the phase measurements presented in the following paragraph were done in conditions where losses developed in the 4th turn and an imperfect combination is measured, see Figure 48, this data is still useful to demonstrate the ability of developed diagnostics to be sensitive to phase errors during the beam combination measurement.
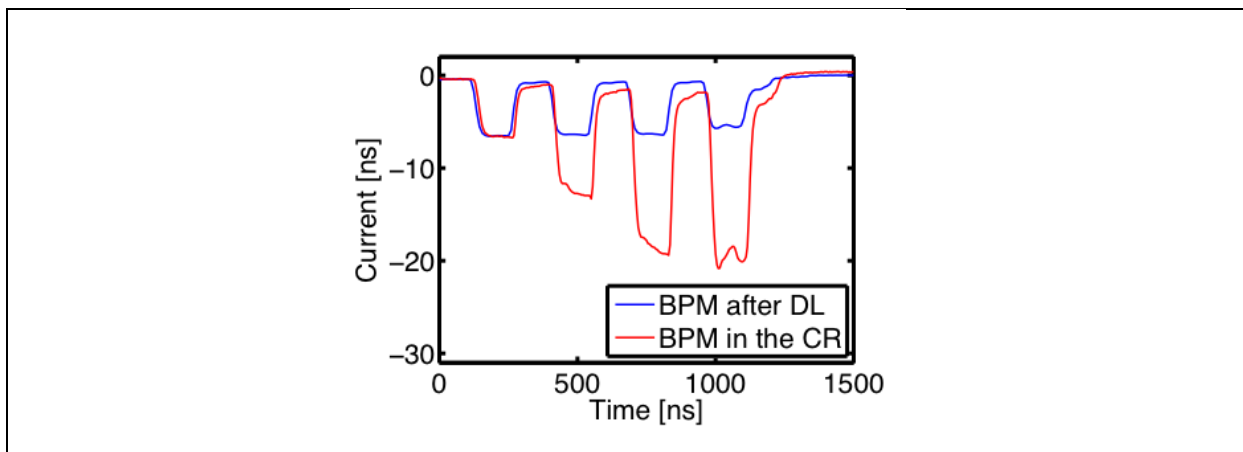
Figure 48: Intensity measurements after the delay loop (blue) and inside the combiner ring (red), as measured during a beam diagnostics commissioning run in November 2009 at CTF3.

The combination factor 4 as measured by the streak camera in the combiner ring is depicted in Figure 49.
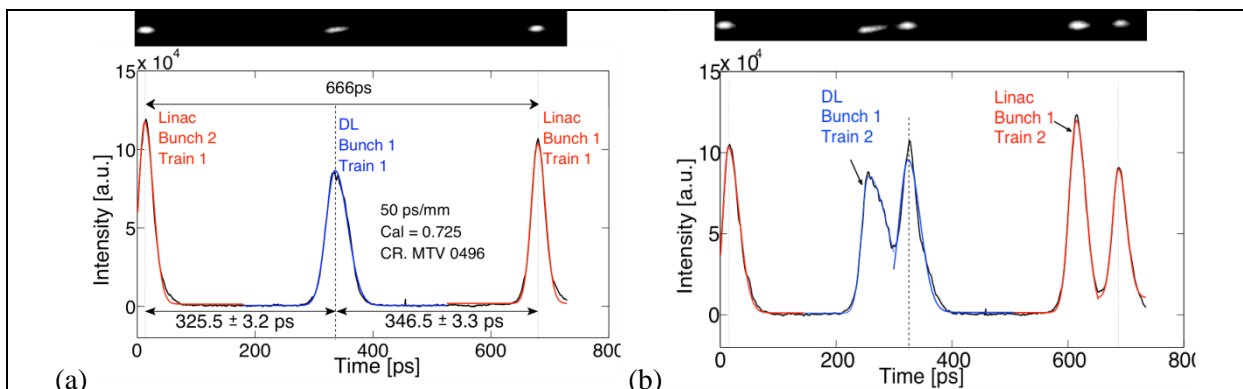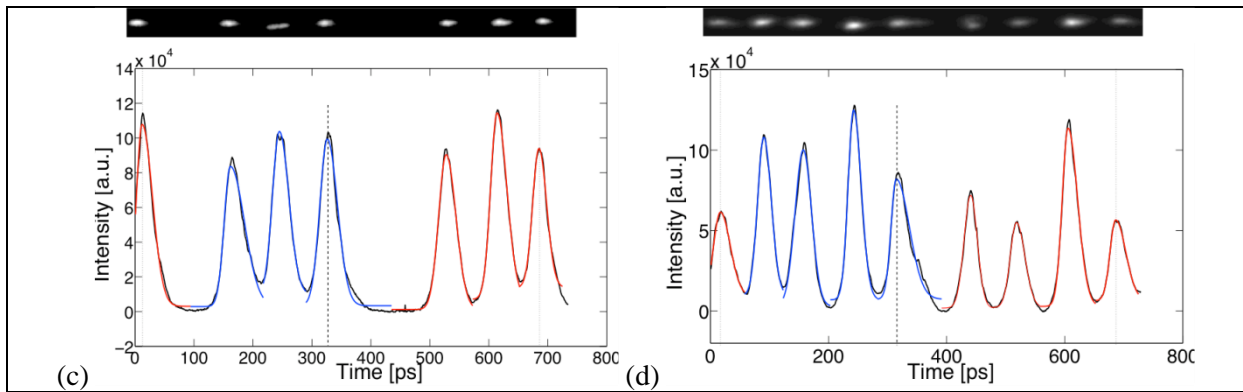
Figure 49: Streak camera bunch spacing measurement for subsequent turns in the combiner ring, showing a sensitivity to measuring phase errors during the bunch frequency multiplication process. 50ps/mm sweep speed – (a) 1st Turn (b) 2nd Turn (c) 3rd Turn (d) 4th Turn

An example of the power measured for the phase monitor on this same measurement day, normalized to current and bunch length, is shown in Figure 50. As expected, the 12 GHz power measurements dominate for the combination. But, due to the poor combination, there is a residual signal from the other frequency components. These unwanted harmonics should be suppressed in the phase monitor measurement during a better combination.
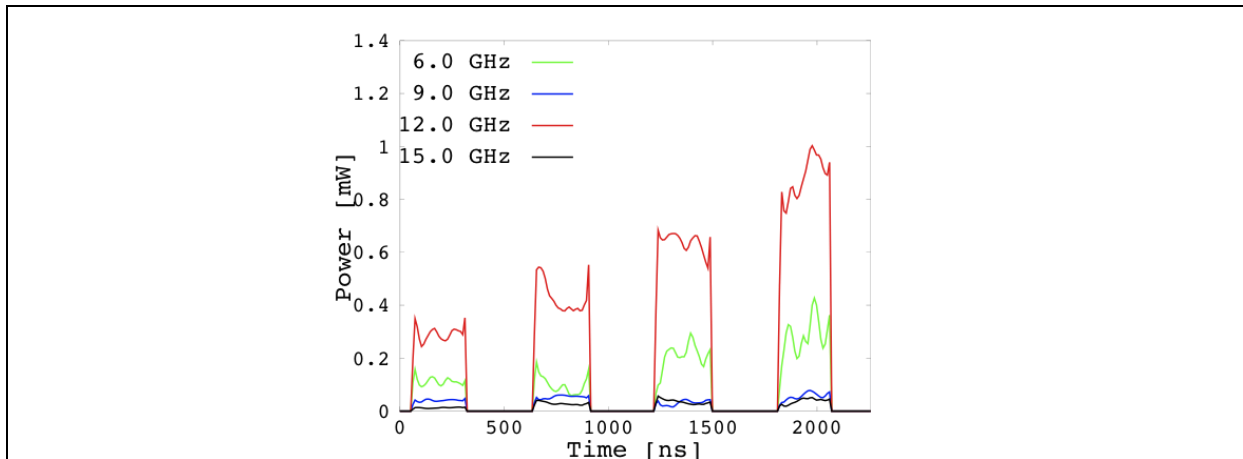
Figure 50: Phase monitor power measurement, normalized to the intensity in FIG BPM and the bunch length measured with the BPRW, where residual 6.0 GHz signals, indicates a phase error during the combination.

The observed bunch spacing error is related to non-zero dispersion at the measurement point [lxiv], and corrections to the dispersion are currently being addressed at CTF3. The dispersion, the ring length and the isochronicity of the rings are all items in the beam optics that are currently being understood at CTF3. The relevant optics tuning knobs are being identified and updated phase measurements are currently being performed.

5.7.4.5 Summary of CLIC longitudinal profile monitors

A summary of the longitudinal profile monitoring systems is presented in Table 13 and indicates what would be the technology choice for the different part of the accelerator complex. It gives baseline scenario, where the technology is mature enough to fulfill the requirements. In many cases, there are two technology mentioned, which basically indicates that two different types of devices are needed to cover the full dynamic range of beam intensities.

Machine Sub-Systems	Quantity	Technology choice	Place to be Tested
Main Beam			

e⁻ & e⁺ injector Complex	10	Streak (^{P}) / RF pick-up (^{R})	CTF3
Pre-Damping and Damping rings	4	Streak (^{P}) / RF pick-up (^{R})	CTF3
RTML	12	EOS (^{P}) / CDR / CSR (^{R})	XFEL's
Main Linac and Beam Delivery system	50	EOS (^{P}) / CDR (^{R})	XFEL's
Drive Beam			
DB source and Linac	8	Streak (^{P}) / RF pick-up (^{R})	CTF3
Frequency multiplication complex	16	Streak (^{P}) / RF pick-up (^{R})	CTF3
Transfer to tunnel	4	Streak (^{P}) / RF pick-up (^{R})	CTF3
Turn-arounds	192	Streak (^{P}) / RF pick-up (^{R})	CTF3
Decelerator and Dump lines	96	Streak (^{P}) / RF pick-up (^{R})	CTF3

Table 13: Longitudinal profile monitors: (^{P}) means full longitudinal profile measurements and (^{R}) for RMS bunch length or form factor measurements

Longitudinal profile monitors for bunches of the order of one picosecond are developed in CTF3 and relies on the use streak camera and RF devices to respectively. For shorter bunches as required in the CLIC Main linac, EO techniques and coherent radiation techniques would be the preferred solution but RF deflecting cavity [lxv] could well be envisaged if necessary to provide reliable cross calibration for these two others technologies. Most likely, the development of very short bunch instrumentation is not possible at CERN at the moment and should be carried out in collaborations with XFEL's project like the ones in PSI, DESY or SLAC.

5.7.5 *Beam Intensity Measurements*

5.7.5.1 *Overview*

An overview of the requirements for beam intensity measurements is presented in Table 14. The change of beam pipe diameter is mentioned in the table, as it would give an indication on possible standardization of devices.

Machine Sub-Systems	Intensity (312 x part/bunch) (A) for DB	Train duration (ns) / Bunch frequency (GHz)	Accuracy / Resolution (%)	Time resolution (ns)	Quantity	Beam aperture (mm)
Main Beam						
e⁻ injector Complex	6 10⁹	156 / 1	2 / 0.5	10	6	40
e⁺ injector Complex	8 10⁹	156 / 1	2 / 0.5	10	34	40
Injector Linac (e⁻/e⁺)	4.4 / 6.4 10⁹	156 / 1	2 / 0.5	10	50	40
Pre-Damping Rings	4.4 / 6.4 10⁹	156 / 1	2 / 0.5	10	10	20/9
Damping rings	4.1 10⁹	156 / 1	2 / 0.5	10	10	20/9
RTML	4.1 10⁹	156 / 2	2 / 0.5	10	54	various
Main Linac	3.7 10⁹	156 / 2	1 / 0.1	10	48	8
Beam Delivery System	3.7 10⁹	156 / 2	1 / 0.1	10	4	various
Spent Beam Line	3.7 10⁹	156 / 2	1 / 0.1	10	3	various
Drive Beam						
Source and Linac	4.2A	1 / 140.3	0.1 / 0.01	10	10	40
Frequency Multi.			0.1 / 0.01	10		80

- Delay Loops	4.2A	288 / 243.7			12	
- TL1	8.4A	288 / 243.7			2	
- Combiner ring 1	8.4→25.2A	96 / 243.7			4	
- TL2	25.2A	96 / 243.7			2	
- Combiner ring 2	25.2→101A	24 / 243.7			4	
- TL3	101A	24 / 243.7			2	
Transfer to Tunnel	101A	24 / 243.7	0.1 / 0.01	10	4	200
Turn arounds	101A	1 / 243.7	0.1 / 0.01	10	96	40
Decelerator	101A	1 / 243.7	0.1 / 0.01	10	96	26
Dump lines	101A	1 / 243.7	0.1 / 0.01	10	48	40

Table 14: Requirements for Beam intensity measurements

5.7.5.2   Accuracy limit of state of the art devices

Drive beam intensity measurement accuracy, resolution, and stability requirements are driven by several applications. Maintaining stable accelerating gradient requires reproducibility and stability of drive beam current to 10^{-3}. Survival of electronics in the tunnel requires drive beam loss less than 10^{-5} while potential access restrictions for personnel due to activation of tunnel components limits losses at less than 10^{-4} in each decelerator sector.

Establishing absolute accuracy better than 1% is very challenging. But combining 1% absolute calibration accuracy with inter-calibration between devices measuring a common beam under low-loss conditions established with loss monitors will suffice. The high drive beam current (100A) makes detection of small fractional beam losses straightforward. The inter-calibration procedure relaxes the need for say 10^{-4} absolute calibration to one of 10^{-4} diurnal stability. Localization of losses within a drive beam decelerator section is facilitated by a combination of loss monitors and beam position monitor sum signals similarly inter-calibrated to the beam charge monitors to a few $x10^{-4}$ in low-loss conditions.

5.7.6   Beam Loss Monitoring Measurements

5.7.6.1   Overview

The main task of a beam loss monitor (BLM) system is to prevent damage to accelerator components. As an integral part of the CLIC machine protection system, the CLIC BLM system should detect potentially dangerous beam instabilities and prevent subsequent injection into the main beam linac and the drive beam decelerators. An additional task of the BLM system is to assist in beam diagnostics and localize and characterize the beam loss distribution. This includes the ability to measure the time structure of the loss, which can indicate the origin of the beam perturbations. These two roles can also be decoupled in two separate systems. In the CDR we focus on the protection requirements of the BLMs. Only for the damping and pre-damping rings have additional requirements been specified. Where further measurements for diagnostics purposes could be desirable, future studies are described.

Table 15 lists the beam parameters and significant loss fraction for each machine sub-system. The estimated number of electrons required to damage a beamline component is based on the structural yield limit for energy deposited in copper, [lxvi]. Limits are more strongly dependent on the charge density, rather than the energy of the beam.

Machine Sub-Systems	Beam Energy (GeV)	Electrons per bunch train	Train Duration	Estimated number of electrons to damage beam line component	Number of electrons for a loss of 1 Watt per meter $(m^{-1}s^{-1})$
Main Beam					
e^- and e^+ injector complex	0-2.86	1.16E+12	156ns		2.18E+09 (at 2.86GeV)
Pre-Damping and Damping Rings	2.86	1.16E+12	156ns	3.48E+08 (at extraction)	2.18E+09
RTML	9	1.16E+12	156ns		6.94E+08
Main Linac	9-1500	1.16E+12	156ns	3.48E+08	6.94E+10 - 4.16E+06
Beam Delivery System	1500	1.16E+12	156ns	1.16E+08	4.16E+06
Spent Beam Line	1500		156ns		4.16E+06
Drive Beam					
Injector complex	0-2.4		140μs	1.54E+13	2.60E+09 (at 2.4GeV)
Decelerator	2.4-0.24	1.53E+14	240ns	1.54E+12	2.60E+09 -2.60E+08
Dump lines	0.25(peak)	1.53E+14	240ns		2.60E+08

Table 15: Beam parameters and loss limits in the CLIC Complex

5.7.6.2 *Summary of CLIC Beam Loss Monitor Requirements & Baseline Choice*

The main requirements for a baseline BLM technology choice are described in this section and summarized in Table 16. A more detailed description of the requirements is given in sections 5.7.6.3 - 5.7.6.8 where the two beam modules, the beam delivery system (BDS), the damping rings and the spent beam line are discussed separately due to their more challenging requirements.

5.7.6.2.1 Response time and time resolution

The machine protection strategy for CLIC will include a 'next cycle permit' system [lxvi] where after each cycle; the next cycle permit is revoked and only re-established once beam and equipment checks are passed. The highest envisaged repetition rate of 100 Hz leads to the required BLM response time of less than 8 ms for all CLIC sub-systems except the pre-damping rings and damping rings, where a response time of 1 ms is required to assist with orbit control.

The time resolution for protection purpose is equal to the cycle repetition interval for all sub-systems (except the pre-damping and damping rings).

5.7.6.2.2   System sensitivity and dynamic range

The system must be sensitive enough to measure the onset of any loss, which exceeds the acceptable threshold. With the exception of the two beam modules and the BDS, the beam losses should not exceed 1W/m. To avoid luminosity losses due to beam loading variations in the two beam modules the total beam losses should not exceed 10^{-3} over each main beam and 10^{-3} over each drive beam decelerator. To detect the onset of these losses, the sensitivity requirements are specified to be the signal produced by a loss rate of a factor of 100 less. For the BDS, the sensitivity requirements are determined by the expected losses on each collimator, as described in 5.7.6.7. The sensitivity requirements are used to define the lower end of the dynamic range.

The upper end of the dynamic range is derived from the signal of a dangerous beam loss (loss causing component damage). In general, during beam operation, losses are required to stay safely (at least a factor of 10) below the estimated damage level. Therefore, to limit the required dynamic range of the BLMs, the upper end is defined as a factor of 10 below the estimated damage level.

5.7.6.2.3   CLIC BLM requirements summary table

Machine Sub-Systems	Dynamic Range	Sensitivity (Gy/pulse)	Response time (ms)	Quantity	Recommended
Main Beam					
e$^-$ and e$^+$ injector complex	10^4	10^{-7}	<8	95	
Pre-Damping and Damping Rings	10^4	10^{-9} (Gy per millisecond)	1	1396	Insensitive to Synch. Rad.
RTML	10^4	10^{-7}	<8	1443	
Main Linac	10^6	10^{-9}	<8	4196	Distinguish losses from DB
Beam Delivery System (energy spoiler + collimator)	10^6	10^{-3}	<8	4	
Beam Delivery System (betatron spoilers + absorbers)	10^5	10^{-3}	<8	32	
Beam Delivery System (except collimators)	$>10^5$	$<10^{-5}$	<8	588	
Post-collision Line	10^6	10^{-7}	<8	56	
Drive Beam					
Injector complex	$5.\,10^4$	$5.\,10^{-6}$	8	4370	
Decelerator	$5.\,10^6$	$5.\,10^{-8}$	8	41484	Distinguish losses from MB
Dump lines	$5.\,10^6$	$5.\,10^{-8}$	8	96	

Table 16: Requirements for BLMs in the CLIC complex

5.7.6.2.4   Baseline Technology Choices

Ionization chambers similar to the ones used at the LHC for example, are specified as the baseline choice of BLM system in all machine subsystems except for the damping and pre-damping rings. The LHC ionization chamber itself has a very high dynamic range of at least 10^8. The LHC readout electronics has a dynamic range of 10^5 and together with the LHC ionization chambers the sensitivity is 7×10^9 Gy (in the shortest time integration interval) [lxvii]. The measurement range can be easily shifted up by 1-3 orders of magnitude by reducing the monitor sensitivity (i.e. reducing sensitive volume and/or gas pressure) and/or by the choice of the electronics components to cover the requirements in Table 16 with the exception of the beam delivery system. The dynamic range of the

LHC readout electronics is 10^5, converging the requirements of most of the accelerator components. Currently under development is a readout electronics for CERN injector machine BLM systems, which is expected to cover a dynamic range of 10^6. The Main Linac and Decelerator could also safely be operated with a somewhat reduced dynamic range, should $1\text{-}5 \times 10^6$ turn out to be technically too challenging.

For the high signals expected in the beam Delivery System, the same type of readout electronics can be used with Secondary Emission Monitors (SEM), [lxviii].

The baseline choice of BLM system in the damping rings is the Cerenkov radiator coupled to a photomultiplier, a system used at the Advanced Photon Source (APS) for the Linear Coherent Light Source (LCLS) free electron laser, [lxix].

The total number of BLMs required is currently estimated to be greater than 50,000. However, the total number of BLMs could be substantially reduced either by halving the number of ionization chambers for the drive beam decelerators or with the use of alternative technologies such as fibres or long ionization chambers in the main tunnel. The reduced number of ionization chambers is presented as an additional cost estimate for comparison to the baseline choice. The alternative technologies are briefly discussed as future activities and options in section 5.6.7.9.

5.7.6.3   Beam Loss Monitoring of the drive beam excluding the two beam modules

The drive beam injector complex consists of the linacs, the delay loops and combiner rings, the long transfer lines and the transfer lines to each drive beam in the main tunnel. Due to the high intensity drive beam, it is currently foreseen to install one BLM per quadrupole, at total of approximately 4300 BLMs. The average distance between BLMs is between 2 and 50 m. In the transfer lines, where the BLM spacing is high, the vacuum chamber is large (100 mm in diameter) and the operational losses are expected to be low. For some subsystems, it is possible that the number of BLMs required would be reduced if destructive losses were detected by the vacuum gauges rather than with BLMs.

5.7.6.4   Beam Loss Monitoring of the main beam excluding the damping rings, two beam modules and beam delivery system

The main beam injector complex (apart from the damping rings) consists of the pre-injector and injector linacs, the booster linac, bunch compressors, diagnostic sections, the turnarounds and the long transfer lines to the main linac. It is foreseen to install approximately one BLM per quadrupole in every subsystem. In the long transfer lines there are only 96 quadrupoles over 21000 m i.e. approximately one every 210 m, whereas in parts of the transfer lines to the tunnel there is one quadrupole every 0.5 m.

5.7.6.5   Beam Loss Monitoring of the damping rings

In each of the damping rings, there are 502 quadrupoles, 102 dipoles, 288 sextupoles, 356 steerers, 48 skew quads and 52 wigglers. In each of the pre-damping rings there are a total of 196 quadrupoles, 38 dipoles, 102 sextupoles, 156 steerers, 38 skew quads and 40 wigglers. It is foreseen to install one BLM for each quadrupole, a total of 1396 BLMs.

To assist with orbit control, the BLM system in the CLIC damping ring complex should respond within 1000 turns, i.e. within about 1 millisecond. To ensure that the superconducting wigglers do not quench, the losses should not exceed 1 W/m corresponding to a loss of 2×10^6 electrons per meter per millisecond. Based on FLUKA simulations of continuous losses for the 2.4 GeV drive beam, this would result in a dose near the beamline of approximately 10^{-7} Gy in one millisecond. To detect the onset of these losses, the BLMs should be sensitive a factor of 100 less, i.e. approximately 10^{-9} Gy.

 At the extraction point of the damping rings, the beam becomes destructive when 0.03% of a bunch train is lost. Using this as an approximation for the damage potential within the damping rings, damage to a beamline component occurs when 3.5×10^8 electrons hit a single aperture restriction.

Based on FLUKA simulations for the 2.4 GeV drive beam, a loss of 3.5×10^8 electrons results in a dose close to the beam line of approximately 10^{-4} Gy. The upper limit of the dynamic range requirement should allow for the detection of 10% of destructive losses. The required dynamic range for the BLM system in the damping rings is 10^4.

To avoid synchrotron radiation, the BLMs in the straight sections should be placed immediately after each quadrupole and absorber. In the arc sections, the BLMs should be placed immediately after each dipole and absorber or between the doublets. Whilst the absorbers are expected to pick up most of the synchrotron radiation, it is possible that some radiation would reach BLMs at these locations. The use of Cerenkov detectors, which are typically insensitive to synchrotron radiation, might lead to more freedom in positioning the detectors to optimize detecting the loss signal. However, exposure to synchrotron radiation should still be limited to avoid radiation damage to BLM components.

5.7.6.6 *Beam loss monitoring of the two beam modules (main linac and drive beam decelerators)*

Beam loss monitoring for the two beam modules requires careful consideration. The system would ideally be able to distinguish between losses from each of the two beams, 65 cm apart. The BLMs should be sensitive to signals from lost electrons with an energy range of 9 to 1500 GeV in the main beam and 2.37 to 0.237 GeV in the drive beam. Table 17 lists the different BLM requirements at various positions in the CLIC tunnel. For the drive beam, they are specified for losses at the maximum and minimum energies. For the main beam they are specified for each of the module types, which depend on the energy of the beam.

	Dynamic Range	Sensitivity (Gy/pulse)	Response Time	Position Resolution (longitudinal)
DB side, (e+, e-), 2.4 GeV	5.10^5	10^{-7}	<8ms	1m
DB side, (e+, e-), 0.24 GeV	2.10^5	5.10^{-8}	<8ms	1m
MB side Type 1, (e+, e-), 9 -100 GeV	10^6	10^{-9}	<8ms	2m
MB side Type 2, (e+, e-) 100-250GeV	10^6	10^{-9}-10^{-8}	<8ms	~5m
MB side Type 3, (e+, e-) 250-750GeV	10^6	10^{-9}-10^{-8}	<8ms	~10m
MB side Type 4, (e+, e-)750-1500GeV	10^5	10^{-8}	<8ms	~10m

Table 17: Summary of the BLM requirements for the two beam modules

To distinguish between losses in the horizontal and vertical planes, one BLM for each quadrupole is required, a total of 41484 for the drive beam decelerators and 4196 for the main beam linacs. The longitudinal resolution of the BLM system should be less than the spacing between quadrupoles, which is approximately 1 m in the drive beam decelerators and always higher in the main beam. The response time should be less than 8 ms to allow the system to react from train to train.

Simulations have been performed using the Monte Carlo code FLUKA [lxx], [lxxi] to determine the sensitivity and dynamic range requirements for BLMs in the two beam modules. Losses at the maximum and minimum energies for each beam were simulated to determine the resulting spatial distribution of absorbed dose. For each beam energy, two loss scenarios were simulated. In one, the loss was simulated at single point representing the location of an aperture restriction, i.e. at the end of a PETS just before the quadrupole in the drive beam and the end of an accelerating structure just before the quadrupole in the main beam. In the other, the losses were simulated continuously along the beam pipe, an approximation of losses at multiple aperture restrictions, to represent standard

operational losses due to beam gas interactions. The simulations are described in greater detail in [lxxii]. Examples of the resulting dose distributions are shown in Figures 51 and 52.

Whilst ideally the BLM system should be sensitive to the losses due to beam gas interaction, it is required that the system is at least sensitive to the losses at which the machine can no longer operate. It is assumed that the limiting factor in normal operation will be imposed by beam dynamic considerations, where losses of no more than 10^{-3} of the total beam intensity along the 20 km main linac, and no more than 10^{-3} of the total beam intensity along each decelerator section (average length 876 m), can be tolerated due to luminosity losses from beam loading variations. From Figure 52, a loss of 10^{-3} of a bunch train along the linac would result in an absorbed dose close to the quadrupole, a possible location of the BLM, of approximately 10^{-5} Gy for the drive beam, and approximately 10^{-7} Gy for the main beam. To see the onset of such losses the sensitivity requirements were determined to be 10^{-7} Gy per pulse and 10^{-9} Gy per pulse respectively. Similar plots for losses at other energies were used to make estimates for the sensitivity requirements in Table 15.
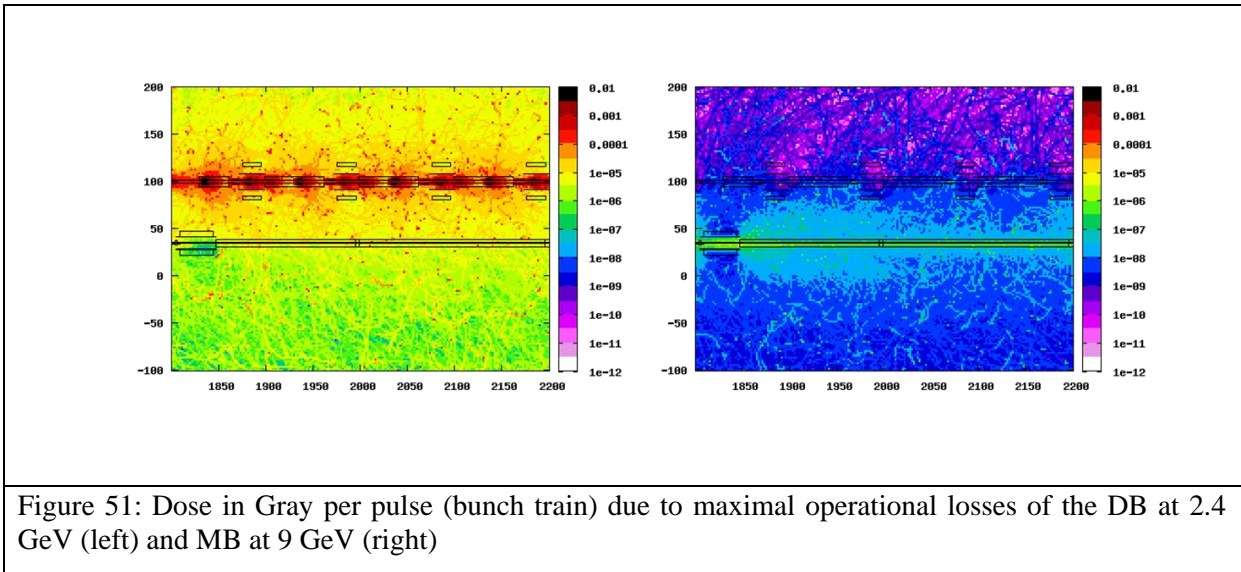
Figure 51: Dose in Gray per pulse (bunch train) due to maximal operational losses of the DB at 2.4 GeV (left) and MB at 9 GeV (right)
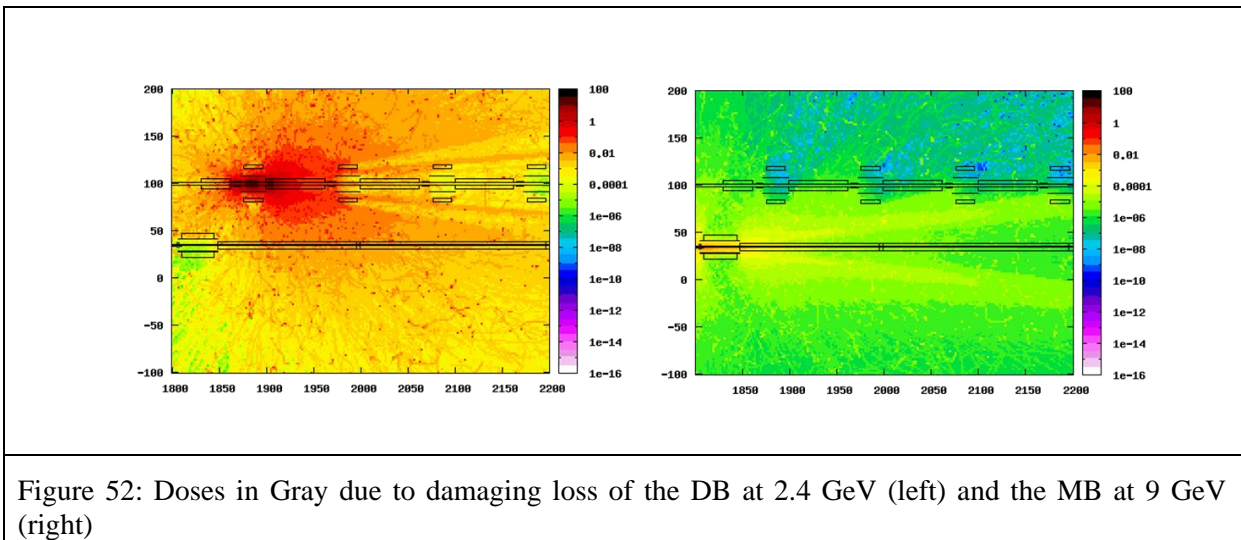
Figure 52: Doses in Gray due to damaging loss of the DB at 2.4 GeV (left) and the MB at 9 GeV (right)

The dynamic range of the BLM system should allow for the detection of beam losses at a factor of 10 below the point at which they become destructive. The losses become destructive respectively on the Drive Beam or the Main beam when 1% or 0.03% of a single bunch train hits a single aperture restriction. This corresponds to approximately 1.5×10^{12} and 3.5×10^{10} electrons from the drive and main beams respectively. In the drive beam, the aperture restrictions are located at the end of the PETS just before a quadrupole and in the main beam at the end of the accelerating structure just before

the quadrupole. From Figure 51, destructive losses at 9 GeV in the main beam and 2.4 GeV in the drive beam result in doses of 0.01 - 0.1 Gy near the beamline. Based on these results, the dynamic range is determined to be between 4×10^5 and 10^6. Similar plots for losses at other energies were used to make estimates for the dynamic range requirements listed in Table 17.

The system should be able to detect the onset of failures in the cold-start up scenario described in [lxvi], where the number of electrons per bunch train would be reduced by a factor of 100 in the drive beam and 150 in main beam. Thus an additional requirement is that the BLM system should always be sensitive to a signal over a factor of 150 less than that produced by a destructive beam loss at nominal intensity. It is clear that this is always the case from Table 17, where the upper limit of the dynamic range is defined by the signal at 10% of destructive loss, and the dynamic range is always greater than 150.

As shown in Figure 51, the absorbed doses are similar from destructive loss at 2.4 GeV at the quadrupole near the loss point and the subsequent upstream quadrupole. This is also the case for losses at 0.24 GeV. Therefore, due to the close spacing between the quadrupoles in the drive beam, it would be feasible for machine protection purposes to place one BLM every two quadrupoles. However the ability to distinguish between losses in the horizontal and vertical planes would be lost.

5.7.6.7 *Beam Loss Monitoring of the beam delivery system (BDS)*

Between the main linac and the interaction point there are 18 collimators (9 spoilers and 9 absorbers), 206 dipoles, 70 quadrupoles and 18 sextupoles for each BDS. As the BDS is highly critical in terms of damage potential, it is foreseen to install one BLM per dipole, quadrupole, skew quadrupole and collimator, a total of 624 BLMs. The BLM response time should be less than 8 ms to allow the system to comfortably react from train to train.

The BLMs should be sensitive to losses on the BDS collimators during standard operation. In the main linac, the largest part of operational losses is expected to originate from beam-gas interactions. It is estimated that, due to the beam-gas interactions in the main linac and BDS, approximately 0.02% of the beam will hit the collimators in the BDS [xxx]. Assuming the losses are evenly distributed over each of the collimators this would correspond to approximately 2×10^7 electrons per bunch train hitting each spoiler. Based on FLUKA simulations of losses at 1.5 TeV in the main linac, a loss of 2×10^7 electrons at a single location would lead to doses of approximately 0.002 Gy in a region near the spoiler.

It is likely that most of the halo losses will occur on the first betatron spoilers whereas the remaining spoilers will see a much smaller fraction of the beam. Therefore sensitivity requirements of the BLMs are specified to be a factor of 10 lower, i.e. 2×10^{-4} Gy, such that significant losses on any spoilers are detected.

The dynamic range of the BLMs for the collimators should allow for the detection of 10% of destructive losses. The first spoiler and the first absorber (momentum cleaning) should withstand the impact of a full bunch train, 1.16×10^{12} electrons. This is to happen regularly during commissioning and not so often during normal operation. The other collimators (betatron cleaning) can only withstand a fraction of the beam (sacrificial devices). To ensure the survivability of the betatron cleaning collimators, the beam loss on each collimator should be no more than approximately 1%, 1.16×10^{10} electrons per bunch train. Based on FLUKA simulations of losses at 1.5 TeV in the main tunnel, this would lead to an absorbed dose in a position near the collimators of approximately 100 Gy for the first (momentum cleaning) spoiler and absorber and 1.0 Gy for the betatron collimators. Using the sensitivity requirement as a lower limit, the dynamic range is required to be approximately 10^6 for the momentum collimators and less than 10^5 for the remaining collimators.

It should be noted that the sensitivity and dynamic range requirements are currently based on estimates of dose distribution from simulations of loss at single aperture restrictions in the main linac. The dose distribution resulting from losses on a spoiler and absorber is likely to be substantially different.

However, for the baseline technology choice, a change in two orders of magnitude of the specified requirements would be reasonably achievable.

The beam becomes destructive to standard BDS beamline components when approximately 0.01% of a bunch train, 1.16×10^8 electrons, is lost at a single aperture restriction. Based on FLUKA simulations of losses at 1.5 TeV in the main tunnel, this results in a dose of 0.01 Gy near the beam line.

5.7.6.8   Beam Loss Monitor in the Post-collision Line

The key components of the spent beam line are shown in Figure 53. The most significant beam losses are expected to occur in the protection absorbers of the window-frame magnets and in the intermediate and main dumps [lxxiii].

 The 4 window–frame magnets separate the electrons, positrons and beamstrahlung photons. The power loss in the magnet absorbers is expected to be between 1 and 11 kW. All "opposite-sign" particles are then stopped by the upper part of the intermediate dump, which should absorb 140 kW of power, whilst "same-sign" particles with energies less than 250 GeV are stopped by the lower part of the dump, which should absorb 170 kW of power. Between the intermediate dump and the main dump there are four C-type magnets to disperse the remaining beam before it impacts on the main dump, which should absorb 14 MW of beam power.

It is currently foreseen to install 28 BLMs for each spent beam line: 4 per window frame magnet, 4 at the intermediate dump (due to the asymmetric losses on the dump), 1 for each C-shaped magnet and 4 at the main dump. However the BLMs might be repositioned when better information about the expected loss distribution at each component is known.

The specifications for sensitivity and dynamic range currently represent collective requirements of all BLMs in the spent beam line. The sensitivity requirement is based on detecting the onset of losses of 1W/m. According to FLUKA simulations of continuous losses at 1.5 TeV along a beam line, the resulting absorbed dose near the beam line is approximately 10^{-5} Gy per pulse, for losses of 1 W/m. The sensitivity requirement is therefore specified to be a factor of 100 less to detect the onset of these losses. Whilst an upper limit for the dynamic range not known, the specified dynamic range is set to match that for the collimators in the BDS. In the case where the upper limit of dynamic might not be consistent with BLMS sensitive enough to detect of 1 W/m, the BLMs would be rearranged with different thresholds for their different measurement purposes. This would be determined for the technical design report and is not considered to be a conceptual problem.
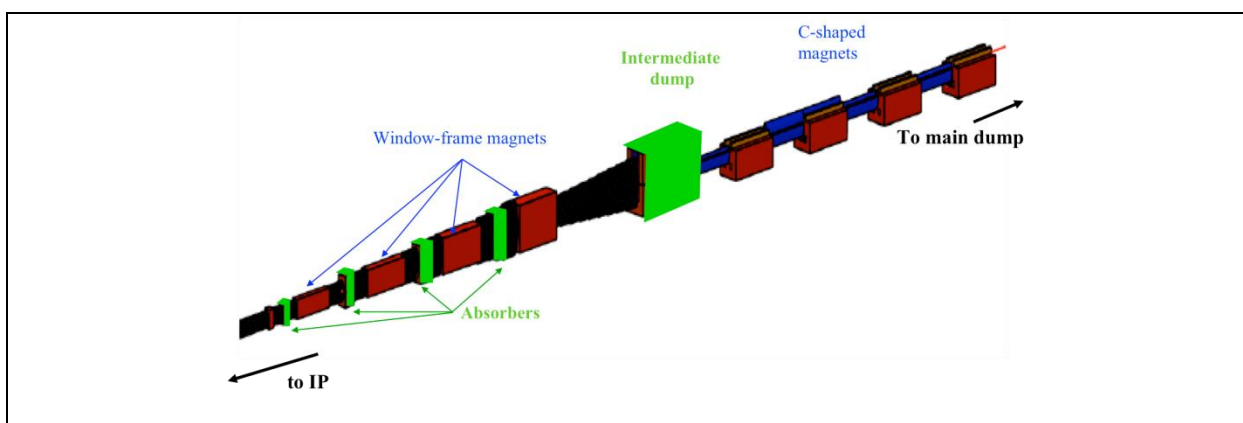
Figure 53: Schematic of the Post-collision line with a succession of absorbers and an intermediate dump

In the time period before the TDR, the focus of future activities will be to reduce the total cost of the system, to refine the BLM requirements listed in the previous sections and to investigate the feasibility of a BLM system for the purpose of beam diagnostics.

The issue of cost will be addressed primarily with testing alternative technologies for the two beam modules, which would account for approximately 85% of the required number of BLMs if ionization chambers (baseline technology choice) were used.

To better determine the BLM requirements, Monte Carlo simulations should be performed that are more specific to each CLIC subsystem, particularly for subsystems such as the damping rings and BDS where detecting beam loss is crucial, and where the estimated loss signals are currently based on simulations of beam loss in the main linac. Simulations will also be adapted to the type of technology considered or tested. Estimates of requirements are currently based on values for absorbed dose in air, a reasonable approximation for the expected loss signal in ionization chambers. However, future simulations for calculating the detector signals for CLIC requirements and for CTF-3 testing must take into account the expected loss signal in the respective detector. For example, the signal in Cerenkov detectors is dependent on the angle and type of incoming radiation so current estimates of absorbed dose near the beam line would not be sufficient for estimating the detector requirements.

A BLM system used for diagnostic purposes should distinguish between losses from each beam in the two beam modules. Current simulations indicate that the worst 'cross-talk' between signals appears to be from losses of the main beam at low energy (9 GeV) and of the drive beam at high energy (2.4 GeV): From Figure 52, in a region close to the main beam, a destructive loss from the drive beam provokes a signal of similar magnitude to that of a destructive loss from the main beam. A single monitor in this region would not be able to distinguish between the losses. For machine protection purposes this is not a problem since the loss would not go unnoticed. For beam diagnostic purposes, Monte Carlo studies will be used to investigate optimizing the position of BLMs for distinguishing the location of loss signals. Furthermore, due to the difference in time structure between the main beam and the drive beams, a BLM system with a very high temporal resolution that could distinguish between the destructive losses from each of the beams could be considered as and alternative technology.

5.7.6.9.1   Alternative Technologies Summary

Some of the detectors to be investigated before the Technical Design Report are summarized in this section. The use of long ionization chambers (lone hollow coaxial cable filled with argon and CO_2) [lxxiv], [lxxv], optical scintillating fibers and Cerenkov fibers [lxxvi] are currently considered for use in the two beam modules and their characteristics are summarized in Table 18.

The advantage of long ionization chambers is that they are cheap, easy to install and have uniform sensitivity. Whilst the potential radiation damage to the cable isolation could be of concern, the system at SLAC survived 20 years running without problems. However, due to the fact that long ionization chambers have to be placed further from the beam line than the standard short ionization chambers, their sensitivity and dynamic range may not meet the requirements for the two beam modules. Optical fibers for the two beam modules would offer a better response time if it is required. Cerenkov fibers have a high tolerance to radiation and are insensitive to synchrotron radiation whereas scintillating materials typically offer much better sensitivity and dynamic range but suffer damage at much lower radiation levels.

A Cerenkov fibre system where two parallel fibers attached to SiPM readout is currently under study [lxxvii] and it is foreseen that several tests will be performed at the CTF3 facility CLEX in 2011.

	Dynamic Range	Sensitivity (nC/Gy)	Response Time	Position Resolution (longitudinal)
Long Ionization Chambers (Ar + CO_2 *FERMILAB*) (Ar + CO_2 *SLAC*)	10^4 (SLAC)	$2.10^2 cm^{-1}$ (FERMILAB)	~µs	m-km
Cherenkov Fibers (- with SiPM) under investigation at CTF-3 *A .Intermite*, *C. Welsch*	10^4 (typical -to be tested)	$10^5 cm^{-2}$	50ns	10 cm
Plastic Scintillating Fibers (with PMT)	$<10^7$	$<10^8 cm^{-2}$	~ ns	m

Table 18: Summary of the alternative BLM systems considered for two beam modules

5.7.7 *Beam Energy Measurements*

5.7.7.1 *Overview*

An overview of the requirements for beam energy measurements is shown in Table 19 for the Main and the Drive Beam respectively. The table presents the evolution of the beam energy and its energy spread through the CLIC complex with the corresponding expected resolution and the number of devices requested. The typical charge densities are mentioned since they will set an upper limit above which intercepting devices like screens or wire scanners would get damaged.

Machine Sub-Systems	Energy (GeV)	Energy spread (%)	Accuracy (%)	Resolution (%)	Time resolution (ns)	Quantity	Charge density (nC/cm^2)
Main Beam							
e$^-$ injector Complex	→ 0.2	3.5 → 0.1	1	0.5	10	2	$< 5\ 10^5$
e$^+$ injector Complex	→ 0.2	6 → 3.5	1	5	10	4	$< 5\ 10^5$
Injector Linac (e$^-$/e$^+$)	→ 2.86	0.1 / 2.7	1	0.5	10	2	$< 5\ 10^5$
Pre-Damping Rings	2.86	0.5	0.1	0.05	10	2	$< 5\ 10^6$
Damping rings	2.86	0.134	0.1	0.05		2	$< 5\ 10^8$
RTML			0.1	0.05	10		$< 5\ 10^8$
- Bunch compressors 1	2.86	1.17				4	
- Booster Linac	2.86 → 9					2	
- Transfer lines	9					2	
- Turn arounds	9						
- Bunch compressor 2	9	1.26				4	
Main Linac	9 → 1500	1.3 → 0.3		0.02	10	48	$< 5\ 10^8$
Beam Delivery System	1500	0.3 → 1		0.02	10	2	$< 5\ 10^8$
Drive Beam							
Source and Linac	→ 2.37	1	0.1	0.01	10	10	**$< 40\ 10^6$**
Frequency Multiplication	2.37	1	0.1	0.01	10	6	**$< 40\ 10^6$**
Transfer to Tunnel	2.37	1	0.1	0.01	10	0	**$< 40\ 10^6$**

Turn arounds	2.37		0.1	0.01	10		$< 1.5 \; 10^6$
- Bunch Compressor 1		0.3				48	
- Turn-arounds							
- Bunch Compressor 2						48	
Decelerator	< 2.37	→90	0.1	0.01	10	0	$> 1.5 \; 10^6$
Dump lines	0.237<x< 2.37	<90	0.1	0.01	10	48	$> 1.5 \; 10^6$

Table 19: Requirements for Beam Energy measurements

The beam energy and its energy spread need to be carefully monitored all along the complex. Once emitted from their conversion target, the positron beam has an energy spread of 6% a factor 2 bigger compared to the electrons. Their energy spread is further reduced in the injector linac and in the damping rings. In the RTML, the two consecutives bunch compression stages introduce a time correlated energy spread necessary to shorten the bunch length. The energy spread increases then up to 1.3% but is reduced by roughly a factor 3 as the beam is accelerated all along the main linac. One must note here that the correct acceleration strongly relies on the precise timing synchronization between the Main and the Drive beam. The scheme is discussed in more details in paragraph 2.7. In the beam delivery system, the beam energy is precisely monitored since very tight beam energy stability is absolutely mandatory to ensure optimum final focusing conditions.

With full beam loading acceleration, the operation of the Drive Beam linac is very sensitive to RF phase and power variations, which must be kept below 10^{-4}. Any intensity variation for the electron source will also directly transfer into energy variation at the end of the linac and must also be controlled to ensure a high stability. Because of the high beam loading in the accelerating structures, transient effects occur during the filling time of the cavity, resulting in a much higher acceleration for the first particles of the pulse. Time resolved measurements along the pulse train are then a must to tune the linac accordingly. In the decelerator the Drive Beam energy is progressively converted into RF power, and the beam at the end of the line have an energy spread of 90%. The precise monitoring of the beam deceleration is one of the key measurements to optimize the RF power production. The beam energy must be then measured before and after each decelerator.

In most case the beam energy and its energy spread are monitored in dedicated spectrometer line as discussed in paragraph 5.7.7.2.

5.7.7.2   *Beam energy and energy spread measurement in Spectrometer line*

A spectrometer uses the Lorentz force, $F=q \cdot [E+p \times B]$, to transfer information about particle momentum into particle position. If a particle of charge q and momentum p passes through a magnetic field B it will 'experience' a force F, which will result in a change in path direction as depicted in Figure 54. Assuming a deflection in the horizontal plane, the measurement of the horizontal beam position and size in the spectrometer line will directly provide a measurement of the beam energy and its energy spread. Experimentally it requires minimizing the natural transverse beam size at the position of the monitors ((d) and (e)) by using a set of quadrupoles (a). The alignment of the beam entering the bending magnet is also crucial and needs to be precisely measured and corrected if necessary.
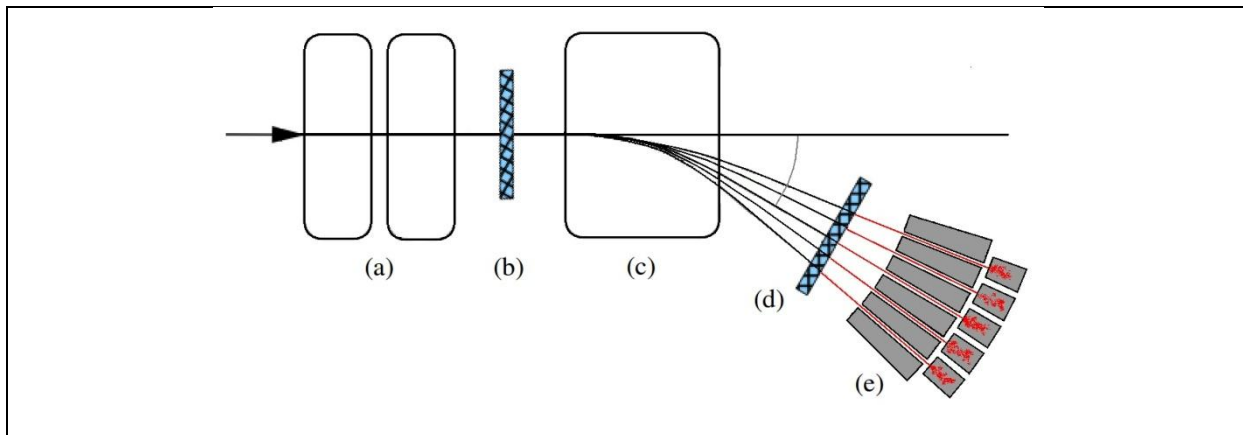
Figure 54: Schematic of spectrometer line: (a) Set of Quadrupoles (b) Beam Position monitoring before the bending magnet (c) Bending Magnet (d) Beam position and profile monitor in the spectrometer line (e) Horizontally segmented beam dump

The monitor accuracy and resolution will depend on the accuracy of the beam position measurement (see paragraph 5.5.2) and on the good knowledge of the bending magnet field relying on its precise calibration. Magnets can be calibrated accurately down to few ppm and state of the art beam position monitors can provide accuracy and resolution respectively of few microns and 50nm, which would provide beam energy measurement with accuracy and resolution respectively better than 10^{-3} and 10^{-5}.

Energy spread is typically measured using beam profile monitor installed at the end of the spectrometer line. Contrary to the beam position monitor, they are most of the time interceptive devices, as discussed previously in paragraph 5.7.3. In this context, thermal limitations have to be taken into account in the choice of the detector technology and implemented as well in the final design of devices.

Energy spread measurement using OTR screens

The optic of the beam line is made in such a way that the beam size at the location of the monitor is large enough in order to minimize the thermal stress in the OTR screen. Typically beam size will be of the order of one centimeter. A limitation of OTR in imaging large beam size is actually illustrated in Figure 55. It shows a decrease of the light intensity captured by the camera, as the beam is moving out of the center of the screen. This effect depends on the electron energy, as the OTR photons are emitted in a cone of $1/\gamma$ aperture, and on the numerical aperture of the optical system.
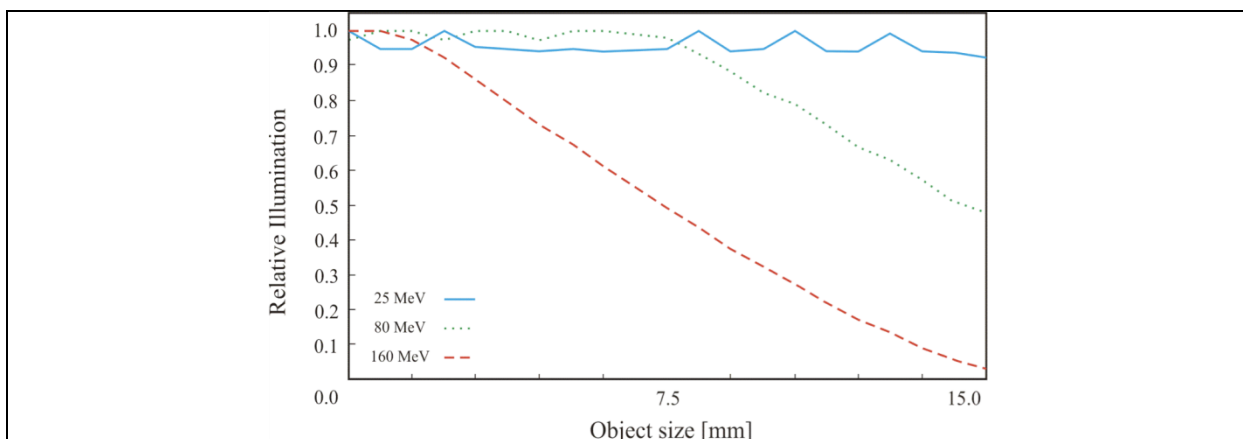
Figure 55: Illumination plot simulating the relative number of OTR photons arriving on the camera with Zemax

The effect has been studied in details on the CTF3 machine, as depicted in Figure 56. As the beam is moved toward the edge of the screen, the light intensity drops out quickly and the beam profile is truncated. Several alternatives have been proposed by developing OTR screens with different surface

shape (parabolic) or different surface state (diffusive screen) and have already shown promising results [lxxviii].
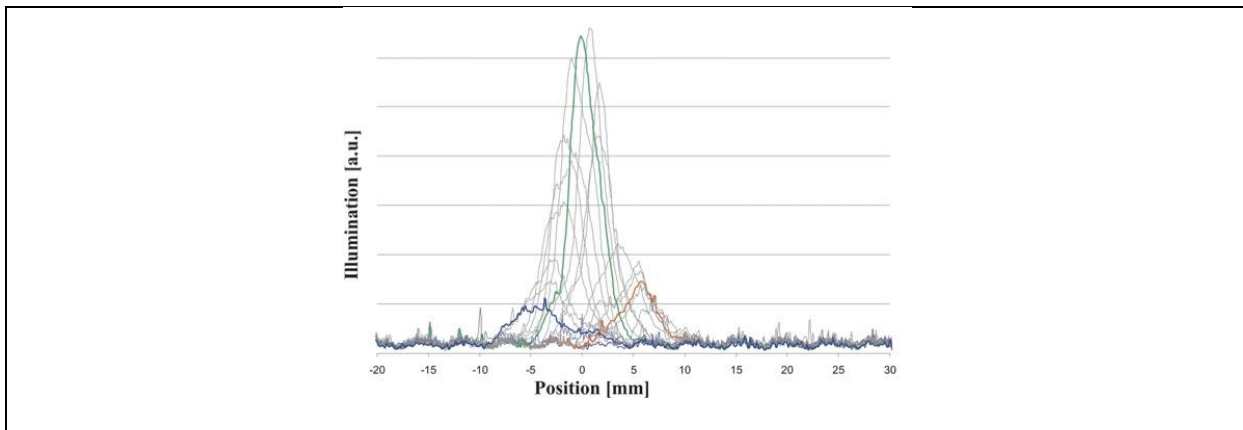
Figure 56: Illumination plot as measured on CTF3 using a flat highly reflective OTR screen in aluminum. The beam energy was 100MeV

Another parasitic effect also observed on CTF3 was due to the synchrotron radiation emitted by the bending magnet at the entrance of the spectrometer line (see Figure 57). Some of the photons were emitted in the direction of the beam, reflected by the OTR screen and detected by the camera, producing then a large background signal potentially degrading the quality of the measurement.
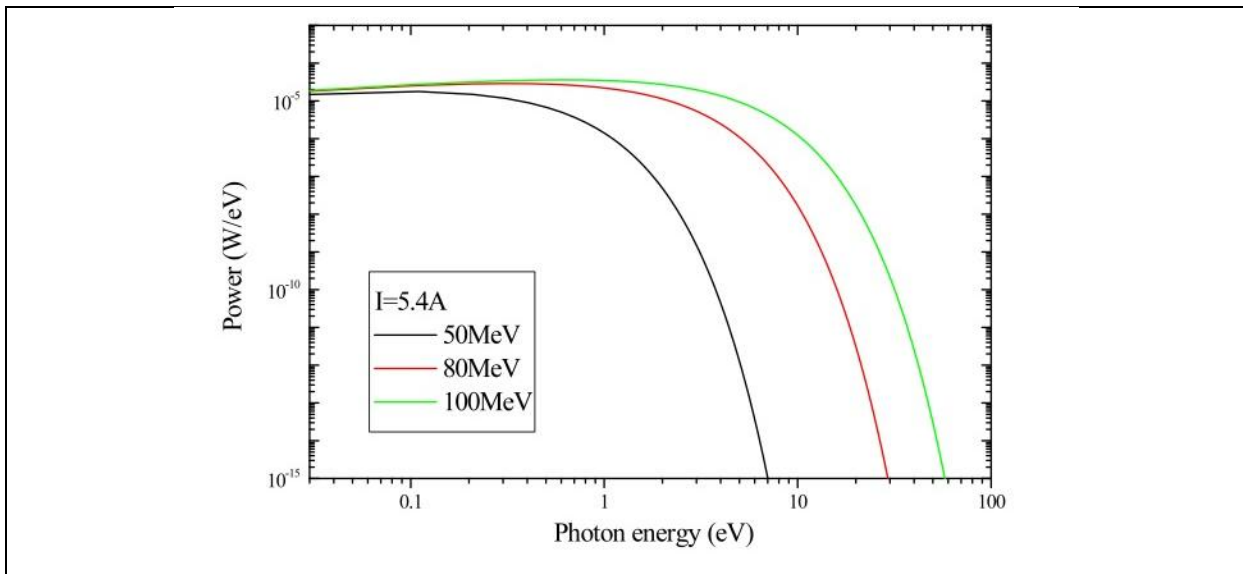
Figure 57: Typical Synchrotron radiation spectrum for several beam energies assuming a bending magnet with a radius of 100cm

In order to overcome this limitation, the mechanical design of the OTR screen was modified to incorporate a thin carbon foil, mounted just upstream of the OTR screen, which will absorb and reflect the synchrotron radiation from the main bending magnet. Such screens [lxxix] (as depicted in Figure 58) are already in use in the present CTF3 spectrometer line imaging system.
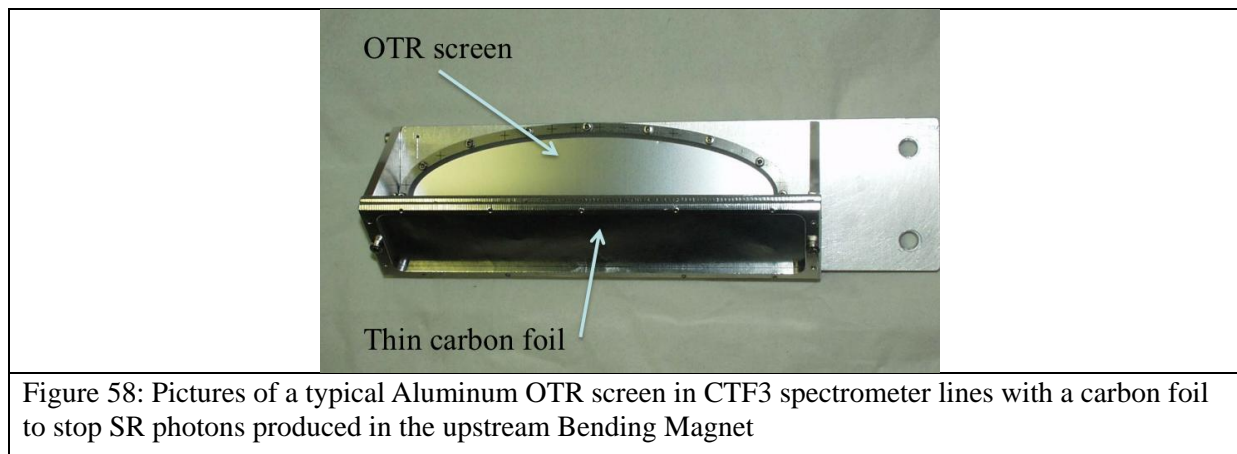
Figure 58: Pictures of a typical Aluminum OTR screen in CTF3 spectrometer lines with a carbon foil to stop SR photons produced in the upstream Bending Magnet

Time resolved energy spread measurement using segmented dumps

Time resolved measurements have been developed during the last years on CTF3, and despite several technologies were tried [lxxx], the detection system found to be the most simple and robust is based on a device, called segmented dump. It is composed of parallel metallic plates designed to stop the incident particles. By measuring the deposited charge in each segment, the beam profile can be reconstructed. The material and the dimension of the segments must be optimized depending on the beam parameters. In particular, they need to be long enough to stop the particles. On the other hand, the segment thickness must be chosen to provide an optimized spatial resolution, which will tend to degrade due to multiple Coulomb scattering [lxxxi] inside the segments. Moreover, because of the high power carried by the beam, thermal changes must be considered as a crucial issue as well as radiation effects that will influence the long-term behavior the detector. An example of a typical geometry developed for the CTF3 linac [lxxxii] and designed for beam energies below 100MeV is depicted in Figure 59. The present system uses of a multi-slit collimator installed just upstream of the segmented dump. Its role is to capture as much beam power as possible, keeping the deposited power in the segments low enough to avoid water-cooling. However the slit width needs to be large enough to detect enough particles and provide comfortable signal amplitudes.
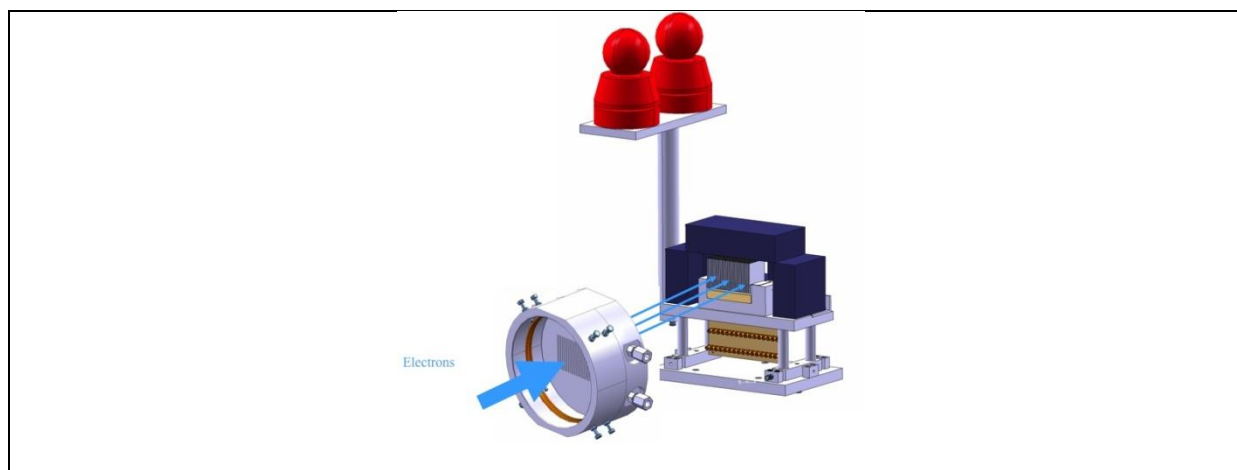
Figure 59: Segmented Beam dump assembly with a 20cm long multi-slit collimator (32 vertical slits, 400um wide each) made out of Iron and 32 Tungsten segments, 2mm wide and 5cm long, spaced by 1mm. Radiation hard ceramics are used as insulating material in between plates.

Monte-carlo simulations using FLUKA [lxx] have been performed in order to choose the optimal material for the collimator and the dump segments and to optimize the detector geometry for best sensitivity and thermal behavior. A typical energy deposition inside the detector is presented in Figure 60 for the CTF3 beam parameter.
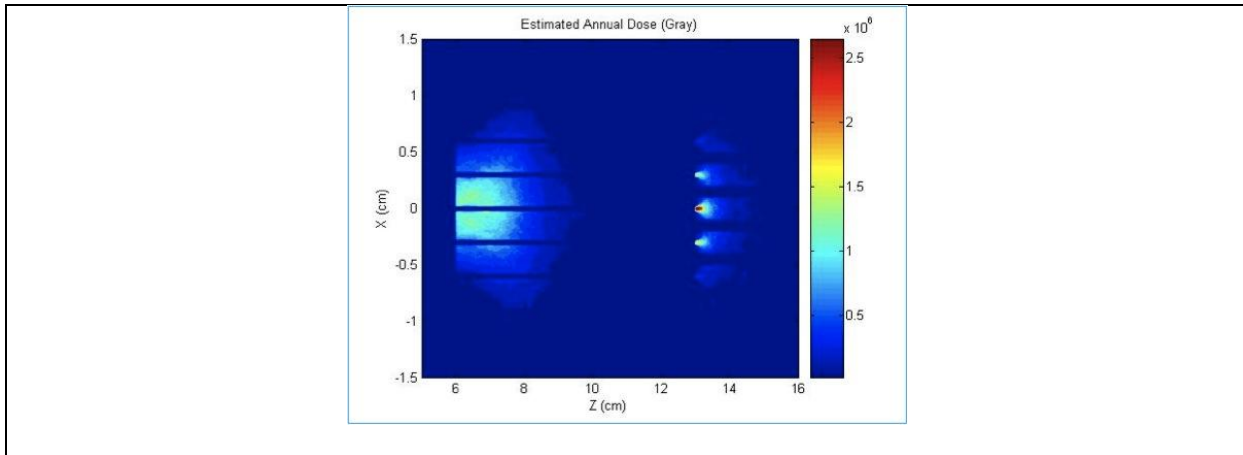
Figure 60: Energy deposition (GeV/cm^3) in a segmented dump simulated using FLUKA. The beam energy is 120 MeV.

Several segmented dumps have been built and installed at several location along the CTF3 linac and are now regularly for the optimization of the machine [lxxxiii]. As an example, a typical energy spectrum is displayed on Figure 61, and shows a fast high energy transient at the beginning of the pulse followed by a long steady state with typically 2-3% energy spread.
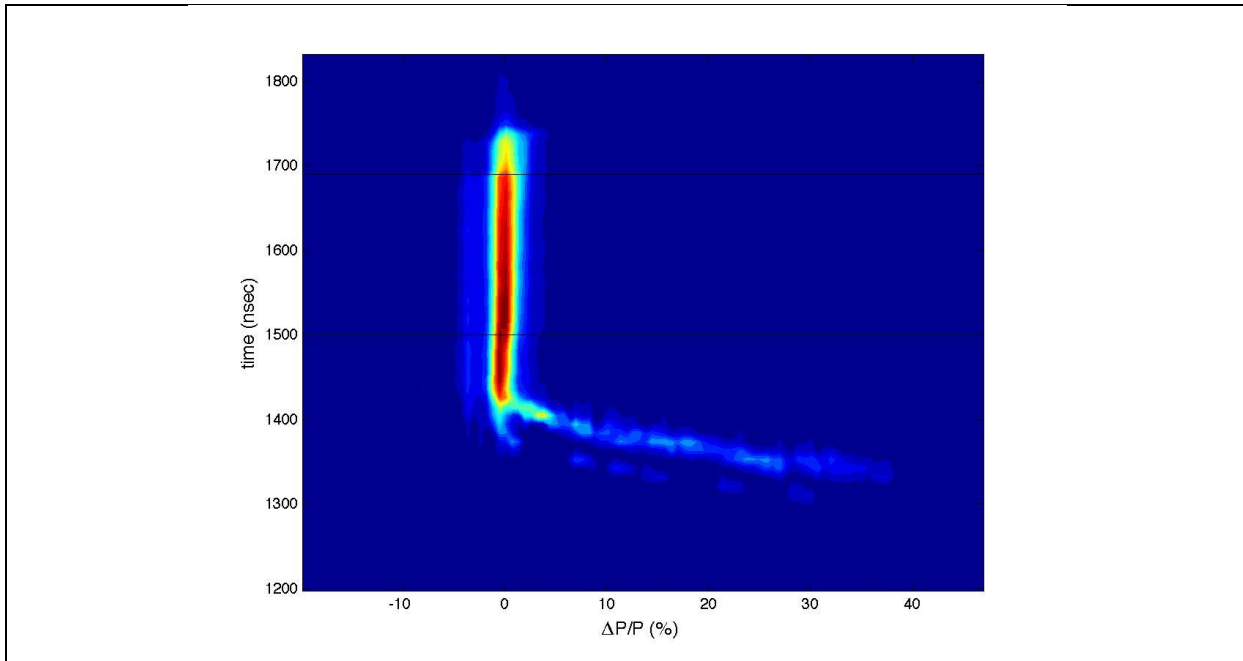
Figure 61: Typical Time resolved energy measurement as measured on the CTF3 linac. Beam energy of 100MeV

5.7.7.3   *High Precision BPM for Energy measurement in the Beam Delivery System*

Beam energy measurements in the Beam Delivery System are crucial because the final focusing system performance is closely related to the good knowledge of the beam energy within a resolution of 2.10^{-4}. It is then foreseen to measure beam energy using using bending magnets (> 200 in total) and the high precision BPMs. As sketched in Figure 62, the BPM, as required for beam position monitoring (see paragraph 5.7.2) would provide measurements with a resolution better than 100nm. By combining several BPMs along the BDS, the estimation of the beam energy will be accurate enough to fulfill the requirements.

Figure 62: Energy measurement scheme as foreseen in the Beam Delivery System
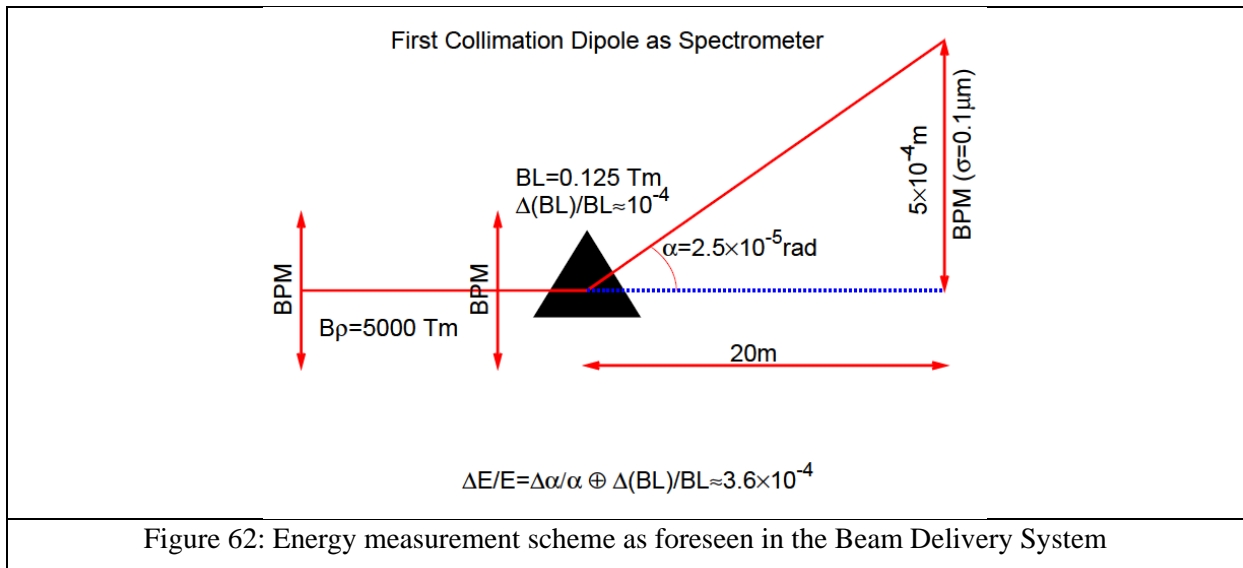
5.7.7.4 Time Resolved Spectrometry on the CLIC Drive Beam Decelerator

In normal beam conditions, the Drive Beam progressively looses its energy as it propagates along the decelerator. A typical time resolved spectrum at the end of the decelerator is shown in Figure 63. It is characterized by a fast transient lasting 100ns. The overall beam energy spread is of the order of 90%. The other extreme case, even if it should not happen frequently, would correspond to the case where all the PETS of a decelerating sector are switched off. The beam will basically not interact with the structures and will not be decelerated at all, as depicted on the second plot of Figure 63.

Figure 63: Minimum and Maximum energy spread at the end of the Drive Beam decelerator
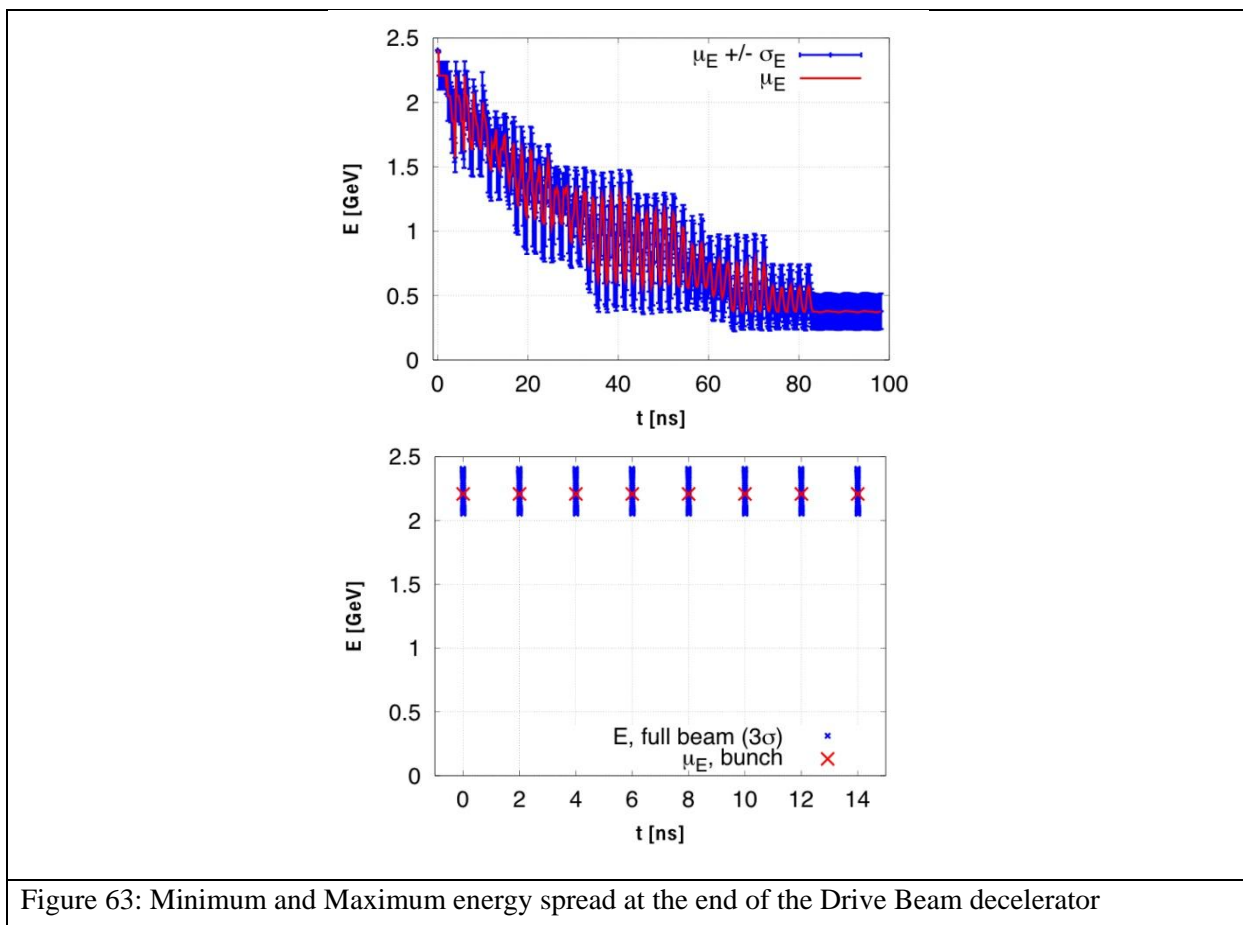
The measurement of the DB energy and energy spread before and after the decelerator is required as a proof of the efficiency of the CLIC RF power production.

Similarly to what is foreseen in the CLIC injector complex, the beam will be dumped in a spectrometer line at the end of each decelerator. The classical techniques to measure energy spread discussed in paragraph 5.7.7.2 cannot be used anymore due to the high beam power carried by the beam. Moreover, due to the high energy spread, the device should be based on a technology, which is not sensitive to energy variation.

A possible solution could use the emission of Cherenkov photons in air (or glass). To highlight the performance on Cherenkov radiation in this particular context, a comparison between OTR and Cherenkov photons yield is presented as a function of beam energy in Figure 64. The calculation assumes a Cherenkov cell of 1cm length. The number of photons produced by OTR is lower than the one produced by Cherenkov in air. The energy threshold to emit Cherenkov photons in air is around 20MeV and, contrary to OTR, the light yield is then perfectly constant with beam energy.
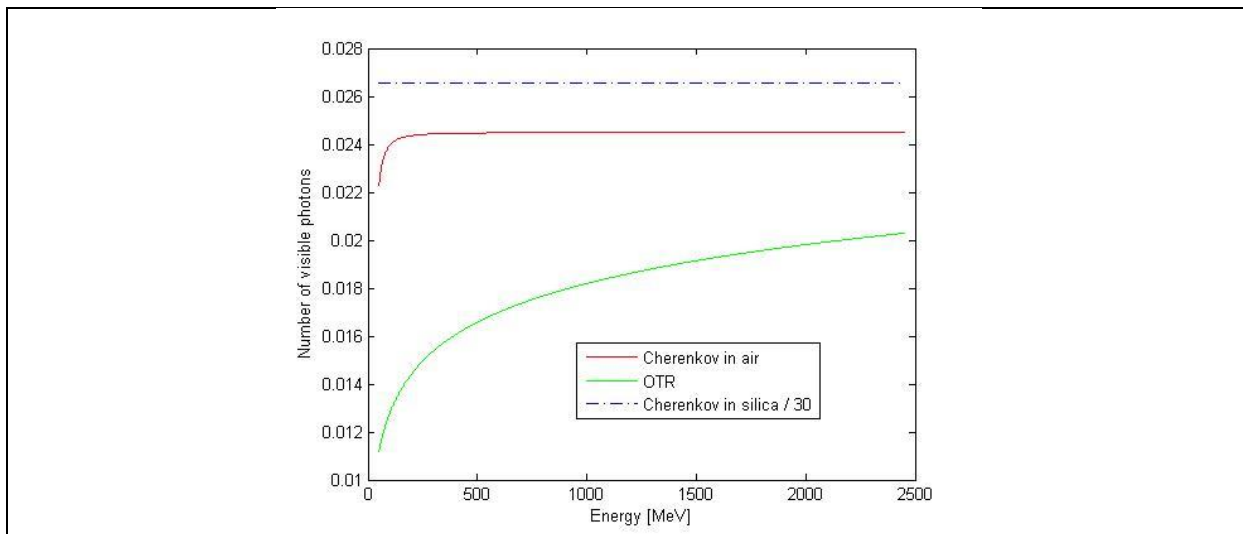
Figure 64: Evolution of the number of photons produced by OTR and Cherenkov in air or quartz as function of beam energy

To measure the beam energy spread, segmented devices would need parallel glass / gas cells, generating Cherenkov photons, which are then transported via optical fiber to a linear CCD or multi-anode photomultiplier. Gas cells can be as small as few cm long and would not suffer from the high beam power. Such a system is currently in preparation to be tested on the CTF3 during the TDR phase.

5.7.7.5   Summary of CLIC beam energy monitors

A summary of the beam energy monitoring systems is presented in Table 20 and indicates what would be the technology choice for the different part of the accelerator complex. It gives baseline scenario, where the technology is mature enough to fulfill the requirements. In many cases, there are two technology mentioned, which basically indicates that two different types of devices are needed to cover the full dynamic range of beam intensities.

Machine Sub-Systems	Quantity	Technology choice	Place to be Tested
Main Beam			
e⁻ & e⁺ injector Complex	8	BPM / OTR / seg. dump	CERN
Pre-Damping and Damping rings	2	BPM / XSR	Sync light sources
RTML	12	BPM / XSR	FEL's

Main Linac and Beam Delivery system	52	BPM	ATF2
Drive Beam			
DB source and Linac	10	BPM / OTR / Cherenkov	CERN
Frequency multiplication complex	6	BPM / OTR	CERN
Turn-around	96	BPM / OTR	CERN
Decelerator and Dump lines	48	BPM / Cherenkov	CERN

Table 20: Overview on energy measurement: color code – Feasibility under investigation / Feasibility proven / CLIC design

5.7.8 *Beam Polarization Measurements*

The Main electron beam is polarized and its polarization must be measured and maintained through the whole complex. The specifications for polarization measurements have not been studied in details so far, but it is however clear the several monitors would be required all along the Complex as indicated in the following table.

Machine Sub-Systems	Quantity
Injector Complex	3
Pre-Damping Rings	2
Damping rings	2
RTML	8
Beam Delivery System	2

Table 21: Quantity of Polarization monitor required in CLIC

No developments were initiated so far concerning the CLIC needs but electron polarization is classically measured using Mott polarimeter [lxxxiv] at low beam energy and Compton back-scattering above few GeVs [lxxxv]. A detailed design of the CLIC polarimeters will be initiated during the TDR phase of the project.

5.7.9 *Luminosity Monitoring*

The concept and the design of the luminosity monitors are currently presented in paragraph 3.7 as a part of the post collision line.

5.7.10 *Component Inventory:*

5.7.10.1 *Summary Table*

The total number of instruments foreseen for the Drive and the Main beams are indicated respectively in Tables 22 and 23. The difference between the 3TeV and the 500GeV machine is mentioned as well. The distinction between instruments located in underground tunnel or in surface building (injector) is also clearly indicated.

Instrument	DB Injector		DB Tunnel		**DB Total**	
	500GeV	**3TeV**	*500GeV*	**3TeV**	*500GeV*	**3 TeV**

Instrument						
Intensity	19	38	160	240	179	278
Position	917	1834	9650	44220	10567	46054
Beam Size	16	32	288	768	304	800
Energy	9	18	152	192	161	210
Energy Spread	9	18	152	192	161	210
Bunch Length	12	24	248	288	260	312
Beam Loss /Halo	865	1730	9650	44220	10515	45950
Beam Phase	8	16	192	192	200	208
Total	1855	3710	15052	90312	22347	94022

Table 22: Number of Beam Instrument for the Drive Beams

Instrument	MB Injector	MB Tunnel		MB Total	
		500GeV	**3TeV**	*500GeV*	**3 TeV**
Intensity	86	58	98	144	184
Position	1539	2168	5648	3707	7187
Beam Size	34	74	114	108	148
Energy	19	14	54	33	73
Energy Spread	19	4	4	23	23
Bunch Length	17	18	58	35	75
Beam Loss /Halo	1936	2374	5854	4310	7790
Beam Polarization	11	6	6	17	17
Tune	4	0	0	4	4
Beam Phase		96	96	96	96
Luminosity		2	2	2	2
Total	3665	4814	11934	8479	15599

Table 23: Number of Beam Instrument for the Main Beams

5.7.10.2 500GeV Collider option

This paragraph discusses the changes related to the beam instrumentation for a CLIC collider working at a reduce beam energy of 500GeV. As a general comment, one could notice that the required performances of most of the beam diagnostics are unchanged, except for the emittance measurement devices. For the 3 TeV CLIC machine the specifications for beam size measurements are at the limit of what is achievable, and it becomes slightly relaxed for lower beam energies. Obviously due to the shorter length of the main linac, the number of required instruments is much smaller.

Impact on the Drive Beam instrumentation

For the 500GeV machine, a single Drive Beam generation complex is foreseen to provide the required beams to generate the e^+ and e^- linacs. The number of Drive Beam decelerator sectors per linacs is reduced from 24 to 5 for a 500GeV collider and as a consequence the total pulse length of the Drive beam is shortened from 140ms to 29ms. This reduction will not have a big impact in terms of instrumentation development. The total charge of the Drive Beam remains high enough in order to impose big restrictions in the use of intercepting devices.

Impact on the Main Beam instrumentation

The Main Beam has a twice-higher charge per train, but this will not have a big impact of the beam diagnostic as well. This should just be taken into account in the specifications so that the electronics does not need to be changed for the 3TeV Collider.

The Bunch length is getting longer with a sigma of 72microns instead of 44microns for the 3TeV machine. This has no impact on the instrumentation as soon as the dynamic range of the corresponding device is already designed to be larger than that. Beam size and emittance will be larger at 500GeV, which would relax the requirement for the spatial resolution of the transverse profile monitors. But the

transverse aspect ratio of the beam is twice more pronounced with a horizontal beam emittance hundred times bigger than the vertical one. The current laser wire system envisaged to measure the beam profiles and emittances would have degraded performances as soon as the beam gets flatter and flatter. The effect needs to be quantified but this is potentially an additional problem.

Number of beam instruments

The total number of instruments is of course reduced significantly for lower energy Collider. As it was mentioned above, the complex will be powered by a single drive beam, which already reduces the number of components for the Drive Beam accelerator complex by a factor 2. The total number of modules installed in the machine is linearly proportional to the final beam energy and the beam instrumentation installed in the tunnel is then reduced accordingly. For a 500GeV machine, the total number of devices is reduced by a factor of 5 compared to a 3TeV collider.

i D. Alesini *et al.*, *"RF Beam deflectors for CTF3 combiner ring"*, Proceeding of the European Particle Accelerator Conference, Paris, France, (2002) pp2115; D. Alesini *et al*, *"Analysis of the vertical beam instability in CTF3 combiner ring and new RF deflector design"*, Proceeding of the European Particle Accelerator Conference, Genoa, Italy (2008) pp2793

ii S. Walston *et al*, "Performance of a High Resolution Cavity Beam Position Monitor System" Nuclear Instruments and Methods in Phys. Rev. A578, 2007, 1-22.

iii S.R. Smith *et al*, "*Commissioning and Performance of LCLS Cavity BPMs"*, Proceeding of the Particle Accelerator Conference, Vancouver, BC, Canada (2009) pp754

iv A. Heo *et al*, "Nanometer Resolution Beam Position Monitor for the ATF2 Interaction Point Region", Proceeding of the Particle Accelerator Conference, Vancouver, BC, Canada (2009) pp3603

v A. Lunin *et al*, *"Submicron Multi-bunch BPM for CLIC"*, Proceeding of the International Particle Accelerator Conference, Kyoto, Japan (2010) pp1185

vi K.Y. Ng and K. Bane, *"Handbook of Accelerator Physics and Engineering"*, pp236

vii E. Bravin and T. Lefevre, *"OTR Studies for the High Charge CTF3 Beam"*, Proceeding of the Particle Accelerator Conference, Portland, USA, (2003) pp2464

viii C. Rimbault *et al*, *"4D Emittance Measurements using Multiple Wire and Waist Scan Methods in the ATF Extraction Line"*, Proceeding of the European Particle Accelerator Conference, Genoa, Italy (2008) pp1257

ix C. Limborg, S. Gierman and J. Power, *"A modified Quadscan Technique for Emittance Measurement of Space Charge Dominated Beams"*, Proceeding of the Particle Accelerator Conference, Portland, USA (2003) pp2667

x P. Tenenbaum, H.H. Braun and F. Chautard, *"Nulling emittance measurement technique for the CLIC test facility"*, Proceeding of the Particle Accelerator Conference, Vancouver, B.C., Canada (1997) pp479

xi K. Honkavaara *et al*, *"Design of OTR Beam Profile Monitors for the Tesla Test Facility, Phase 2, (TTF2)"*, Proceeding of the Particle Accelerator Conference, Portland, USA (2003) pp2476

xii C.H. Back *et al*, *"A Novel Wire Scanner for High Intensity Pulsed Beams"*, SLAC Publication 8061 (1999)

xiii M. Castellano and V.A. Verzilov, *"Spatial resolution in optical transition radiation beam diagnostics"*, Physical Review special topics – Accelerators and Beams **1** (1998), 062801; M. Ross e*t al*, *"A Very High Resolution Optical Transition Radiation Beam Profile monitor"*, SLAC-PUB-9280 (2002)

xiv T. Okugi *et al*, *"Evaluation of Extremely Small Horizontal Emittance"*, Physical Review Special Topics – Accelerators and Beams **2** (1999) 022801; H. Hayano, *"Wire Scanners for Small Emittance Beam Measurement in ATF"*, Proceeding of the Linear Accelerator Conference, Monterey, California, (2000) pp146

xv A. Hofmann, "The Physics of Synchrotron Radiation", Cambridge university press (2000)

xvi K. Ida *et al*, *"Measurement of an electron-beam size with a beam profile monitor using Fresnel zone plates"*, Nuclear Instruments and Methods in Phys. Rev. A **506** (2003) 41; S. Takano *et al*, *"X-ray imaging of a small electron beam in a low-emittance synchrotron light source"*, Nuclear Instruments and Methods in Phys. Rev. A **556** (2006) 357

xvii M. Kocsis and A. Snigirev, *"Imaging using synchrotron radiation"*, Nuclear Instruments and Methods in Phys. Rev. A **525** (2004) 79

xviii A. Andersson *et al*, "*Electron beam profile measurements with visible and X-ray synchrotron radiation at the Swiss Light Source"*, Proceeding of the European Particle Accelerator Conference, Edinburgh, Scotland (2006) pp1223; M. Sjostrom *et al*, *"Characterization of the Max-II electron beam: Beam size measurements"*, Proceeding of the European Particle Accelerator Conference, Edinburgh, Scotland (2006) pp1193

xix T. Lefevre, *"Laser Wire Scanners: Basic process and perspectives for the CTF's and CLIC Machines"*, CERN note 2002-010.

xx   I. Agapov, G. A. Blair, M. Woodley, *"Beam emittance measurement with laser wire scanners in the International Linear Collider beam delivery system"*, Physical Review Special Topics –Accelerators and Beams **10**, 112801 (2007)

xxi M. Ross *et al*. Nuclear Instruments and Methods in Phys. Rev. **A379** (1996) 363-365

xxii Y. Honda *et al*, *"Upgraded laser wire beam profile monitor"*, Nuclear Instruments and Methods in Phys. Rev. **A538** (2005) 100-115

xxiii A. Bosco *et al*, " ", Nuclear Instruments and Methods in Phys. Rev. **A592** (2008) 162–170.

xxiv S.T. Boogert *et al*, *"Micron-scale laser-wire scanner for the KEK Accelerator Test Facility extraction line"*, Physical Review Special Topics –Accelerators and Beams **13**, 122801 (2010)

xxv L. Corner *et al*, " ", Proceeding of the International Particle Accelerator Conference, Kyoto, Japan (2010) pp3227

xxvi http://www.nktphotonics.com/side5215.html

xxvii F.O. Ilday, J. Buckley, L. Kuznetsova and F.W. Wise, *"Generation of 36-femtosecond pulses from a ytterbium fiber laser"*, Optics Express 11, 3550 (2003)

xxviii A.E. Siegman, *"Lasers"*, University Science Books (1986) pp664–669

xxix A. Bosco *et al*, "A large aperture electro-optical deflector", Applied Physics Letters **94** (2009) 211104

xxx I. Agapov, H. Burkhardt, D. Schulte, A. Latina, G. A. Blair, S. Malton, J. Resta-Lopez, *"Tracking studies of the Compact Linear Collider collimation system"*, Physical Review Special Topics –Accelerators and Beams **12** (2009) 081001

xxxi L. Deacon, G.A. Blair, S.P. Malton, I. Agapov, A. Latina, D. Schulte, *"Simulation of Beam halo in the CLIC Collimation systems"*, Proceeding of the European Particle Accelerator Conference, Genova, Italy (2008) pp2859

xxxii A. Aryshev *et al*, *"A novel Method for sub-micrometer transverse electron beam size measurements using optical transition radiation"*, Journal of Physics **236** (2010) 012008; D. Xiang and W. Huang, *"Theoretical considerations on imaging of micron size electron beam, with optical transitions radiation"*, Nuclear Instruments and Methods in Phys. Rev. **A570** (2007) 357

xxxiii P. Karataev *et al*, *"Experimental observation and investigation of the prewave zone effect in optical diffraction radiation"*, Physical Review Special Topics –Accelerators and Beams **11** (2008) 032804

xxxiv E. Chiadroni et al, *"Non-Intercepting electron beam transverse diagnostics with optical diffraction radiation at the DESY FLASH facility"*, Proceeding of the Particle Accelerator Conference, Albuquerque, New Mexico, USA, (2007) pp3982

xxxv A.H. Lumpkin *et al*, *"Near-field imaging of optical diffraction radiation generated by a 7-GeV electron beam"*, Physical Review Special Topics –Accelerators and Beams **10** (2007) 022802

xxxvi P. Karataev *et al*, *"Beam-size measurement with Optical Diffraction Radiation at KEK Accelerator Test Facility"*, Physical Review Letters **93** (2004) 244802; P. Karataev *et al*, *"Pre-wave zone effect in transition and diffraction radiation: Problems and Solutions"*, Physical Letters **A345** (2005) 428

xxxvii T. Lefevre *et al*, *"A Large Scintillating Screen for the LHC Dump Line"*, Proceeding of the Diagnostic and Instrumentation Particle Accelerator Conference, Venice, Italy, (2007), pp132

xxxviii C. D. Johnson, *"The Development and Use of Alumina Ceramic Fluorescent Screens"*, CERN/PS/90-42

xxxix AF995R from Saint Gobain Céramiques Avancées Desmarquest : *http://www.ndfc.saint-gobain.com*

xl K. J. MacCarthy *et al*, *"Characterization of the Response of Chromium-doped Alumina Screens in the Vacuum Ultraviolet Using Synchrotron Radiation"*, J. Appl. Phys. **92** (2002) 6541

xli R. Jung *et al*, "*Single Pass Optical Monitoring*", Proceeding of the Diagnostic and Instrumentation Particle Accelerator Conference, Mainz, Germany, (2003) pp10

xlii C.P. Welsch *et al*, *"Longitudinal beam profile measurements at CTF3 using a streak camera"*, Journal of Instrumentation **1** (2006) P09002

xliii X. Yan, A.M. MacLeod, W.A. Gillespie, G.M.H. Knippels, D. Oepts, A.F.G. Van der Meer, W Seidel, *"Subpicosecond electro-optic measurement of relativistic electron pulses"*, Physical Review Letters **85** (2000) 3404 ; I. Wilke, A.M. MacLeod, W.A. Gillespie, G. Berden, G.M.H. Knippels, A.F.G. Van der Meer, *"Single-shot electron-beam bunch length measurements"*, Physical Review Letters **88** (2002) 1248011

xliv Hamamatsu Streak camera – model FESCA 200: http://jp.hamamatsu.com/products/opto-meas/pd357/pd360/fesca/index_en.html

xlv C. Martinez, *"Determination of Longitudinal Electron Bunch Lengths on Picosecond Time Scales"*, PhD Thesis Univ. Polytec. Catalunya 1999

xlvi A. Dabrowski *et al*, *"Non-destructive single shot bunch length measurement for the CLIC Test Facility 3"*, Proceeding of the Particle Accelerator Conference, Albuquerque, New Mexico, USA, (2007) pp4069

xlvii A Dabrowski *et al*, *"Measuring the longitudinal bunch profile at CTF3"*, Proceeding of the Linear Accelerator Conference, Tsukuba, Japan, (2010) pp1107

xlviii S.P. Jamison, A.M. MacLeod, W.A. Gillespie, B. Redlich, A.F.G. van der Meer, *"Electro-optic technique*

with improved time resolution for real-time, nondestructive, single-shot measurements of femtosecond electron bunch profiles", Physical Review Letters **93** (2004) 114802-06

xlix A. L. Cavalieri et al, "Clocking femtosecond X-rays", Physical Review. Letters **94**, 114801 (2005)

l G. Berden, S. P. Jamison, A. M. MacLeod, W. A. Gillespie, B. Redlich and A.F.G. Van der Meer, "Real-time, non-destructive, single-shot electron bunch-length measurements", Physical Review Letters **93**, 114802 (2004)

li G. Berden, W.A. Gillespie, S.P. Jamison, E.-A. Knabbe, A.M. MacLeod, A.F.G. Van der Meer, P. J. Phillips, H. Schlarb, B. Schmidt, P. Schmüser, and B. Steffen, "Benchmarking of Electro-Optic Monitors for Femtosecond Electron Bunches", Physical Review Letters **99** (2007) 164801

lii B. Steffen et al, "Electro-optic time profile monitors for femtosecond electron bunches at the soft x-ray free-electron laser FLASH", Physical Review Special Topics – Accelerators and Beams **12** (2009) 032802

liii S.P. Jamison, A.M. Macleod, G. Berden, D.A. Jaroszynski and W.A. Gillespie, "Temporally resolved electro-optic effect", Optic Letters **31** (2006) 1753-55

liv S.P. Jamison, G. Berden, P. J. Phillips, W.A. Gillespie, A.M. MacLeod, "Upconversion of a relativistic Coulomb field THz pulse to the near-IR", Applied Physics Letters **96** (2010) 231114

lv R. Lai and J. Sievers, "Determination of Charged Particle Bunch Shape form Coherent far-infrared Spectrum", Physical Review E **50** (1994) 3342; R.B. Fiorito and D.W. Rule, "Diffraction radiation for moderate to high energy charged particle beams", Nuclear Instruments and Methods in Phys. Rev. B 173 (2001) 67

lvi M. Castellano et al, "Measurement of Coherent Diffraction Radiation and its Applications for Bunch Length Diagnostics in Particle Accelerators", Physical Review **E63** (2001) 056501

lvii M. Castellano et al, "Effects of diffraction and target finite size on coherent transition radiation spectra in bunch length measurements", Nuclear Instruments and Methods in Phys. Rev. **A435** (1999) 297

lviii R. Bartolini, G Rehm and P. Karataev, "Observation of Longitudinal Microbunch Instabilities in Diamond Storage Ring", Proceeding of the Particle Accelerator Conference, Vancouver, B.C., Canada (2009) pp4707

lix M. Micheler et al, "Coherent Diffraction Radiation Longitudinal Beam Profile Monitor for CTF3", Proceeding of the International Particle Accelerator Conference, Kyoto, Japan (2010) pp 1143; M. Micheler et al, "Longitudinal beam profile monitor at CTF3 based on coherent diffraction radiation", Journal of Physics: conference series **236** (2010) 012021

lx E. Adli, presentation CLIC Beam Physics Meeting, 03 November 2010.

lxi A. Ferrari et al, "Development of a bunch frequency monitor for the Preliminary Phase of the CLIC Test Facility CTF3", Proceeding of the Diagnostic and Instrumentation Particle Accelerator Conference, Mainz, Germany, (2003) pp211

lxii A Dabrowski et al, "Measuring the bunch frequency multiplication at CTF3", Proceeding of the International Particle Accelerator Conference, Kyoto, Japan (2010) pp1107

lxiii Private communication with S. Smith, SLAC

lxiv R. Corsini et al, "Experimental Results on Electron Beam Combination and Bunch Frequency Multiplication", Physical Review Special Topics – Accelerators and Beams **7**, 04101, (2004)

lxv R. Akre, L. Bentson, P. Emma and P. Krejcik, "A Transverse Deflecting Cavity for Bunch Length and Phase space Diagnostics", Proceeding of the Particle Accelerator Conference, Chicago, IL, USA (2001) pp2353

lxvi M. Jonker, E.B. Holzer, S. Mallows, D. Manglunki, G. Morpurgo, T. Otto, F. Tecker, M. Sapinski, J. Uythoven, "The CLIC Machine protection", Proceeding of the International Particle Accelerator Conference, Kyoto, Japan (2010) pp2860

lxvii E.B. Holzer, "Beam loss monitoring system for the LHC", NSS '05. IEEE (2005) p.1052, CERN-AB-2006-009 BI

lxviii D. Kramer et al, "Very High Radiation Detector for the LHC BLM System Based on Secondary Electron Emission", NSS '07. IEEE (2007) pp2327, CERN-BE-2010-028 BI

lxix W. Berg et al, "Development of a Beam Loss Monitor System for the LCLS Undulator Beamline", Proceeding of the International Particle Accelerator Conference, Kyoto, Japan (2010) pp2860

lxx A. Fasso`, A. Ferrari, J. Ranft, and P.R. Sala, The FLUKA code: Description and benchmarking, CERN-2005-10 (2005), INFN/TC_05/11, SLAC-R-773, NIM Z 265(1938) 581-598

lxxi G. Battistoni, S. Muraro, P.R. Sala, F. Cerutti, A. Ferrari, S. Roesler, A. Fasso and J. Ranft, **"FLUKA: a multi-particle transport code**", Proceedings of the Hadronic Shower Simulation Workshop 2006, Fermilab 6-8 September 2006, M. Albrow, R. Raja eds. AIP Conference Proceeding 896, 31-49, (2007)

lxxii M. Sapinski, B. Dehning, E.B. Holzer, M. Jonker, S. Mallows, T. Otto, C.P. Welsch, "Requirements of CLIC Beam Loss Monitoring System", Proceeding of the International Particle Accelerator Conference, Kyoto, Japan (2010) pp2869

lxxiii M.D. Salt, R.B. Appleby, A Apyan, K. Elsener, E Gschwendtner, A Ferrari "Background at the Interaction Point form the CLIC Post-Collision Line", Proceeding of the International Particle Accelerator Conference, Kyoto, Japan (2010) pp3389

lxxiv W. Panofsky, SLAC Internal Report TN-63-57 (1963)

lxxv F.P. Krueger, *"Tevatron Beam Loss Monitor Specifications,"* Fermilab Engineering Note. 1680.00 ES 158450 (FNAL, Batavia, IL, 1982)

lxxvi W.F. Wulf and M. Korfer *"Beam Loss and Beam Profile monitoring with optical fibers"*, Proceeding of the Diagnostic and Instrumentation Particle Accelerator Conference, Basel, Switzerland (2009) pp

lxxvii A. Intermite, M. Putignano, C.P. Welsch, "*Feasibility Study of an Optical Fibre Sensor for Beam Loss Detection Based on a SPAD Array*", Proceeding of the Diagnostic and Instrumentation Particle Accelerator Conference, Basel, Switzerland (2009) pp228

lxxviii C. P. Welsch, E. Bravin, T. Lefèvre, *"Investigations of OTR Screen Surfaces and Shapes"*, Proceeding of the European Particle Accelerator Conference, Edinburgh, UK (2006) pp1220

lxxix T. Lefèvre *et al*, *"Time Resolved Spectrometry at CTF3"*, Proceeding of the European Particle Accelerator Conference, Edinburgh, UK (2006) pp1205

lxxx T. Lefèvre *et al*, *"Time Resolved Energy Measurements at CTF3"*, Proceeding of the Diagnostic and Instrumentation Particle Accelerator Conference, Lyon, France (2005) pp60

[lxxxi] J. W. Motz, H. Olsen and H.W. Koch, *"Electron scattering without Atomic or Nuclear Excitation"*, Review of Modern Physics **36** (1964) 881

lxxxii T. Lefevre *et al*, "*Segmented Beam Dump for Time resolved Spectrometry on a High Current Electron Beam*", Proceeding of the Diagnostic and Instrumentation Particle Accelerator Conference, Venice, Italy (2007) pp340

lxxxiii A. Dabrowski *et al*, *"Transient Beam Loading Compensation in CTF3"*, Proceeding of the Linear Accelerator Conference, Victoria, BC, Canada, (2008) pp585

lxxxiv J.M. Grames *et al*, "Unique electron polarimeter analyzing power comparison and precision spin-based energy measurement", Physical Review Special Topics – Accelerators and Beams **7**, 042802, (2004)

lxxxv M. Woods, *"Compton Polarimetry at a 1TeV collider"*, SLAC-PUB-7744